Università degli Studi di Padova

Dipartimento di Ingegneria Industriale

Scuola di **D**ottorato di **R**icerca in **I**ngegneria **I**ndustriale

Tool wear compensation and energy efficiency in micro milling Electrical-Discharge Machining

Direttore della Scuola: Ch.mo Prof. Paolo Colombo
Coordinatore d'indirizzo: Ch.mo Prof. Enrico Savio
Supervisore: Ch.mo Prof. Paolo F. Bariani

Dottorando: Gianluca Tristo
Matricola: 1017823

UNIVERSITÀ
DEGLI STUDI
DI PADOVA

Sede Amministrativa: Università degli Studi di Padova

Dipartimento di Ingegneria Industriale

SCUOLA DI DOTTORATO DI RICERCA IN: Ingegneria Industriale
INDIRIZZO: Ingegneria Chimica, dei Materiali e della Produzione
CICLO: XXVI

Tool wear compensation and energy efficiency in micro milling Electrical-Discharge Machining

Direttore della Scuola: Ch.mo Prof. Paolo Colombo
Coordinatore d'indirizzo: Ch.mo Prof. Enrico Savio
Supervisore: Ch.mo Prof. Paolo F. Bariani

Dottorando: Gianluca Tristo

Tool wear compensation and energy efficiency in micro milling Electrical-Discharge Machining

Gianluca Tristo
Doctoral School of Industrial Engineering
Department of Industrial Engineering
University of Padua, Italy

January 28, 2014

Preface

The activities described in this work were carried out in the context of a three-year Doctoral School of Industrial Engineering at the University of Padua, Italy. Most of the research activities and experiments were performed at the Te.Si. laboratory (Laboratory For Precision and Micro Manufacturing) in Rovigo, University of Padua, department of Industrial Engineering.

I wish to thank my supervisor Prof. Paolo F. Bariani, for the patient guidance, encouragement and foresight he has provided throughout my growth as a Ph.D. student.
I could never praise Prof. Giuliano Bissacco enough for teaching the methods to conduct scientific researches with passion and for being an inspiring role model.
My sincere gratitude to Dr. Joško Valentinčič and Dr. Izidor Sabotin, for all the exciting time and the long nights spent together performing experiments at Te.Si. laboratory. I would like to thank ERASMUS program and Prof. Hans N. Hansen for the opportunity to increase my knowledge and expertise at the Technical University of Denmark. Prof. Enrico Savio, coordinator of the Doctoral School, and Dr Simone Carmignato are acknowledged for the help and advices. Special thanks to all the Te.Si. laboratory staff I've worked with, in particular to Riccardo Manzetto and Dr Manuel Balcon.

I would like to dedicate this work to my family. To my parents, for helping to make my higher education possible. To my daughters and Marina, for the strong motivation that they gave to me and for the so many unforgettable moments and feelings that we experienced together.

Padua, January 28, 2014

Gianluca Tristo

Abstract

Abstract in English language

This thesis is aimed at enhancing the accuracy and the sustainability of the micro Milling Electrical-Discharge Machining process.
A framework for the simulation and validation of tool wear compensation models is developed. An on-line tool wear compensation method based on discharge counting and tool wear per discharge is proposed. The mean discharge energy and the variability of the characteristics of the discharges acquired during a pocketing operation are analysed. Optimal trigger values for discharge counting are defined.
A custom hardware interface and software protocol to command the micro EDM machine from Matlab programming language is developed and tested.
A strategy to perform on-machine volume measurement is developed and the repeatability and uncertainty of measures are studied. An evaluation of the errors affecting μEDM on-machine measurements is carried out.
The custom communication interface and the on-machine measurement procedure are employed in automatic assessment of material removal and tool wear per discharge. The procedure is tested in a wide range of process parameters and the variability of MRD and TWD values are evaluated.
A material removal simulation tool for accurate workpiece representation of the machined geometry, based on MRD and counted discharges, is developed and validated.
Finally, a low-cost, modular framework for remote energy monitoring, based on open-hardware and open-source software is developed and employed for the energy efficiency analysis of the micro EDM machine. Expedients to improve the energy efficiency of the micro EDM machine and of the process are suggested.

Abstract in Italian language

Le attività descritte in questa tesi si prefiggono come obiettivo il miglioramento nell'accuratezza e nell'efficienza energetica del processo di micro elettroerosione nella configurazione in fresatura.
A tal fine, è stato sviluppato un pacchetto hardware e software necessario per la simulazione e la validazione di strategie per la compensazione on-line dell'usura utensile. È stato definito un metodo di compensazione usura utensile basato sul conteggio delle scariche elettriche e sul valore di usura utensile per singolo impulso. L'energia media delle scariche elettriche acquisite durante una lavorazione tipo e la loro variabilità sono state analizzate e sono stati definiti i valori di soglia ottimali per il conteggio degli impulsi tramite frequenzimetro.
Una interfaccia hardware e un protocollo software sono stati implementati e testati al fine di comandare la macchina per micro elettroerosione attraverso un personal computer esterno, programmando in linguaggio Matlab. E' stata definita una strategia per la misura in macchina del volume di materiale rimosso sia dall'utensile sia dal pezzo durante il processo di elettroerosione. Sono stati quindi valutati la ripetibilità, l'incertezza e l'errore relativo caratteristici delle misure effettuate in macchina con la procedura proposta.
L'interfaccia di comunicazione e la strategia per la misura in macchina sono stati quindi adottati in una procedura automatizzata per la stima dei valor medi di materiale rimosso ed usura utensile per singola scarica elettrica. La procedura è stata testata con un ampio campo di parametri di processo, al fine di valutare la variabilità dei risultati.
Uno strumento software per la simulazione del processo di rimozione del materiale dal grezzo basato sul volume rimosso per singola scarica e sul numero di impulsi contati, è stato sviluppato al fine di rappresentare in modo accurato le geometrie effettivamente ottenute durante un generico processo di micro elettroerosione. Le simulazioni sono state validate per mezzo di risultati sperimentali.
Infine, un sistema modulare a basso costo per il monitoraggio remoto del consumo di energia, basato su open-hardware e software open-source è stato sviluppato ed utilizzato per l' analisi dell'efficienza energetica della macchina per micro elettroerosione. Dall'analisi dei risultati sono state individuate delle possibili soluzioni per migliorare l'efficienza energetica della macchina e del processo di micro elettroerosione.

Contents

Preface **i**

Abstract **iii**

List of Figures **vii**

List of Tables **ix**

Acronyms and abbreviations **xi**

1 Introduction **1**
1.1 Electrical-Discharge Machining 2
1.2 Material removal mechanism 2
1.3 Main configurations 4
1.4 Micro EDM 4
1.5 Dissertation objectives 5
1.6 Dissertation outline 6

2 Tool wear **9**
2.1 Compensation methods 10
2.2 Examples 12
2.3 Proposed method 14

3 Discharge population **17**
3.1 Experimental setup 19
3.2 Design of experiments 24
3.3 Results 24
3.4 Energy distribution 29
3.5 Mean energy stability 33
3.6 Trigger levels 40

4 Machine control **43**
4.1 Data transmission 43
4.2 Communication interface 44
4.3 Communication protocol 45
4.4 Test of the protocol 46

5 On-machine measurements **47**
5.1 Tool wear assessment 49
5.2 Estimation of material removed 50
5.3 Experimental setup 50
5.4 Preliminary experiments 51
5.5 Experimental results 53
5.6 Influence of dielectric fluid and debris 60

6 TWD and MRD assessment **63**
6.1 Setup of the experiments 64
6.2 Analysis of TWD and MRD variability 66
6.3 In-process experimental re-estimation 70
6.4 TWD and MRD at different machine parameters settings . . 70

7 Applications **73**
7.1 A test bench framework 74
7.2 Material removal simulation 76

8 Energy efficiency analysis **83**
8.1 Sustainability 84
8.2 Measuring the electrical energy consumption 86
8.3 Experimental setup 87
8.4 Experiments 95
8.5 Results 96
8.6 Possible improvements and best practices 99

9 Conclusions **103**

Bibliography **105**

Appendix A **115**

List of Figures

1.1 Sarix SX-200 micro EDM milling machine 1
1.2 Phases of electrical discharges 2

2.1 Micromixer mould detail 9
2.2 Micromixer prototype main channel 12
2.3 Textured surface detail 13

3.1 Sarix SX-200 and oscilloscope 17
3.2 Setup for discharges sampling 19
3.3 Effect of ground lead to energy distribution 23
3.4 Discharge Explorer software 26
3.5 Discharge main characteristics 27
3.6 Histogram energy E105 31
3.7 Waveforms E105 32
3.8 Normality test E105 34
3.9 Normality probability plot E105 34
3.10 Overlapping histograms 3 repetitions E105 35
3.11 Mean energy scatter plot for E105 39
3.12 Trigger level selection E105 41
3.13 Trigger level selection E350 42
3.14 Discharge explorer displaying low energy waveforms 42

4.1 Work-flow for the on-line tool wear compensation 44
4.2 Interface for bidirectional communication between Matlab and Sarix 45

5.1 Image of the sphere being measured with a cylindrical tool-probe 47
5.2 Influence of probing speed on measurements 52
5.3 Reference features used in probing tests 52

5.4 Repeatability test relative to different axis 52
5.5 SEM image of the tool-probe electrode 53
5.6 Dimensional characteristics of the cylindrical pocket 55
5.7 Main causes of error in volume measurements 56
5.8 Cross section of the cylindrical pocket 56
5.9 SEM image of the trough hole 58
5.10 Estimation of the relative error in volume measurements . . . 59
5.11 Image of spherical tool-probe electrode 59
5.12 SEM image of particles produced in micro EDM 60
5.13 SEM image of the particles accumulated on the tool-probe . . 61

6.1 Setup used to test the automatic MRD and TWD evaluation procedures 63
6.2 Variability of tool wear per discharge 69
6.3 Variability of material removal per discharge 69
6.4 MRD and TWD with different process parameters 71

7.1 Voxel discretization of tool and workpiece electrodes 73
7.2 Image of a freeform surface 74
7.3 Image of the square pocket captured with a confocal microscope 75
7.4 Example of model based on the heat transfer equations . . . 78
7.5 Molecular dynamics geometrical representation 78
7.6 Material removal simulation tool 80
7.7 Image of the straight groove 81
7.8 Comparison between simulation and experimental data 82

8.1 Arduino Uno microcontroller board and Ethernet Shield . . . 83
8.2 Setup of the experiments based on Arduino 90
8.3 Calibration curve for a current sensor 95
8.4 Image of the cylindrical pocket 97
8.5 Energy distribution between SX-CU and SX-DA 98
8.6 Power required by subsystems 100
8.7 Example of data recorded during the experiments 100
8.8 Sankey diagram of energy distribution 101

List of Tables

3.1 Process parameters settings 21
3.2 Oscilloscope settings 24
3.3 DOE for discharges sampling 25
3.4 Discharges main energy and max current 30
3.5 Mean energy samples and repetitions E105 38

5.1 Process parameters used during the experiments 51
5.2 Tool-probe diameter measurements 54
5.3 Influence of the dielectric fluid on measurements 61

6.1 Material removed from the workpiece and tool electrode . . . 67

7.1 Depth of the square pocket 77
7.2 Results of material removal simulation 82

8.1 List of Sarix SX-200 main subsystems 88
8.2 Machining operation details 96
8.3 Energy consumption per cubic millimetre of material removed 98
8.4 Total discharge energy and total machine energy 99

Acronyms and abbreviations

CAM	Computer Aided Manufacturing
CNC	Computer Numerical Control
CMM	Coordinate-Measuring Machine
CPU	Central Processing Unit
EDM	Electrical-Discharge Machining
μEDM	micro Electrical-Discharge Machining
LSM	Laser Scan Micrometer
LTW	Linear Tool Wear
MCU	Motors Control Unit
MRD	Material Removal per Discharge
MPS	Micro Pulse Shape generator
OMM	On Machine Measurements
RMS	Root Mean Square value of a signal
PSU	Percentage Standard Uncertainty
PWR	Erosion Power Supply
TWD	Tool Wear per Discharge
UART	Universal Asynchronous Receiver/Transmitter
WEDG	Wire Electrical-Discharge Grinding

Chapter 1

Introduction

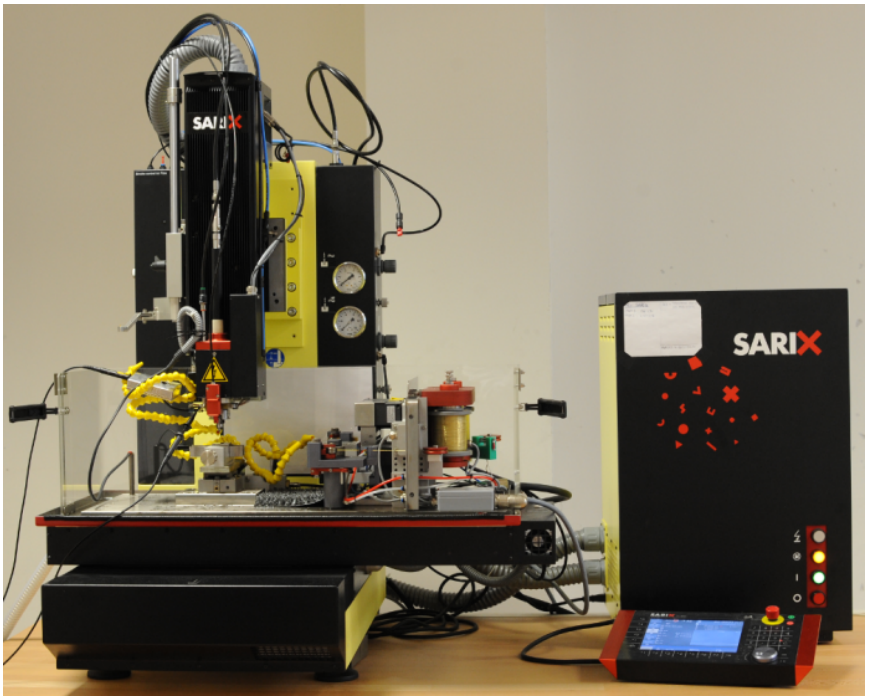

Figure 1.1: Sarix SX-200 micro EDM milling machine at Te.Si. laboratory for precision and micromanufacturing in Rovigo, University of Padua, Italy.

1.1 Electrical-Discharge Machining

Electrical-Discharge Machining (EDM) is an electro-thermal process where material is removed from the workpiece electrode by means of recurring electrical discharges [1]. The EDM process was developed by the end of the 1940s and with the advent of computer numerical control (CNC) and more powerful and sophisticated generators based on transistors has established itself as one of the most frequently used non-conventional manufacturing process. Given its peculiar characteristics EDM is considered an attractive solution for the manufacturing of microcomponents [2, 3].

1.2 Material removal mechanism

Electro discharge machining (EDM) is a thermal process where material removal is achieved by means of electrical discharges occurring inside the small gap between two or more electrically conductive electrodes.
The process is ruled by the generator [5], which is connected to anode and cathode electrodes. The performance of the process such as surface roughness,erosion speed and accuracy can be controlled by modifying the characteristic parameters of the generator as open voltage, current, frequency and duty cycle.
The small gap between tool and workpiece surfaces is filled by the dielectric fluid, which is usually either deionized water or an hydrocarbon oil. The dielectric fluid has an important role in achieving a stable performance during the machining process, by guaranteeing a constant dielectric breakdown strength, by removing excess heat from the electrodes and by washing away from the working area the particles of material produced during the process [6].

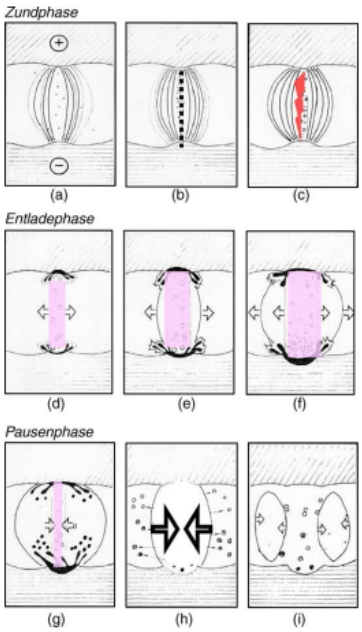

Figure 1.2: Phases of electrical discharges [4].

The most important phases of the electrical discharge material removal process in practical electrical discharge machining is well described by Schu-

macher [4] (figure 1.2). The potential difference applied to the electrodes by the generator induces an electro-magnetic field inside the gap. Accordingly to the studies carried by Kunieda et al. [7], the electrostatic forces in the narrow discharge gap filled by dielectric fluid are the cause of the motion of the debris particles, that were generated during the material removal process. Debris particles have oscillatory movements between the two electrodes because of the electrophoresis and their velocity is high enough to form numerous chains of particles that bridge the gap between the electrodes. Clusters of debris are continuously generated when potential difference applied to the electrodes by the generator and then broken by the explosive expansion of the bubble.

The probability of dielectric breakdown is locally increased by the presence of bridges of debris particles between the two electrodes [8]. At this point ionization begins and small particles start to evaporate. This first phase is in preparation of the discharge and is called ignition-delay. Successively spark occurs and plasma channel grows up till it reaches the equilibrium, producing high pressure on surfaces. The electric current passing from anode to cathode electrodes through the sparking gap, is converted into thermal energy, causing high temperatures at both sparking spots. As a consequence, electrodes material evaporates and liquefies.

When the generator is turned off, the plasma channel de-ionizes quickly, but the gas bubble re-dimensions relatively slowly, the pressure on the molten material decreases and it starts to boil and liquid globules are ejected from the crater. These, once in contact with the dielectric are shock hardened.

Once the concentration of debris particles around the previous discharge crater and the dielectric breakdown strength are recovered, the generator can be turned on and the discharge procedure is repeated in a different location.

The driving force that promotes the discharge movement outside the previously discharged channel, all around the sparking gap, is essential for precision EDM and is defined as spark mobility [9]. High spark mobility means uniform and high performance machining, while low spark mobility means arcing, surface deterioration and process instability. Surface roughness, gap width, concentration of erosion debris and other particles, dielectric strength of pure and decomposed oil, pulse-off time affect spark mobility.

For each spark a crater is generated on both tool and workpiece electrodes. The final shape of the crater, as a consequence of a single discharge, is a depression with edges that are raised above the original surface. Protruding borders are formed during plasma on-time, when the molten metal is kept in place under plasma pressure, eventually escaping from the borders and

re-solidifying immediately, until the plasma collapses and the molten metal is violently expelled from the crater [10].

1.3 Main configurations

Electrical discharge machining is one of the most extensively used non-conventional material removal processes. EDM as well as micro EDM can be performed in different configurations [11, 12]. The following are the most common.

Sinking In Die-Sinking EDM the tool electrode is moved towards the workpiece surface, usually along the Z axis, while material is being removed from the workpiece by discharges. At the end the shape of the tool electrode is replicated on the workpiece [13].

Drilling Drilling EDM [14] is performed by means of a rod that is rotating and moving around and along its axis in order to produce a hole on the workpiece. High aspect ratio micro holes can be machined by flushing the high pressure dielectric fluid through a tubular tool electrode to remove the debris from the bottom of the cavity.

Wire In Wire EDM [15] a thin wire is tensed between two spoons and used as tool electrode to cut the workpiece material. The wire is continuously unwounded and hence regenerated, thus the effects of tool wear are avoided.

Milling In Milling configuration shapes of the tool electrodes are standardized into a cylindrical form and constant rotation is given to the electrode so that the electrode wear is axisymmetric [16]. The material is removed layer-by-layer [17] with layer thickness as low as 0.1 µm. The diameter of the tool can vary from few microns (micro EDM) to dozens of millimetres. This method is based on the stabilization of the tool wear phenomenon after the machining of few layers. Complex 3D shaped microfeatures and high accuracy machining can be achieved by implementing tool wear compensation strategies.

1.4 Micro EDM

The miniaturization of parts could be the next technological revolution [18, 19]. EDM is a contactless process that provides an attractive alternative

machining technique in the production of microcomponents that are smaller than 100 µm [2]. Given the very small forces exerted on both the work piece and tool electrode during the material removal process, it is possible to produce round or irregular-shaped holes as small as 50 µm as well as narrow slots of 50 to 300 µm wide [12, 20].
In order to machine microparts by EDM, it is necessary to increase the accuracy and the resolution of the process, in terms of minimum machinable feature size and surface roughness. To this end, it is necessary to reduce the minimum achievable material removal per single discharge [18], which is proportional to the discharge energy [21].
The discharge generators that are employed in micro EDM, are designed to provide very short and low energy discharge pulses. Discharge energies as small as 3 nJ were obtained by using an RC circuit [22]. Han et al. achieved an improvement on machining characteristics of micro-EDM by using a transistor type iso-pulse generator, further improvements can be achieved by implementing a servo feed control [23]. Kunieda developed a pulse generator for nano EDM based on capacity coupling which eliminates the inuence of the stray capacitance, obtaining discharge craters of 0.43 mm in diameter [24].
However iso-energetic generators are still under development and relaxation type generators based on RC circuits are used in commercial micro EDM machines.
The tool electrodes used in EDM processes are subject to severe wear during machining, because the material is removed by electrical discharges on both anode and cathode electrodes. Tool wear must be studied and quantified in order to manufacture accurate microcomponents.

1.5 Dissertation objectives

The activities described in this work were carried out with the aim of enhancing the micro milling EDM process. To this end, two different objectives were pursued.
The first objective is to verify the applicability to existing commercial micro EDM machines of the proposed on-line tool wear compensation method, which is based on discharge counting and on the tool wear per discharge information only. To this end the validity of the assumptions on which the method is based will be investigated by analysing the variability of mean discharge energy, tool wear and material removal per discharge through a wide range of process parameters settings and machining depths. Finally, a

framework to directly validate the method through experimental data will be developed.
The second objective is related to sustainability: the energy consumption of the micro EDM machine and its main subsystems will be studied in order to define the measures that could improve the energy efficiency of the process. The measurements will be carried on by means of a modular and low cost energy monitoring system, based on open hardware and open-source software, that was developed expressly for this task but that could be easily adapted to a large variety of machine tools.

1.6 Dissertation outline

Chapter 2 introduces the problem of tool wear and explores the possible solutions with a succinct literature survey. The proposed on-line tool wear compensation method based on discharge counting and tool wear per discharge is described.

Chapter 3 analyses the discharges voltage and current waveforms, relative to a wide range of process parameter settings, in order to evaluate the stability of mean energy for a given set of process parameters. The variability of mean energy values of sampled discharges is studied during long and deep machining pocketing operations. The software tool programmed in Matlab language that was used to explore the experimental data is presented. A procedure to select the optimal trigger value for discharge counting is defined.

Chapter 4 describes the development and test of a custom interface and protocol for bidirectional data transmission between Matlab software and the micro Milling EDM machine.

Chapter 5 presents the strategy that was developed to perform on-machine measurement for the assessment of the volume of tool wear and material removed. The repeatability and uncertainty of measures are evaluated.

Chapter 6 defines the automatic procedure for on-machine measurement of the material removal and tool wear per discharge that are characteristic for a selected set of process parameters. The variability of the values during the pocketing operation is evaluated.

Chapter 7 shows the application of tool wear and material removal per discharge parameters for on-line tool wear compensation based on discharge counting and for micro milling EDM simulation.

Chapter 8 analyses the energy efficiency of a micro EDM machine. The modular framework for remote energy monitoring that was developed to accomplish this task is presented. The overall energy consumption is compared to the energy consumption of its main subsystems. Possible solutions to increase the energy efficiency of the micro EDM machine and process are suggested.

Chapter 9 summarises the activities carried on in this work and the results achieved.

Chapter 2

Tool wear

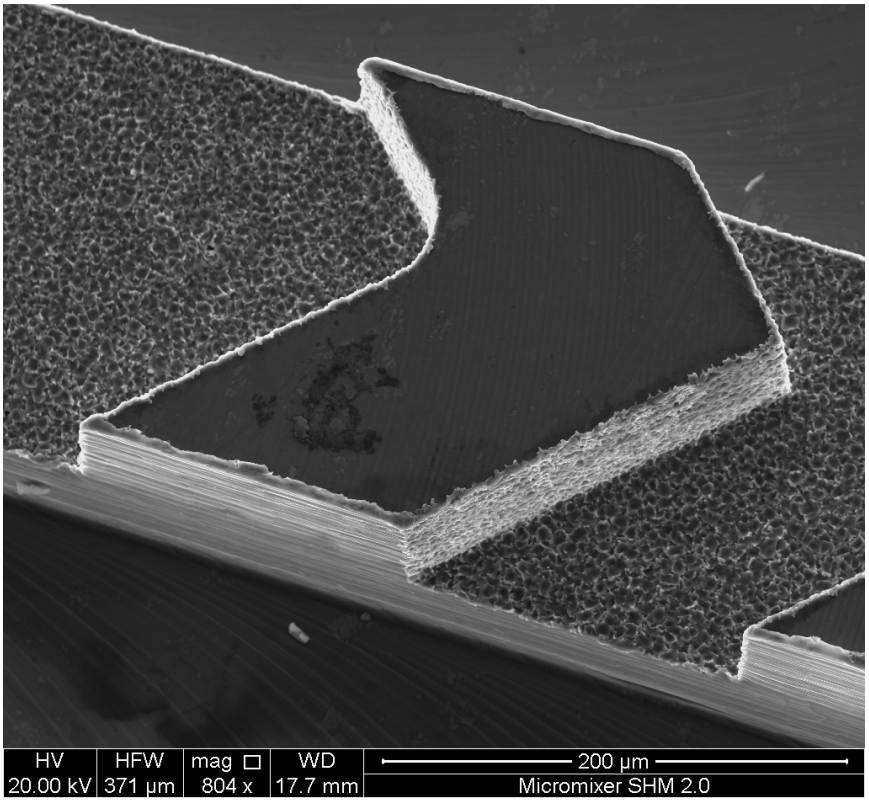

Figure 2.1: SEM image of the functional microfeatures of a mould insert for the mass fabrication of a micromixer by means of micro injection moulding.

In Electrical Discharge Machining the material is removed from both anode and cathode electrodes by successive discrete electrical discharges. The ratio of the material removal to the tool wear depends on many factors such as electrode materials, process parameters and dielectric fluid, but in some circumstances tool wear rate can be greater than material removal rate. During the erosion process the tool electrode is affected by wear both frontally and laterally. Lateral wear can be caused by the abrasion of particles formed during the material removal process and by secondary discharges occurring between the side walls of tool and workpiece electrodes [25].
As a consequence of tool wear, the tool electrode is changing its shape and dimensions continuously during the machining process [13], modifying the tool and workpiece relative position. Given the small sizes of typical tool electrodes used in micro Milling EDM, electrode wear must be studied and effectively compensated in order to achieve high machining accuracy.

2.1 Compensation methods

Electrode wear compensation in macro and micro EDM was investigated by several researchers. Snoeys et al. [26] developed an Adaptive Control System for minimizing tool-wear in wire EDM, Dauw et al. [27] investigated the theoretical basic rules that govern the tool wear in Die-Sinking EDM, Yu et al. [17] proposed the uniform wear method based on layer by layer milling EDM, Pham et al. [28] proposed a simple model for volumetric wear ratio estimation in micro EDM drilling, Tsai et al. [29] evaluated the wear resistance of different electrode materials in μEDM, Uhlmann et al. [30] applied novel materials characterized by high thermal conductivity and high melting/sublimation point to reduce the tool wear.
Since milling EDM is performed in very thin layers (usually in the range of 0.5 to 3 µm) compared to the tool diameter (50 to 300 µm) [17], the tool profile stabilizes rapidly and wear correction can be performed by applying a uni-directional downward feeding movement during the machining.
Recent electrode wear compensation approaches in conventional milling EDM use either an estimation of the volumetric wear ratio with a continuous downward electrode movement proportional to the relative movement along the toolpath (anticipated tool wear compensation), real time wear sensing or a combination of the two [31]. Furthermore, real time compensation can be based on discharges energy measurement [32] or on discharge counting and statistical treatment of the discharge population [33].

Off-line methods are implemented in CAM software during the post processing of the toolpath, by applying a linear compensation continuously or in a small increments along the tool path. Jian-Zhong et al. [34] proposed a method where the area that is scanned by the tool electrode is calculated in order to apply a continuous and constant compensation along the toolpath. The coordinates of the toolpath are adjusted to compensate the tool wear before the part program is loaded by the milling EDM machine. Narasimhan et al. [35] developed a model for tool path generation in macro and micro milling EDM.

The anticipated approach requires a sophisticated CAM software [36] in order to be effectively applied. Working conditions must be known before machining and represented with high fidelity in the CAM software, that uses this information to generate the toolpath. Extensive experiments are required in order to evaluate the appropriate ratio of the tool feed to the tool movement. Real time sensing for wear compensation was implemented by Bleys et al. [37] in conventional size milling EDM, by employing tubular electrodes and an isoenergetic pulse generator. Wear compensation was based on counting effective discharges and using a constant volumetric wear per discharge.

However the method is not directly applicable to resistance-capacitance type relaxation generators found in commercial micro EDM machines, because the produced discharge pulses are not isoenergetic. Aligiri et al. [32] have recently developed a tool wear compensation method based on real time estimation of material removal for micro EDM drilling.

The approach used by Aligiri is based on discharge discrimination and material removal characterization through measurement of crater volume for single discharges. The size of the single crater is predicted by using a thermal model. However, the single discharges are not representative of the actual process and measurement of single crater volume is affected by high inaccuracy.

Jung et al. [38] have implemented real time tool wear compensation based on discharge pulse monitoring and pulse frequency control.

However, due to the very short pulse duration, down to 30 ns, full discharge discrimination is not practical in micro EDM because of the limitations in signal processing speed and because of the larger relative measurement uncertainties. Therefore in such conditions, pulse discrimination is bound to be inaccurate.

2.2 Examples

In the following paragraphs two examples of micro Milling EDM process are presented to describe the practical outcomes of the anticipated tool wear method. The machining operations were performed on a Sarix SX-200.

2.2.1 Micromixer

The first example regards the machining by micro Milling EDM of a micromixer, a microfluidic device that is used to enhance the mixing of two fluids [39].

Microfluidic devices are usually composed of a number of microchannels, having typically a width of 100÷200 µm, a depth of 30÷80 µm and can reach a length of several millimetres.
The geometrical characteristics of the functional microfeatures are optimized with the assistance of CFD analysis, in order to exploit the advantages offered at the microscale, usually in laminar flow regime [40]. Since any form error can compromise the performance of the micromixer, high precision micromachining is required.

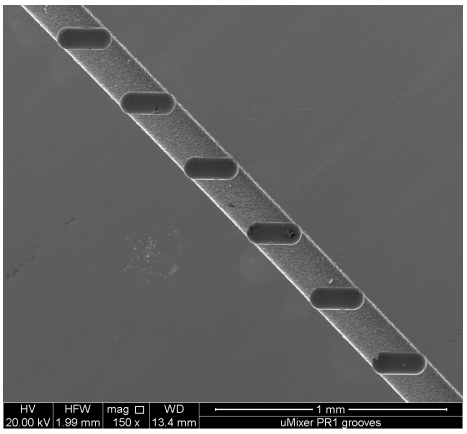

Figure 2.2: SEM image of the main channel of a micromixer prototype.

In order to validate simulations results by comparison with experimental data, a number of prototypes of the micromixer were manufactured by means of micro milling EDM (figure 2.2). Particular attention was given to the empirical estimation of the adjustment factor, which is required by the CAM software to calculate the tool path with the correction for the tool wear compensation. Indeed, considering the considerable length of the toolpath, an under or over estimation of the adjustment factor would lead to an error of several microns in the depth of the microchannels. The bottom of the microchannels would be characterized by a slope angle and consequently a constant variation in depth. Thereby, the cross section area, the flow speed, the Reynolds number would be different from the optimal values, compromising the micromixer

performance.
Once the final design of the micromixer was defined, a mould was manufactured to produce a number of replicas by means of microinjection moulding (figure 2.1). The protruding microfeatures of the mould were machined by ultra precision micro milling, and the functional microfeatures were finished by means of micro milling EDM with a tool having a diameter of 40 µm. The tool electrode was fabricated on-machine by Wire Electrical-Discharge Grinding (WEDG) [19, 41].
With the anticipated tool wear compensation method the toolpath is defined by the CAM software before machining, and the tool length reduction is compensated on the basis of the volume of material removed. In this case, a misalignment of the tool reference on the micro EDM machine, produces a different engagement of the tool electrode during machining, and hence an error in the tool wear compensation. The tool reference coordinate system is set by using the tool electrode tip as a probe on a Coordinate Measuring Machine (CMM), hence, a misalignment is highly probable. When an over compensation occurs, the machining is ended at a lower level than the specifications, and the main microchannel could be reduced in depth, compromising the fluid flow.

2.2.2 Textured surface

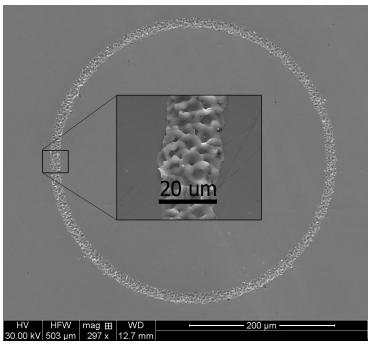

Figure 2.3: SEM image of an optical surface textured by micro milling EDM and detail of the texture.

The second example concerns the surface texturing of a mould insert for the mass production of biomedical components. The manufactured parts were characterized by a mirror like surface on which very thin marks were machined by micro milling EDM (figure 2.3).
The lines had a specified width of about 20 µm and a depth of few microns by specifications. In order to produce such thin marks, considering the sparking gap, tool electrodes with a diameter of about 12 µm are required.
Given the small footprint of the tool electrode, the tool length was shortening very rapidly during machining by effect of the tool wear. Tool wear was being compensated with the anticipated method, using a

continuous and constant downward feeding movement.
The empirical evaluation of the adjustment factor was of paramount importance because an under compensation of the tool wear would lead to the non-homogeneousness of line width. A slight tilt of the workpiece surface, originating from a clamping misalignment, would produce the same defects. On the other hand an over-compensation would produce a greater depth than specified, more material removed, an increase of the tool wear and as a consequence more tool electrodes would be necessary to machine all the microfeatures. Since the microfabrication of the microtools at the wire dress unit can last 7 to 10 minutes, the loss in productivity is noticeable.

2.3 Proposed method

The proposed on-line tool wear compensation method can be applied to micro milling EDM and is based on discharge counting rather than on single discharge energy measurements. The method relies on a statistical approach to the evaluation of discharge energy, therefore the statistical distribution of discharge characteristics, namely the average discharge energy, is considered. Assuming that tool wear and material removal can be strictly related to discharge energy, if the average energy is constant then the average values of Material Removal per Discharge (MRD) and Tool Wear per Discharge (TWD) can also be considered constant. Thus, it is sufficient to count the number of pulses occurring during the process in order to implement an effective on-line tool wear compensation with this method.
The statistical approach is valid for a stable process, when discharge population is expected to be stable.
Tool wear compensation in micro EDM milling can thus be obtained by counting the discharges and multiplying the number of discharges by the population TWD value. Similarly, material removal can be estimated by multiplying the number of discharges by the average MRD of the population.
Once the volumetric tool wear and the tool diameter are known, the wear length can be calculated and the electrode wear compensated by adjusting the tool-workpiece relative position. The tool wear compensation can be performed continuously during the machining operation.
Uncontrollable changes in the machining conditions can occur, due for instance to a loss in washing efficiency of the dielectric fluid when machining high aspect ratio microfeatures. In this case, the tool wear and material removal per discharge values can be updated in order to achieve high accuracy

machining.
The advantage of this method is the simplicity and the low cost of the necessary equipment.

Chapter 3

Discharge population

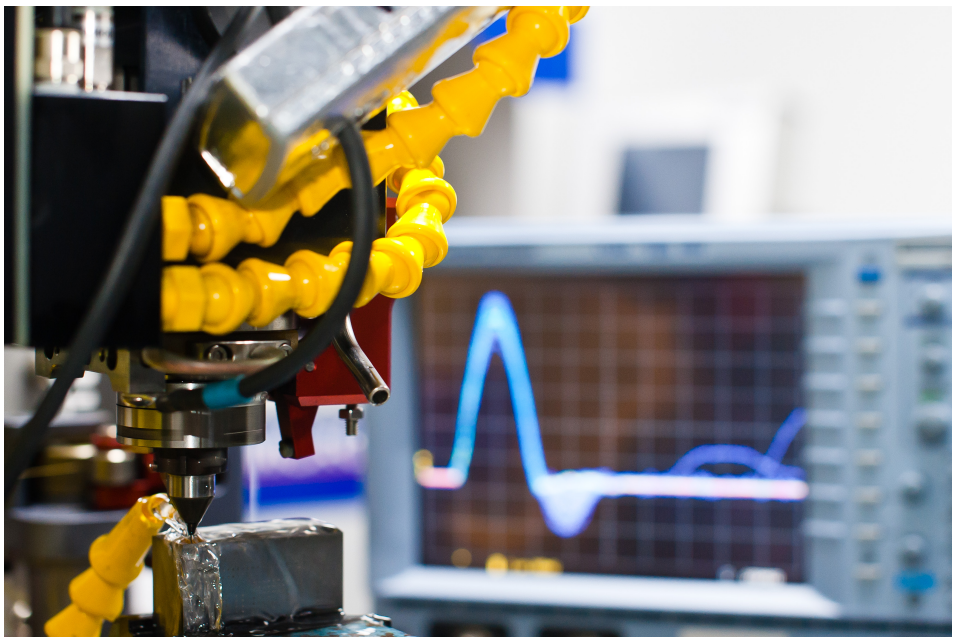

Figure 3.1: Sarix SX-200 during a machining operation while discharges are recorder by an oscilloscope.

The evolution of EDM machines has seen the development of better generators capable of a more accurate control of the discharge parameters with the transition from resistor-capacitor circuits to transistors.
In micro EDM the trend is to increase the resolution of the process by reducing the energy of the single discharge, in order to remove a smaller volume of material. At the same time it is necessary to preserve the productivity and hence the competitiveness of the technology, and for this reason it is necessary to increase the frequency of the discharges. Indeed, micro EDM machines are usually equipped with generators based on resistance capacitance circuits, because these can easily generate very short pulses with relatively high peak currents at higher frequencies. On the other hand, this kind of generators is not able to produce isoenergetic discharges.
As a consequence, micro EDM processes are characterized by a relatively large range of discharge energies, even under the condition of constant process parameters settings. This variation in discharge energy is due to the stochastic charge and discharge of the RC circuit. Furthermore the generator circuits that are typically used to provide the high energies required in roughing operations, include a number of capacitors, characterized by different capacitance. In this case the discharges population is characterized by clusters of discharges with completely different voltage and current waveforms and energy can vary from 4 µJ to 240 µJ for constant settings (table 3.1, energy index 305).
Even considering a set of process parameters typical for fine finishing operations that uses a generator with only one capacitor (table 3.1, energy index 015), the discharge energy can vary from 0.01 µJ to 0.99 µJ. In this case voltage and current waveforms have a similar shape, and the variation in energy is due mainly to differences in voltage and current peak values and pulse duration.
For this reason, although the energy information is not used during the online tool wear compensation with the statistical approach, it is important to completely characterize the pulses in terms of the statistical distribution of the entire population, in order to confirm the applicability of the method and perform a proper setup.
In particular, it is important to verify that the statistical distribution of the discharges energies, sampled during a generic process, is constant over a reasonable amount of time. As a matter of fact, assuming that the material removed from the workpiece by a given discharge is dependant on the energy supplied by the generator [32], it is reasonable to suppose that if the mean energy per discharge is constant then it will be constant also the material removal per discharge [31, 37].

This chapter has three main objectives: to determine if there is an influence of the machining depth over the samples, to evaluate the consistency of the populations of different repetitions of the same experiment and to identify the optimal trigger value for the frequency counter that will be used to count the discharges. The population of discharges energies relative to a broad range of process parameters setting, from roughing to fine finishing, will be analysed. A statistical analysis of data will be performed to discern between systematic differences in samples means and chance variability.

3.1 Experimental setup

In order to characterize the discharges occurring during a generic μEDM process with different sets of process parameters, it is necessary to measure and evaluate the electric current and the electrical potential that are delivered to the workpiece and tool electrodes by the generator during the machining operations.

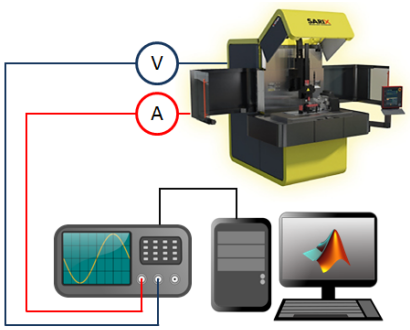

Figure 3.2: Setup used during the experiments, consisting of a Sarix SX-200 micro EDM milling machine, LeCroy Waverunner 2 LT584L oscilloscope, personal computer.

Voltage and current analogue signals are produced by two probes, which can be considered as the sensors of the acquisition system. Electrical potential has been measured with a Velleman passive probe with a bandwidth of 250 MHz. Commercially available current probes with sufficient bandwidth are rare and expensive. Thus, the probe to sense the electric current was designed and built by the research partners at the Technical University of Denmark, specifically for this application. Construction details of the probe are deliberately not explained.
The signals generated by these two probes have then to be digitized using an analogue to digital converter. The challenge of accurately digitizing the current and voltage signals of the discharges in μEDM comes from the duration of the short pulses that are typical in fine finishing operations and can last only few tens of nanosecond, thus demanding a high sampling rate. Not only the equipment that is capable to

digitize analogue signals continuously at a sampling rate of 200-500 MS/s is expensive, but a machining process can easily last several hours. Hence, the volume of data generated during the experiments for the acquisition and digitalization of the waveforms is large, causing issues in data throughput, data storage and post processing time. Real time processing of the input signals with an FGPA board is a possible solution to eliminate the post processing and reduce the amount of data that is necessary to transfer and record, but at the time of writing high speed DAQ boards with on-board signal processing are extremely expensive.

However, considering that discharges have a consistent width, and that the empty signal between discharges can be discarded, it is possible to reduce the amount of data sensibly. To this end, an oscilloscope can be used to record data only when a trigger event occurs, for a predetermined fixed timespan. With the appropriate trigger level, voltage and time per division values it is possible to minimize the number of bytes per discharge, and thereby to use the buffer of the oscilloscope to store hundreds or thousands of discharges. Unfortunately, the limited amount of memory available in oscilloscopes is not sufficient to store all the discharges occurring during a typical μEDM process. Although only a limited number of pulses can be stored in a row, it is possible to sample these in batches at time intervals and to use the pause between samples to transfer the data from the oscilloscope memory to an external mass storage. Eventually, the oscilloscope can be programmed by using an external application, so that this procedure can be repeated automatically for all the duration of the machining process.

This strategy was exploited by employing a LeCroy Waverunner 2 LT584L oscilloscope (figure 3.1), which is characterized by the following specifications: 4 channels, a maximum sampling rate of 4 GS/s, 1 GHz of analog bandwidth, a memory of 4 Mpoints per channel, a vertical Resolution of 8 bits and a sensitivity of 2 mV per division up to 10 V per division. The oscilloscope was programmed remotely through a GPIB connection by a Matlab script, that was running on a computer (3.2). The segments that were stored on the internal memory of the oscilloscope were transferred and saved to a computer hard drive in binary format, in order to reduce both the transmission time and the size of the files. All the files relative to the same experiment were then interpreted in Matlab to reconstruct the waveforms for a visual inspection and the evaluation of energy, maximum and minimum values of current and voltage, width, rise time and fall time of every discharge recorded.

The experiments were performed on a Sarix SX-200 micro EDM machine. Tungsten carbide cylindrical rods with a nominal diameter of 300 µm were

Energy index	Pol. -	Width index	Freq. KHz	Curr. A	Volt. V	Gain index	Gap index	Layer µm
015	-	6.0	100	70	80	75	65	0.5
105	-	6.0	100	65	100	75	90	0.9
206	-	5.0	130	50	130	80	100	2.5
250	-	5.0	130	50	130	50	97	2.0
305	-	4.6	130	50	130	100	106	2.5
315	-	4.6	130	50	130	60	100	2.5
350	-	4.6	130	50	130	50	100	2.5

Table 3.1: Process parameters used during the experiments

used as tool electrodes, while the workpiece material was a martensitic stainless steel (Uddeholm Stavax ESR). The workpiece was flooded with dielectric fluid, HEDMA 111 hydrocarbon oil.

3.1.1 Reference feature

The feature that has been selected as reference to be machined during the experiments is a circular pocket having a diameter of about 500 µm and a depth of about 300 µm.
It is machined layer by layer, with layer thickness ranging from half of a micron to few microns depending on the process parameters settings (table 3.1). Machining is performed with the undressed electrode, which has a nominal diameter of 300 µm with a variability guaranteed by the manufacturer of +2 and -4 µm. The circular pocket is machined by imposing an orbital movement to the tool electrode while the tool is rotating around its own axis. The toolpath consisted of circular interpolations around the centre of the pocket, and the direction of circular interpolation was changed alternatively from clockwise to counter-clockwise at every new layer in order to uniformly distribute the excess of rest material induced by tool wear on the floor of the pocket. No tool wear compensation was applied either before nor during machining.

3.1.2 Signal fidelity

Voltage and current values, measured and recorded using the setup described in section 3.1, are generated by two different probes, that have to be con-

nected to the discharge circuit of the machine. Intuitively, in order to measure the energy that effectively contribute to the material removal, avoiding noise, parasite current and other disturbances, these probes should be placed as close as possible to the working area, where the discharges occur. For instance, the probe ground lead length influences the inductance of the circuit. The longer the ground lead, the greater the inductance and the greater the likelihood of seeing on fast pulses the typical oscillations that result when a circuit resonates (ringing effect). However a compromise has to be made in order to maintain a sufficient signal fidelity without limiting or compromising the capabilities of the machine in tool positioning. Indeed, to use a long lead to connect the ground of the voltage probe would be convenient to be able to perform all the machining operations, in particular the electrode dressing at the wire dress unit, without having to remove and then fix again the probe.
A test to verify the influence of the probe setup on the measurements has been conducted, to compare results obtained when the ground signal is alternatively connected to the main voltage source pole on the machine table through a 700 mm long wire (WL in figure 3.3) or to a thin copper plate inserted between the workpiece and the clamp (CU in figure 3.3).
Voltage and current signals of 8000 discharges have been acquired for each setup, and the tests were repeated 3 times. The discharges energy has been calculated from the voltage and current signals and results have been compared. Figure 3.3 shows the sensible difference in discharge energy distributions between the two setup.

Signal fidelity, source loading and noise immunity should be taken carefully into consideration when the aim is to perform accurate analysis of the energy of every discharge, for instance by using sophisticated and expensive hardware as power line isolation transformers, isolation amplifiers and active or differential probes.
This problem has far less influence on the accuracy of the machining process when the on-line tool wear compensation method is based on discharge counting.
In the experiments described in this work the setup with the thin copper plate was used (CU in figure 3.3) in order to reduce the inductance of the circuit.

Oscilloscope setup

The experimental setup described in 3.1 has been used to acquire samples of discharge population relative to the seven sets of process parameters detailed

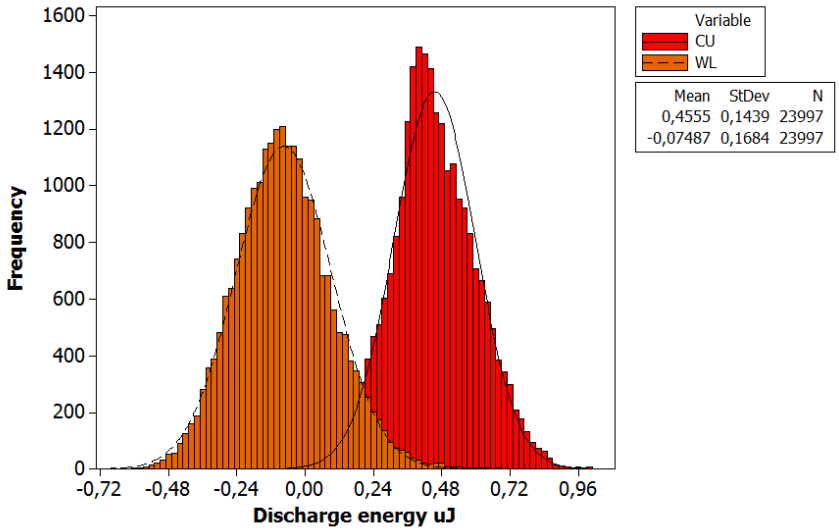

Figure 3.3: Difference in energy distribution due to different setup of the voltage probe ground lead. Energy 015.

in table 3.1. These settings are representative of the main operations that are often adopted for the fabrication of microcomponents and are referenced using the same name, or energy index, defined in the machine documentation.
These sets of process parameters (table 3.1) are typical for a wide range of operations, from roughing to fine finishing, and consequently produce waveforms that are very different in amplitude and duration. For this reason, it was necessary to perform a series of preliminary experiments in order to optimize the oscilloscope parameters for the data acquisition. The main parameters for each oscilloscope configuration used during the experiments are reported in table 3.2. The trigger levels were set as close as possible to zero, in order to acquire all the variety of discharges. As a consequence, also short circuits and arches have been recorded. Voltage per division and vertical offset values relative to both current and voltage probes channels have been selected in order to avoid the clipping of data in correspondence of peaks and valleys and at the same time to maximise the resolution of the waveforms. The same for the time per division. The attenuation of the voltage and current probes were set to 10:1 and 1:1 respectively.

Energy index	Time/div µs/div	Voltage V/div	Current mV/div	Trigger mV	Sampling rate MS/s
015	0.1	20	20	30	500
105	0.1	50	100	50	500
206	0.2	50	200	60	500
250	0.5	50	200	60	500
305	0.5	50	200	60	500
315	0.5	50	200	100	500
350	0.5	50	200	100	500

Table 3.2: Main oscilloscope settings

3.2 Design of experiments

The populations of discharges relative to the seven set of process parameters in table 3.1 were sampled at a fixed time interval along all the machining process, in order to verify if there is a correlation between the average energy of the samples and the depth of the layer that was being machined during the acquisition. The number of discharges that were stored in memory per sample ranges from 1000 to 4000, as specified in table 3.3. The differences of this value between different energy indexes is due to the timebase setting of the oscilloscope: for a constant sampling rate the shorter the timebase, the more the segments that can be stored in memory.
In the following sections energy index 105 will be examined in detail as an example. For this set of process parameters, 34 samples with a size of 4000 observations have been recorded during each experiment, and the experiment has been repeated 3 times.

3.3 Results

After the experiments were performed, a number of files were saved on the computer hard drive. Each file represents one sample and contains the information about voltage and current over time of 1000 to 4000 discharges, which are the observations of the experiment (table 3.3). The number of samples per experiment range from 16 to 64. As a consequence the total number of discharges that have to be processed is relatively large and, indeed, the maximum worksheet size in Microsoft Excel, which is 65536 rows by 256 columns, is easily exceeded even when only few descriptive parame-

Energy index	discharges per sample	samples	repetitions
015	4000	23	1
105	4000	34	3
206	2000	16	1
250	1000	18	1
305	1000	64	1
315	1000	20	1
350	1000	24	1

Table 3.3: Design of experiments with sample size, number of samples and repetitions.

ters per discharge are stored in a single row.
In order to deal with this large amount of data a graphical user interface for a qualitative inspection of every discharge recorded was developed in Matlab. Matlab was also used to post process raw data, in order to extract the main characteristics of the waveforms, that were then analysed using the statistical software Minitab.

3.3.1 Discharge explorer

In order to better understand the behaviour of the micro EDM process and to check the consistency of the experimental results, it is useful to explore the data, visualizing the waveforms and searching for anomalies that could have occurred during the acquisition of data. It is convenient to have a tool that can cluster and order the discharges in base of their most interesting characteristics, such as energy, width, current or voltage peak and then display the waveform relative to the selected discharge. To this end, a graphical user interface has been developed in Matlab environment (figure 3.4) to simplify the navigation between the discharges and to facilitate the recognition of evident trends over time or groups with clear differences.

The graphical user interface is composed of three plots and a number of buttons and menus. The main plot is used to display both the current and voltage waveforms relative the segment, which is unequivocally identified by the number reported on the text field on the top right angle of the window. The two smaller plots below the main one, are used to display all the segments relative to the sample that has been loaded. Entries are by default ordered chronologically, in order to evaluate the trends over time of a par-

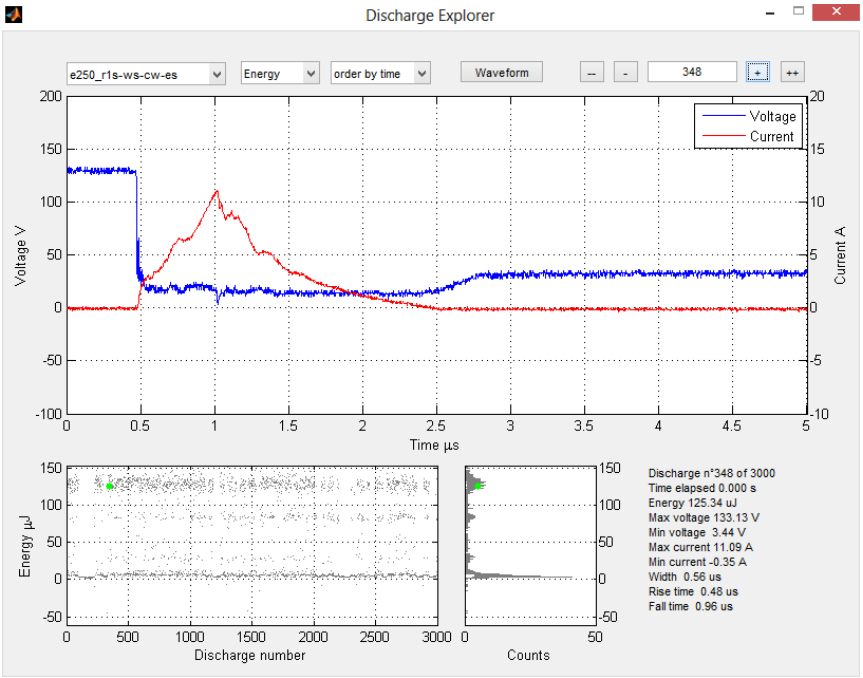

Figure 3.4: Screenshot of the software developed to explore the discharges that were acquired during the experiments.

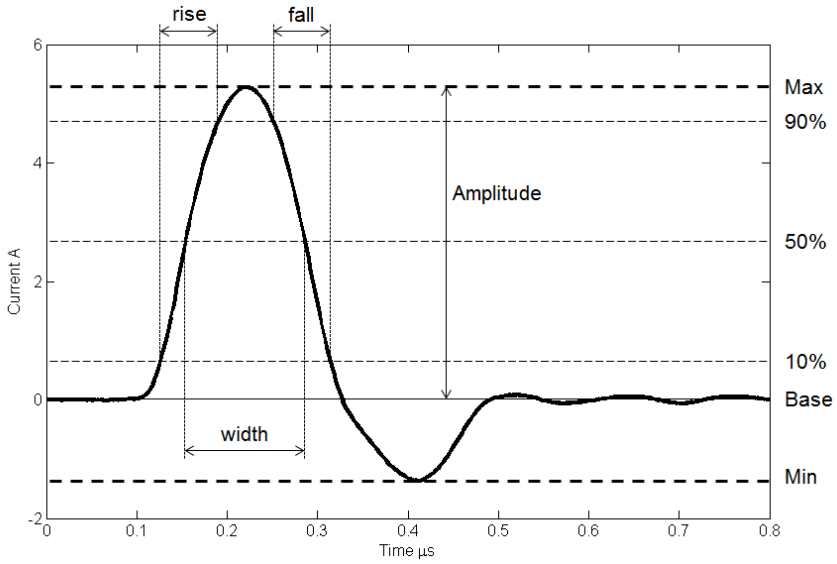

Figure 3.5: Main characteristics of the current waveform of a generic discharge. The illustration is based on a typical discharge obtained with E105 process parameters.

ticular parameter, such as energy or peak current.
Thanks to the graphical user interface the inspection can be carried out relatively quickly and with ease: it is sufficient to select the desired item in one of the secondary plots with the pointer and the waveform plot will be immediately updated. When desired it is possible to save the waveforms as a graphic file for sharing or publications.
This qualitative analysis can give a preliminary overview of the experiments and help in deciding if the quality of data is sufficient for the statistical analysis, understanding the behaviour of the process, identifying and examining the waveforms of outliers and groups with different characteristics.

3.3.2 Data post processing

After the qualitative inspection of the recorded data, the files containing the waveforms have been converted from binary into a human readable format and then post processed in Matlab, in order to evaluate the following characteristics for every trigger event that has been recorded:

Energy The energy E of the discharge is equivalent to the integral over time of the instantaneous power, which is the product between instantaneous voltage and current, as in formula (3.1). The instantaneous voltage $v(t)$ and current $i(t)$ are values that corresponds to a specific time t.

The energy has been calculated in Matlab as the sum of the products between Δt instantaneous voltage and current, where Δt is the time gap between two consecutive voltage or current values (3.2). During the experiment the signals were sampled at a fixed rate of 500 MS/s, hence Δt is a constant and it is equal to 2 ns. The digital representation of the pulse has a total duration of T, variable dependant on the length of the pulse, and is made of $n = \frac{T}{\Delta t}$ points.

$$\begin{aligned} E &= \int_0^T P(t)\mathrm{d}t \\ &= \int_0^T v(t) \cdot i(t)\mathrm{d}t \end{aligned} \tag{3.1}$$

$$E = \sum_{k=0}^{n} v(k) \cdot i(k) \cdot \Delta t \tag{3.2}$$

Max/Min Maximum and minimum values for both voltage and current signals are calculated: V_{max}, V_{min}, I_{max}, I_{min}. It is assumed that the maximum value is equivalent to the peak and to the amplitude of the waveform.

Thresholds Considering the current signal only, three thresholds levels are calculated at 10%, 50% and 90% of the amplitude. These three values correspond to three lines parallel to the base of the signal (zero value). The upper threshold (90%), mesial (50%) and lower threshold (10%) intercept the signal in six points, three on the left side of the peak ($TR_L^{10\%}$, $TR_L^{50\%}$, $TR_L^{90\%}$) and three other two on the right side ($TR_R^{10\%}$, $TR_R^{50\%}$, $TR_R^{90\%}$).

Rise/Fall Time Rise time of the current signal is calculated as the time difference between the two points relative to the lower and upper thresholds on the left side of the peak ($TR_L^{90\%} - TR_L^{10\%}$). Similarly for the fall time, but considering this time the points on the right side of the peak ($TR_R^{10\%} - TR_R^{90\%}$).

Width The width of the discharge has been calculated by measuring the maximum time difference between the intersection between the pulse and the mesian line ($TR_L^{50\%} - TR_R^{50\%}$).

3.4 Energy distribution

As already mentioned in the introdution of this chapter, the work described in this section aims to provide an estimation of the main statistical characteristics of the variety of discharges that are typical of different process parameters settings in micro EDM, and not to accurately qualify every single discharge, for the reasons explained in section 3.1.2.
As can be expected, discharges that are produced with a set of process parameters that is typically used in roughing machining can have an average energy up to three orders of magnitude greater than those occurring during a fine finishing process, as can be seen in table 3.4. Interestingly, also inside each energy index it is possible to define a number of groups of discharges that are characterized by different values of average energy, maximum and minimum voltage and current, width and shapes of waveforms. This is the case when roughing energy indexes are selected because usually in this case the circuit of the generator has more than one capacitor.

The trigger level of the oscilloscope was set at a very low level (table 3.2) in order to acquire all the different pulses, that can be very different in terms of average energy and pulse shape. However, an unwanted effect of the low trigger level setting is that short circuits have also been recorded, in particular for energy indexes 250 and 315. Given that short circuits are not significantly contributing to the material removal process, and that they should be avoided by optimizing the process parameters settings, the information relative to this kind of pulses has been discarded. For the most part of the considered process parameters settings, it was possible to distinguish between discharges and short circuits considering their energy, voltage and current values. However, the results relative to low energy groups inside each energy index could be affected by the presence of outliers, in particular for energy indexes 250 and 315.
Groups of discharges generated with the same set of process parameters are characterized by a bell-shaped distribution and the discharges that are typical of each group are usually characterized by waveforms with different shapes. Mean values of energy and current peak, together with their relative standard deviations, are reported for each group of discharges in table 3.4. Histograms and waveforms relative to energy index 105 are represented

Energy index	Group number	No. of disch.	Energy µJ mean	(std)	Current peak A mean	(std)
015	1	92000	0.43	(0.14)	1.24	(0.10)
105	1	379372	13.03	(1.26)	5.62	(0.21)
206	1	6879	23.74	(2.33)	7.54	(0.11)
206	2	20802	50.26	(3.79)	8.68	(0.25)
206	3	2796	73.61	(4.06)	11.56	(0.16)
250	1	2645	7.51	(1.20)	2.84	(0.26)
250	2	860	32.79	(9.64)	4.85	(1.06)
250	3	1653	83.51	(5.85)	8.41	(0.48)
250	4	5899	127.94	(7.39)	10.95	(0.31)
305	1	19192	23.24	(15.4)	6.70	(0.70)
305	2	29118	161.81	(12.98)	14.01	(0.86)
315	1	5046	46.55	(4.31)	11.25	(0.38)
315	2	1141	88.64	(12.71)	11.49	(0.62)
315	3	133	129.17	(5.60)	12.02	(0.76)
315	4	8726	172.18	(6.73)	13.08	(0.41)
350	1	7189	9.69	(2.69)	4.54	(0.41)
350	2	359	57.88	(18.02)	11.29	(1.86)
350	3	16452	119.02	(15.47)	15.11	(0.52)

Table 3.4: Mean and standard deviation of energy and maximum current for the different process parameters and subgroups of discharges.

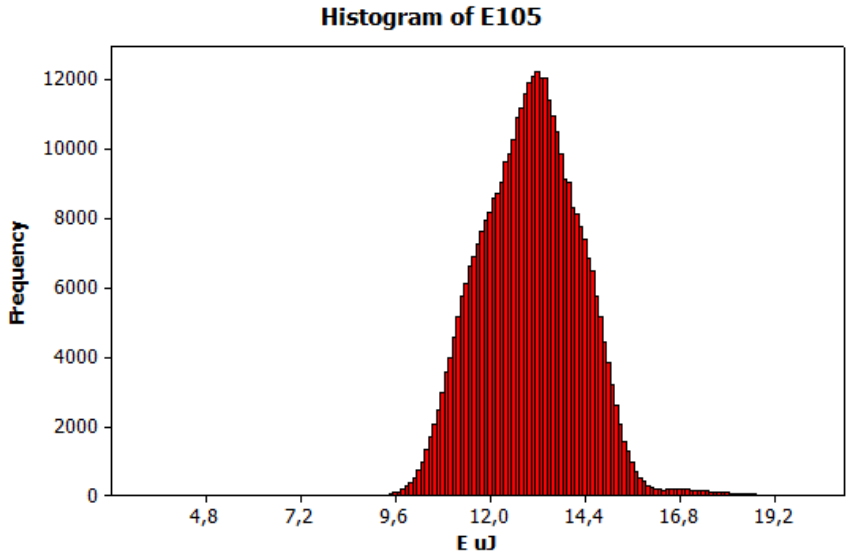

Figure 3.6: Energy distribution of discharge population relative to energy index 105.

in figures 3.6 and 3.7, while those relative to the other energy indexes are reported in Appendix A (9, page 115).

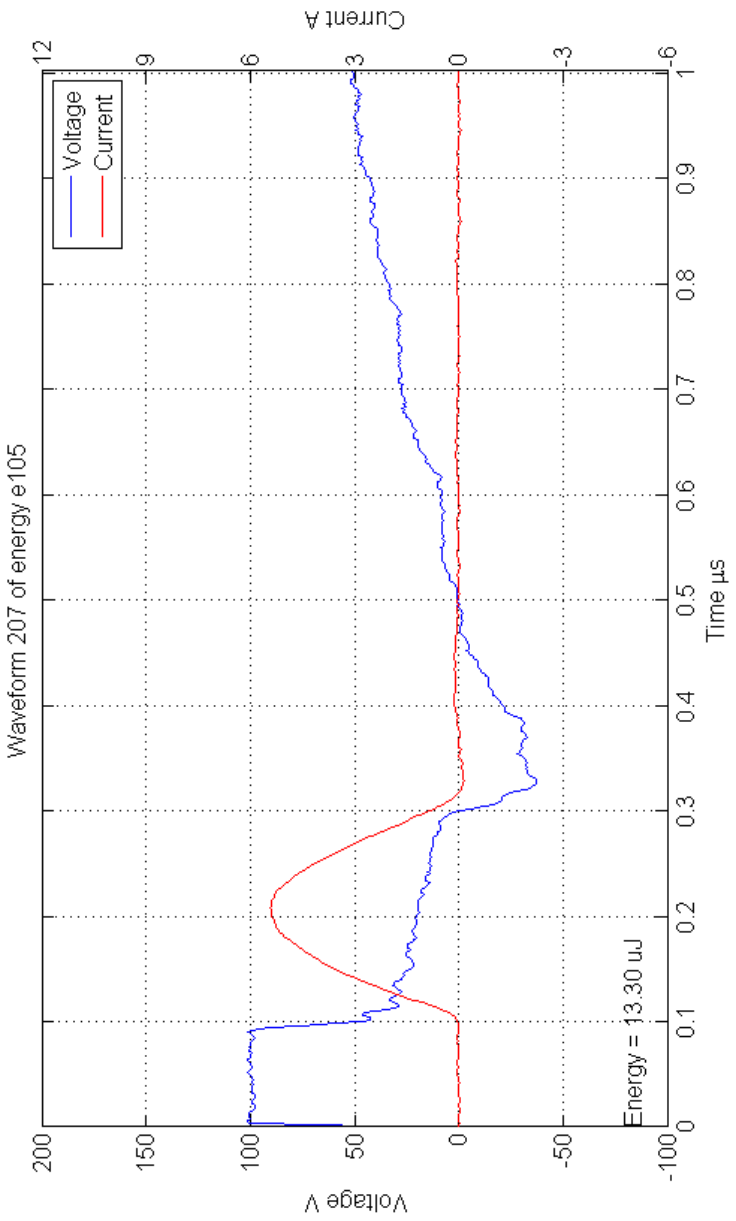

Figure 3.7: Typical voltage and current waveforms relative to energy index 105.

3.5 Mean energy stability

The assumption of the on-line tool wear compensation method based on discharge counting is that mean energy during machining is sufficiently stable and, consequently, the samples that are counted during machining are representative of the same population. It is not strictly necessary that the mean energy is constant during all the machining operation, because it is possible to perform a tool wear and material removal per discharge re-assessment during the operation, with an automatic procedure that will be detailed in the following sections. However, it is relevant to verify the variability of the mean energy of the discharges sampled during the process, in order to estimate the accuracy of the tool wear compensation method and to have a first information about how often it is necessary to perform the TWD and MRD re-assessment procedure.
To this end, the data that was acquired during the experiments has been analysed sample by sample, by evaluating the variations in samples characteristic through all the machining process.
It is also important to verify the consistency of data between different experiments, because unwanted modification of the working conditions and experimental setup could lead to different results, thus affecting the performance of the tool wear compensation method.
The experiment has been repeated three times to test also the stability of the mean values within different repetitions of the same experiment.
The analysis relative to energy 105 is reported here because of its simple waveform, the absence of different groups of discharges, good sample size and number of samples (table 3.3), but similar results can be obtained from the data of other process parameters settings.

3.5.1 Normality test

Considering energy 105 distribution in figure 3.6, it is possible to notice that the energies of the discharges are distributed around the mean value with a bell-shape, which is typical of normal distributions. However, the Anderson-Darling normality test indicates that, at α levels greater than 0.005, there is evidence that the data do not follow a normal distribution, as can be seen in figure 3.8. This result was expected because of the presence of a number of outliers at the extremes, and the test is highly influenced by outliers when the number of samples is high, as in this case.

When the normality test is performed on the means of the 34 samples, instead, the result is different: the test fail to reject the null hypothesis.

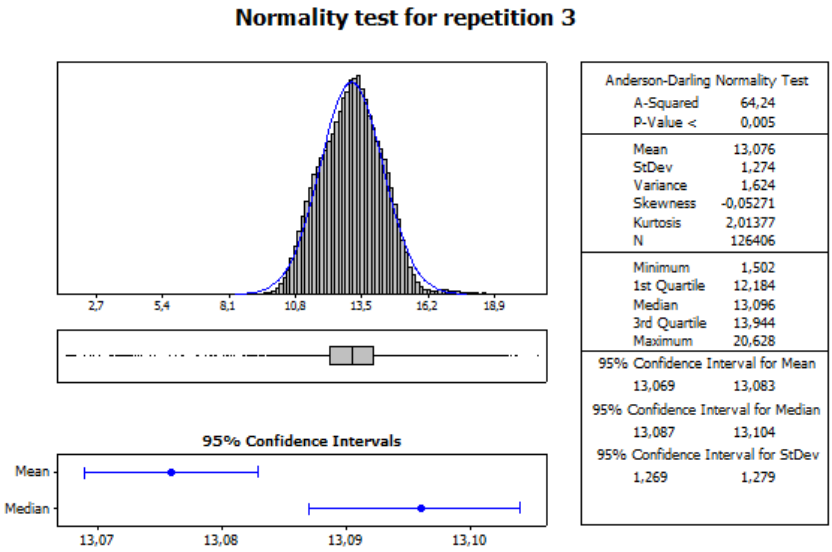

Figure 3.8: Anderson-Darling normality test applied on the raw data of the third repetition of experiment relative to energy index 105.

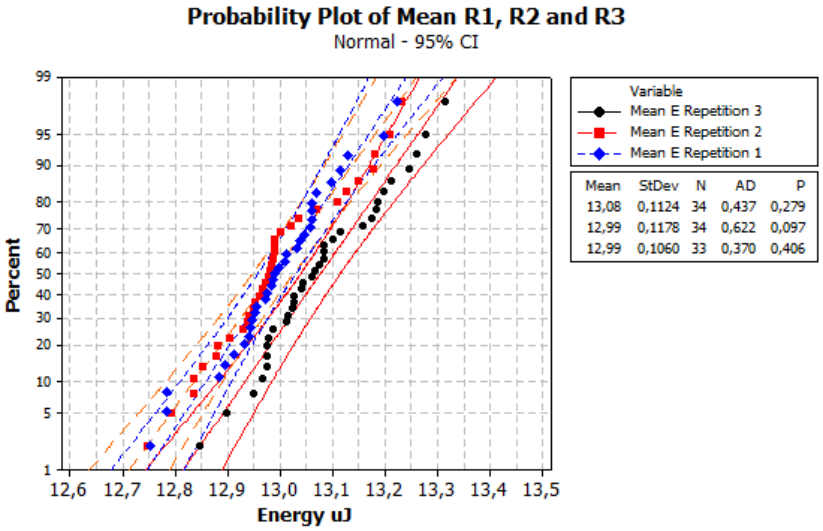

Figure 3.9: Normal probability plot of the 32 samples of energy index 105, 3 repetitions.

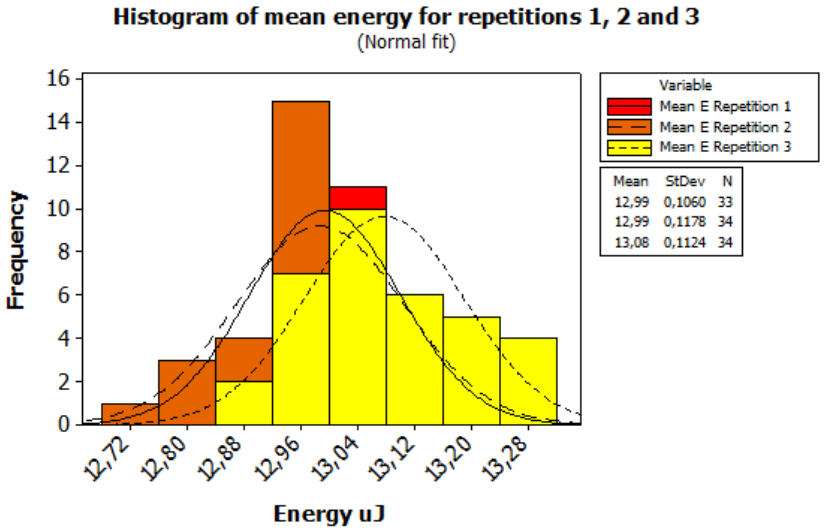

Figure 3.10: Overlapping histograms relative to the mean energy of the samples of three repetitions for energy index 105.

This is confirmed for each of the three repetitions. Results are summarized in the probability plot in figure 3.9. It is then highly probable that a discharge observed at any point of the machining process will fall inside the distribution relative to the data acquired during these three experiments. This result indicates that the experiments were performed correctly, but more information are needed to verify the repeatability of the process in terms of mean discharge energy during the same experiments and between different repetitions of the same experiment.

3.5.2 Stability over repetitions

In the previous paragraph the normality of the distribution of the mean energies of the samples has been verified, hence it is possible to assume with a high confidence that the samples do represent the population of discharges that occurred during the experiments. It is interesting to see if the samples of the three repetitions are representative also of the very same population. Figure 3.10 shows the three distributions with their normal fit on the same chart, and while repetition 1 and 2 are overlapping, the distribution number 3 has a greater mean value, mostly because of its antisymmetric heavy tail on the right side of the chart.

A numeric estimation of the differences between the populations is provided by the mean and standard deviation relative to all the observations for the three repetitions. These results are reported in the last row of table 3.5. The three mean values ranges from 12.99 to 13.08 µJ and the minimum standard deviation is 1.26 µJ. From a practical point of view, the differences can be neglected.
However, in order to have a statistical evaluation of the differences between samples of repetition 2 and 3, a 2-Sample t-test was performed in Minitab. The test assumes that the two set of data belong to two normal distributions and have equal variances. In order to determine if samples means relative to repetition 2 and 3 have a different variability, the 2 Variances procedure was followed. The procedure uses the F-test to test the null hypothesis that the two variances σ are equal (eq. 3.3), against the two-tailed alternative (eq. 3.4).

$$H_0 : \sigma_1^2/s_2^2 = 1 \tag{3.3}$$

$$H_1 : s_1^2/s_2^2 \neq 1 \tag{3.4}$$

The 95% confidence intervals for ratios of the standard deviation (0.741, 1.484) and variance (0.549, 2.202) contains one, then there is insufficient evidence to suggest that the population variance varies by population. Furthermore, the F-test fails to reject the null hypothesis that the standard deviations are equal, because the p-value of 0.786. Thus, it is reasonable to assume equal variances when using a 2-Sample t-test to compute a confidence interval of the difference.
The null hypothesis that the difference between two population means μ is zero (eq. 3.5), against the two-tailed alternative (eq. 3.6), was tested assuming equal variances.

$$H_0 : \mu_1 - \mu_2 = 0 \tag{3.5}$$

$$H_1 : \mu_1 - \mu_2 \neq 0 \tag{3.6}$$

The 95% confidence interval for the difference in population means (-0.146, -0.035) doesn't include zero, thus suggesting that there is difference between the means. The p-value is equal to 0.002 and since it is smaller than 0.05, the correspondent of the α-level, the test rejects the null hypothesis (3.5).
Although the difference between the means of the two populations can be considered negligible in practice, the result of the statistical test is that the means are significantly different. This suggests that either the machining

conditions changed within repetition number 2 and 3 or the experiments could be affected by a systematic error. The source of the systematic error could be identified in one of the factors affecting the signal fidelity discussed in section 3.1.2, or to unpredictable and not yet completely understood phenomena that give a stochastic behaviour to the process, such as an accumulation of debris inside the sparking gap, as well as other external perturbations occurred during the experiments.

3.5.3 Stability over samples

The machining of the cylindrical pocket that was selected as reference feature for the experiments was lasting on average about one hour before reaching the desired depth of about 350 µm, depending on the selected process parameters. The efficiency of the flushing in removing the debris from the sparking gap could decrease when machining at greater depths. It is then important to verify the stability of the discharges mean energy through all the machining time.
To this end, for energy index 105, the pulses occurred during the micro EDM pocketing operation were sampled in groups of 4000 observations periodically every 2 minutes, for a total of 34 samples.
The scatter plot of the mean energies of the samples relative to the three repetition of the experiments in figure 3.11 was generated using data in table 3.5 and gives a first qualitative information about the variation of the mean energy. When the range of the standard deviations of the measures is considered, which is represented in the plot by the vertical error bars, there is no clear evidence of a trend along the machining process. A greater dispersion of the mean values can be noticed in correspondence of the first half and towards the end of the machining operation.

µJ	Repetition 1		Repetition 2		Repetition 3	
Sample	mean	std	mean	std	mean	stdev
1	13.68	0.91	13.18	1.14	13.08	1.09
2	12.99	1.14	13.11	1.14	13.08	1.14
3	13.00	1.21	13.15	1.16	13.04	1.17
4	13.07	1.17	13.23	1.20	13.09	1.18
5	12.98	1.19	13.18	1.19	13.26	1.20
6	12.78	1.24	13.21	1.19	13.25	1.20
7	13.23	1.24	12.98	1.26	13.28	1.23
8	13.20	1.24	12.94	1.24	13.19	1.27
9	13.13	1.29	13.02	1.25	13.32	1.24
10	13.06	1.27	12.94	1.27	13.18	1.29
11	12.91	1.23	13.04	1.30	13.21	1.24
12	12.99	1.32	13.00	1.33	13.18	1.32
13	12.75	1.26	12.88	1.29	13.09	1.27
14	13.10	1.28	12.98	1.26	13.20	1.28
15	12.93	1.27	13.13	1.25	13.16	1.28
16	12.95	1.27	12.97	1.33	13.02	1.32
17	12.98	1.31	12.93	1.27	13.03	1.30
18	12.94	1.25	12.99	1.24	13.06	1.31
19	13.06	1.33	13.07	1.24	13.10	1.39
20	13.05	1.28	12.97	1.29	13.07	1.28
21	12.90	1.30	12.96	1.26	12.98	1.33
22	13.12	1.29	12.98	1.28	12.98	1.27
23	12.94	1.28	12.95	1.26	13.04	1.29
24	12.88	1.30	12.99	1.30	12.98	1.29
25	13.04	1.28	12.99	1.29	12.90	1.31
26	13.06	1.30	12.95	1.25	12.95	1.29
27	13.01	1.29	12.85	1.24	12.85	1.35
28	13.01	1.29	12.99	1.27	12.99	1.29
29	13.03	1.32	12.90	1.25	13.01	1.34
30	12.97	1.29	12.84	1.30	12.98	1.26
31	12.95	1.29	12.88	1.27	13.03	1.29
32	13.06	1.30	12.79	1.30	13.12	1.30
33	12.78	1.29	12.75	1.25	12.97	1.28
34	12.95	1.28	12.83	1.29	13.02	1.28
1÷34	13.02	1.27	12.99	1.26	13.08	1.27

Table 3.5: Mean energy values and relative standard deviation relative to the 34 samples and 3 repetitions, energy index 105. Sample size ranges between 3500 and 4000 observations, with an average of 3720 observations per sample.

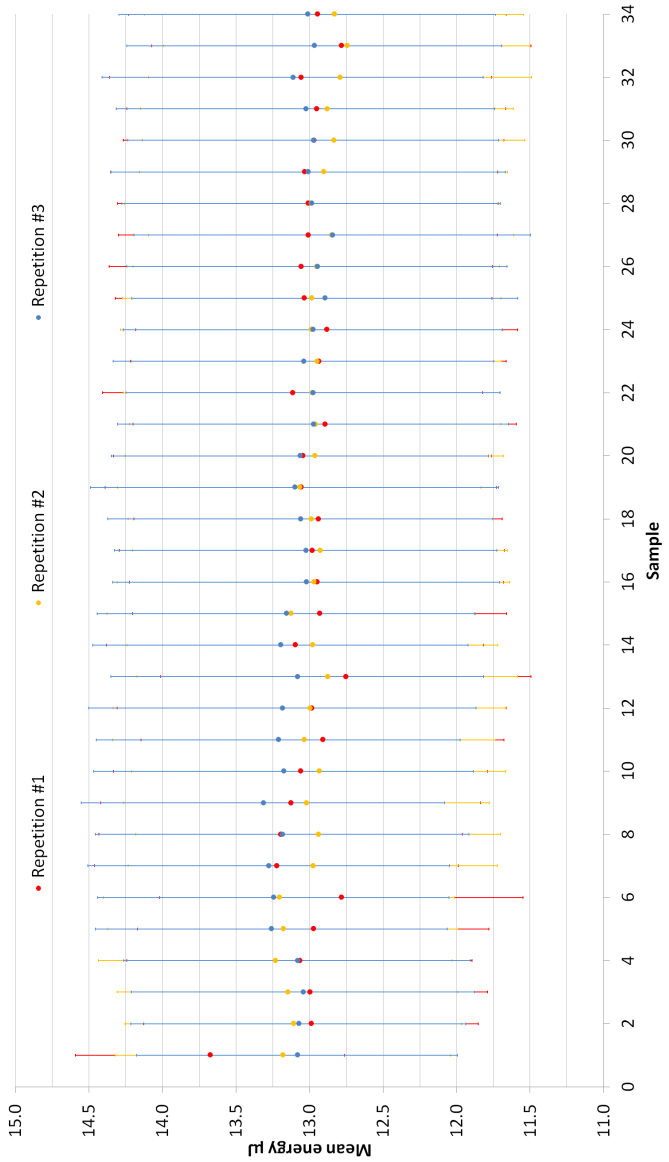

Figure 3.11: Scatter plot of the mean energy relative to the 32 samples and 3 repetitions for energy index E105.

3.6 Trigger levels

Discharges are counted by means of an Agilent 53131A frequency counter, by scanning the signal from the current probe and *totalizing* all the number of trigger events occurring while the gate is open. For frequency measurements the trigger is automatically adjusted to about 50% of the sensed amplitude of the signal, while with the totalize function the trigger level can be set manually.
The selection of the trigger level gives the opportunity to threshold the signal, filtering out undesired noise or random events like short circuits, that are unpredictable and don't concur in material removal and tool wear. As a matter of fact, for the applicability of the tool wear compensation method, to have a good repeatability of the measurement is very important, to some extents it is even more important than to know the exact quota of population that is being effectively counted. This is because the material removal and tool wear per discharge are determined empirically, hence as far as the measurement of the number of discharges can be performed with a good repeatability, also the results of the methods based on MRD and TWD is expected to be consistent. On the other side, the exact percentage of the population that has been counted is a necessary information for the estimation of the quantity of energy involved in the material removal process.
The counter will sense the rising signal of a pulse with the condition that the trigger level is set below the peak value, and sufficiently higher than the noise level. The percentage of the population that has been counted or missed can be estimated by comparing the trigger level to the distribution of peaks in current signal as illustrated in figure 3.12.
It is also important to be aware of the minimum pulse width that the counter is able to detect and the accuracy of the trigger.
The data-sheet of the Agilent 53131A specifies that the minimum width is 10 ns. Although the shortest pulses have a larger width than the minimum requirements, the shape of the pulses has also to be considered. As a matter of fact, the width of the pulses is narrowing going towards the peak, and at the extreme values it could not be sufficient for the minimum requirements of the trigger of the counter.
The accuracy of the Agilent 53131A Universal Counter is defined by the manufacturer with the equation (3.7). For this application, in the worst case the accuracy of the trigger is then equal to ± 50 mV. The uncertainty range is plotted together with the trigger level in figure 3.12 to help in considering the accuracy of the trigger when selecting the trigger level.

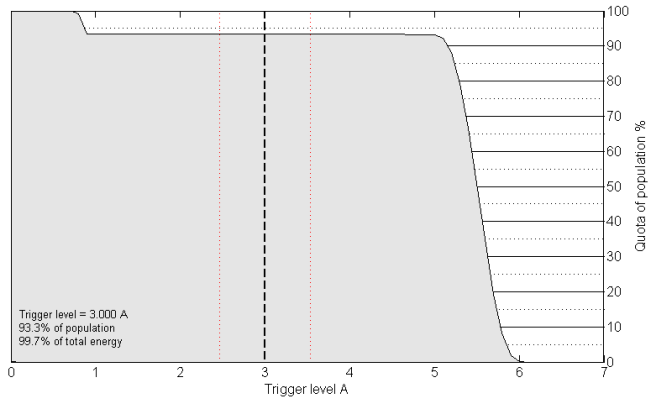

Figure 3.12: Quota of population counted as a function of the selected trigger level. Energy E105.

$$tl_u = \pm(15\text{mV} + 1\%\text{trigger level}) \tag{3.7}$$

Figure 3.12, which is relative to energy index 105, shows that with a trigger level that corresponds to 3 A, 93.3% of the population would be counted and only the 0.3% of the total energy would be discarded. In figure 3.14 are represented the voltage and current waveforms of one typical pulse characterized by a peak current that is below the trigger level, one of the 6.7% of the population that is not considered by the counter. Clearly, the pulses that are discarded in this case are not discharges but short circuits, hence, the result provided by the counter is relative to 100% of the population.

Discharges belonging to energy index 105 have a very well defined bell-shaped distribution of the discharge energies and current peak values. Instead, the selection of the trigger level is more complicated in case of energies that are characterized by a multimodal distribution, as in the case of energy index 350. In this case the presence of two different groups of discharges is evident, figure 3.13, and indeed, the corresponding histogram shows a bimodal distribution (figure 6). To count all the discharges the trigger should be set at a very low level, and the measurement would be unreliable because of the trigger accuracy and the sporadic occurrence of short circuits.

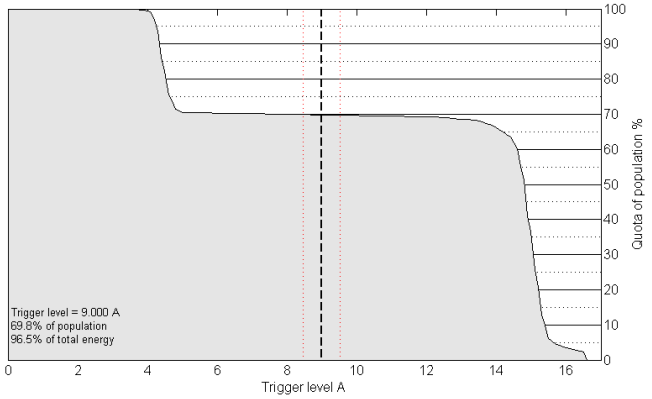

Figure 3.13: Quota of population counted as a function of the selected trigger level. Energy E350.

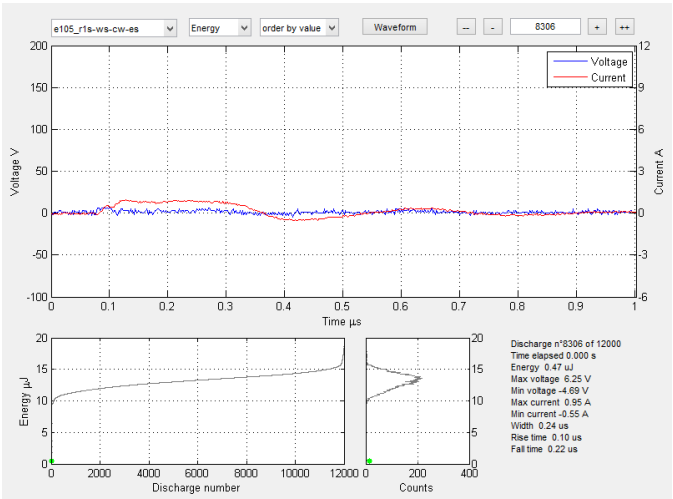

Figure 3.14: Using the graphical user interface to select one of the low energy pulses and to display its waveforms.

Chapter 4

Machine control

The implementation of the on-line tool wear compensation method based on discharge counting, requires the capability to read the number of discharges occurred during the machining process and counted by the frequency counter, calculate the tool wear and then adjust the tool trajectory in real-time. Possibly, this should be performed for each infinitesimal movement along the toolpath. In order to accomplish these tasks directly on the μEDM machine, it would be necessary to have access to the control unit at a very low level. Unfortunately, this is not possible without modifying the firmware of the machine, hence, an external computer was employed to manage the operations and elaborate the commands that were then executed by the μEDM machine (figure 4.1). To exchange information between the CNC machine and the PC it was necessary to develop a custom communication interface and protocol.

4.1 Data transmission

The μEDM machine is provided with different communication interfaces: CAN bus, Ethernet, USB, serial RS232, a number of digital and analogue input and output ports.
The CAN bus is suitable for real time prioritised communications systems but, being used by the machine boards, is restricted to manufacturer personnel for safety reasons and to preserve the reliability of the machine. The other options are not suitable for real time communications. The RS232 serial port of the embedded computer is already used to retrieve data from the laser micrometer. Ethernet and USB ports are also options, but dedcated commands should be implemented in the machine firmware by the

manufacturer in order to grant the access to these ports to a part program during a machining operation.

At the end, the communication between the CNC machine and the computer was established taking advantage of the logical ports. As a matter of fact, the digital Input/Output ports of the machine can be read and set high and low from the part program. With a proper hardware interface the voltage level of the Inputs can be changed and the Outputs read by the external computer. Ten Inputs and ten Outputs are available on the I/O board of the Sarix SX-200 machine. Values and commands can then be associated to a particular combination of status of the logical ports.

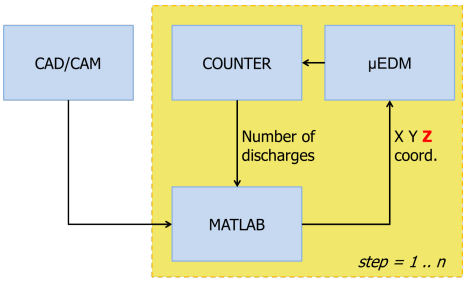

Figure 4.1: Work-flow diagram describing the generation and on-line modification of the toolpath with the proposed setup. The Z coordinate is adjusted on the base of the number of discharges counted, in order to compensate for the shortening of the tool length which is caused by the tool wear.

Using this approach a custom protocol has been developed for bidirectional communication of commands and numerical variables between the part program running on the control unit of the μEDM machine and the Matlab script running on the external PC.

4.2 Communication interface

The Agilent 53131A frequency counter can be programmed remotely through the GPIB interface. An Agilent 82357B GPIB to USB adapter was used to connect the counter to the computer and to retrieve the number of discharges, reset, start and stop the counter remotely from Matlab.
The laptop running Matlab software, had no Input/Output ports, hence, an Arduino Uno connected via USB to the computer were used as digital I/O expansion board. Arduino was controlled by Matlab by using MATLAB Support Package for Arduino (ArduinoIO Package). The logical pins of the compact developer board have a reference voltage of 5 V, while Sarix SX-200 I/O ports are designed to pilot auxiliaries at 24 V, which is a standard in

industrial automation. A circuit board based on 4N35 opto-isolators was developed to convert the digital signals from 0÷5 to 0÷24 V and vice versa.

4.3 Communication protocol

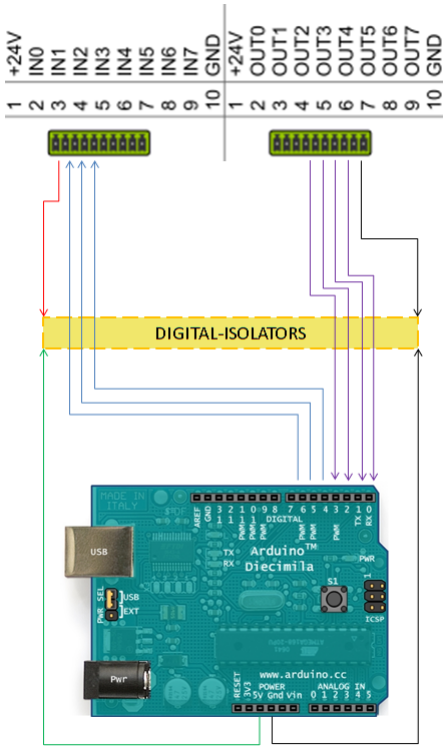

Figure 4.2: Schematics of the hardware interface used to connect the PC running Matlab and the Sarix SX-200 through I/O digital ports.

The software developed for the bidirectional transmission of data is made of four main parts: transmitter, receiver, Matlab script and part program. The software emulates a half duplex serial communication protocol, that are usually managed by dedicated hardware called Universal Asynchronous Receiver/Transmitter (UART). This technique is known as *bitbanging*. In this case, numeric variables are converted from decimal to binary to minimize the number of bits necessary for its representation and then the bit array is transmitted bit after bit, by using a maximum of 6 wires, 3 inputs and 3 outputs.
The transmission procedure is managed on both sides by an high level software running on a personal computer and for this reason the process in not real-time. Indeed, the priority in CPU usage is shared with a number of other processes, instances and services that are running in background and could interrupt the execution of the program. When a lag in either the transmitter or receiver occur, the transmission gets out of sync, and one or more bits are lost. Of course, a missing bit in the sequence can determine a huge difference between the transmitted and received number.
For this reason, two clocks are used to impose the timing of the sequence of

bits. One is used by the sender to apprise when the new bit is ready and the level of the second is changed by the receiver once the bit has been read. With this method the transmission speed is not based on a fixed baud rate but it will adjust on the actual capabilities of the line, sender and receiver. For this reason the average transmission speed will be lower, but an eventual glitch in any of the two sides of the communication interface won't affect the output of the transmission.

4.4 Test of the protocol

The reliability of the communication interface and data transmission protocol was evaluated by performing an extended ping test. The pattern of the test consisted of 1000 random values ranging from -1.9999 to 1.9999. The list of numbers was transmitted from Matlab to Sarix and then values received and submitted were compared.
The test was passed 5 times with a success rate of 100%.

Chapter 5

On-machine measurements

Figure 5.1: Image of a 10 mm steel sphere being measured on the μEDM machine with a 0.2 mm cylindrical tool-probe.

During the μEDM milling process, material is removed by electrical discharges not only from the workpiece but also from the tool electrode, at rates that are strongly dependent on selected set of process parameters, dielectric fluid and electrodes materials. In order to achieve a high accuracy machining, it is fundamental to optimize the process settings and in particular the tool wear compensation strategies, before actual machining. To this end, empirical procedures are preformed on a sacrificial workpiece to evaluate the tool wear and material removal rates per unit of time or energy, or per discharge. The accuracy in assessing the amount of material removed from both tool and workpiece is thus of paramount importance, as tool wear compensation and machining prediction software rely on these information. In micro EDM, on-machine volume measurements enable tool wear strategies and process parameters optimization based on iterative, automatic, self-learning procedures, simplifying the adaptation of the process to industrial environments. On-machine dimensional measurements are commonly performed to inspect and measure both tool and workpiece electrodes with additional instruments such as laser micrometers, touch probes and optical microscopes [42]. However, in commercially available EDM machines it is possible to exploit the hardware that is used for the electrical discharge machining process also to obtain dimensional data. In EDM machines tool and workpiece electrodes are insulated and the electrical potential that is provided by the generator is continuously monitored. This is necessary to keep a constant gap between tool and workpiece during the erosion process, by continuously adjusting their relative position. When a short circuits, or contact between tool and workpiece occurs, a voltage drop is sensed and the machine can take the appropriate countermeasures. Short circuits occur very often during machining, especially if the process has a poor stability, and in this case the sparking gap is automatically restored by the programmed servo feed algorithms. When voltage drops are sensed during rapid movements, the command in execution is interrupted and a collision warning is displayed on the user interface. It is also possible to slowly approach the workpiece and record their relative position in X, Y and Z axes when the voltage drop occurs and the tool tip is in contact with the workpiece surface. As a matter of fact in μEDM on-machine dimensional measurements based on the short-circuits detection system are common practice: it is employed to set the workpiece coordinate system, but also to measure the tool diameter during its fabrication process and to update the tool length at regular intervals during machining operations for tool wear compensation.
The drawback of this method is that the electrical contact can eventually produce a small amount of erosion, which could cause an error in the mea-

surements, but the wear due to few contacts can be neglected [28].
The short-circuit detection system has been adopted for roundness deviation evaluation [43] and the repeatability and reliability of tool length measurements performed with this method has been assessed [44]. However the use of the short-circuit detection system and the tool electrode to perform bidirectional coordinate measurements similarly in a CMM have not been reported and a metrological validation of the method is missing [45].
It is thus important to estimate the accuracy of the μEDM machine in performing volume and dimensional measurements using the short-circuit detection system and the tool electrode as the probe in a CMM.

5.1 Tool wear assessment

Bissacco et al. [44] compared the repeatability of two on-machine measurement methods applied to volumetric and linear tool wear assessment, on the same Sarix SX-200 μEDM machine employed in this work.
The first method exploits the short circuit detection system of the μEDM machine by touching the predefined reference point with the tip of the tool electrode before and after machining a certain number of layers. The difference in z values equals to the linear wear.
The second method uses the laser micrometer to measure the linear wear by interrupting the laser beam with the electrode tip when moving in z direction and the volumetric wear by acquiring the tool tip profile.
In their work, Bissacco et al. drew the following conclusions:

- The mean value of the five repetitive measurements obtained by touching the reference point gives a good estimation of the electrode length and consequently also the linear wear.
- The method based on the laser micrometer does not bring a significant contribution to the accuracy of the linear wear measurement since uncertainties of both measurement methods strongly depend on the machine tool repeatability in Z axis.
- The acquisition of the electrode profiles takes into account also the rounding of the electrode edges, which is not considered in the calculation of the volume based on the linear wear.
- The corner wear on the electrode tip varies even when using the same energy index, hence the wear profile is not stable.

- In the case of smaller electrode diameters, the corner wear becomes more significant. For very small electrode diameters (down to 20 µm) the measurement of the linear wear is not sufficient for effective wear compensation, thus the volume wear has to be considered.

- In order to accurately measure volumetric wear, the best result is obtained by acquisition of the electrode profile. Standard uncertainty and percentage standard uncertainty are significantly smaller when the volumetric wear is calculated based on the electrode profile measurements.

- Standard percentage uncertainty of volumetric wear measurements is higher in the case of smaller linear wear.

Hence, the touch method can be used to estimate the linear and volumetric tool wear when the tool diameter is large relatively to the edge rounding. In this work tool electrodes with diameters ranging from 300 to 200 µm will be used in tests for the assessment of tool wear per discharge and for tool wear compensation method validation. In this case the use of a more expensive laser micrometer does not bring a relevant contribution to the accuracy of the measurements.
Since the touch method has proven to have acceptable repeatability and accuracy, it will be implemented in the procedure to evaluate the linear and volumetric tool wear by means of on-machine measurements.

5.2 Estimation of material removed

The amount of material removed from the workpiece during the machining process is required information for the simulation of the process based on MRD and number of discharges, as well as for the setup of the process when the on-line tool wear compensation method is based on MRD. The performance of on-machine volume measurement has to be evaluated in order to verify the feasibility of the method.

5.3 Experimental setup

On-machine measurements tests as well as machining of reference microfeatures were performed on the Sarix SX-200 μ milling machine. The machine is equipped with a wire dress unit for micro tool fabrication and a Mitutoyo

LSM 500S laser micrometer (resolution and repeatability of 0.01 µm and 0.03 µm respectively) for on-machine micro tool calibration.

Parameter	Value	Unit
Energy	015	index
Width	6	index
Frequency	100	KHz
Current	70	A
Voltage	80	V
Gain	75	index
Gap	65	index

Table 5.1: Set of process parameters used during the experiments.

A low viscosity hydrocarbon oil (HEDMA 111) was used as dielectric medium and rods made of tungsten carbide with a nominal diameter of 300 µm were chosen as tool electrodes.
Werth VIDEO-CHECK-IP 400 multisensor CMM was employed in optical and tactile configurations to calibrate the reference features for comparison with on-machine measurement tests. Sensofar PLμ NEOX confocal microscope with 100x magnification lens (maximum slope of 51 degrees and XY and Z resolution respectively of 0.166 µm and 2 nm) was used for surface characterization. FEI Quanta 400 scanning electron microscope (SEM) was employed for qualitative inspection of surfaces and microfeatures.

5.4 Preliminary experiments

In order to evaluate the accuracy of the measurements that are performed on the μEDM machine a series of preliminary tests were performed to identify the optimal probing speed and tool-probe tip size. Then specific experiments were conducted to estimate typical volume measurements errors and the uncertainty of on-machine dimensional measurements.

5.4.1 Probing speed

The relation between probing speed and probing accuracy was investigated repeating unidirectional measurements with speeds ranging from 0.015 to 1.9 $\mathrm{mm\,min^{-1}}$ along each of the machine linear motion axes (figure 5.2). A step specimen assembled as shown in figure 5.3-B and calibrated with the CMM was used as reference. Results were compared to the reference measure obtained with the CMM. For further experiments a probing speed of about 0.4 $\mathrm{mm\,min^{-1}}$ was selected as a compromise (figure 5.4) between maximum probing speed, minimum error and minimum standard deviation relative to all of the three machine axes.

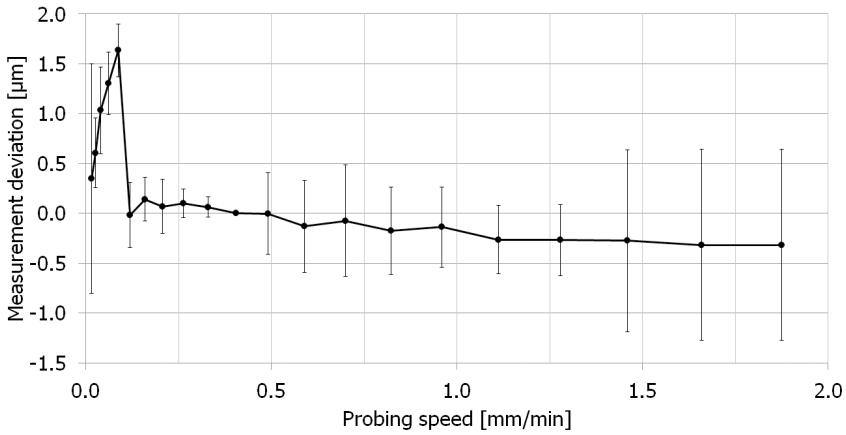

Figure 5.2: Test for the evaluation of the influence of probing speed on unidirectional measurements along the X axis.

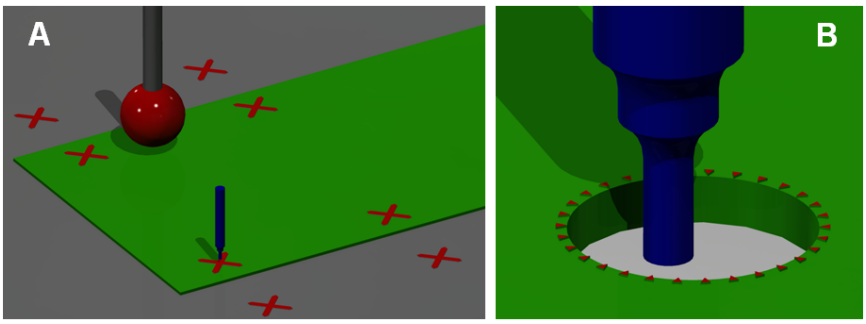

Figure 5.3: On-machine probing of step height (A) and through-hole diameter (B).

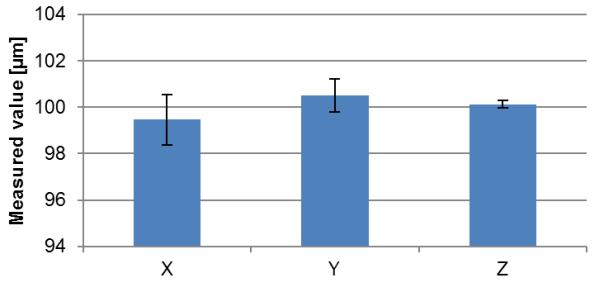

Figure 5.4: Average values with range error bars obtained measuring 10 times the length of a calibrated 0.1 mm gauge block, with a probing speed of about 0.4 mm min^{-1} along each of the machine axes.

5.4.2 Probe diameter

The tool-probes that were fabricated at the wire dress unit to be used for on-machine measurements had a cylindrical shape and were characterized with the laser micrometer.

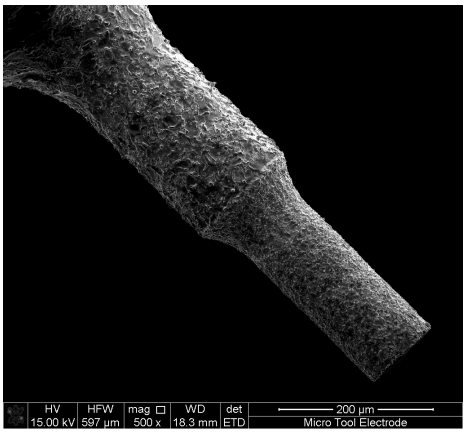

Figure 5.5: SEM image of a typical tool-probe fabricated at the wire dress unit. The tip has a diameter of 100 µm and is 250 µm long.

The tool-probe used for the evaluation of dimensional measurement uncertainty was scanned with the laser micrometer before and after the experiments. The diameter of the tool tip was measured on 40 levels along its axis at every 5 µm starting from the tip and at 0, 45 and 90 degrees of spindle axis positions. After the tests the tool-probe was characterized also with an optical CMM and qualitatively inspected with SEM (figure 5.5). The profiles of the tool-probe have been reconstructed from data acquired with laser micrometer and optical CMM and then compared section by section as reported in table 5.2.

To determine the optimal tool-probe diameter a through hole with a diameter of about 500 µm was used as reference(figure 5.9). The diameter of the hole was measured with the CMM and then on the Sarix SX-200 using 3 tool-probe tips with the same length of about 250 µm and different diameters, namely 50, 100 and 200 µm. Experimental results showed no differences that could be imputable to tool-probe diameter, as a consequence the tool-probes required for further experiments were fabricated with a diameter of about 100 µm.

5.5 Experimental results

5.5.1 Pocket characterization

Surface roughness, taper angle and corners rounding of the features machined by μEDM were appreciable at the microscope (figure 5.7). However,

µm	Average	Std dev	Min	Max	Range
Laser	106.5	0.6	105.8	107.9	2.1
CMM	106.0	0.7	104.9	107.4	2.5

Table 5.2: Comparison between the tool-probe diameter measurements obtained with a laser micrometer and the optical CMM.

on-machine volume measurements were simplified to the evaluation of the volume of an ideal cylindrical pocket. Thus, measures were performed by measuring the circumference and the depth of the machined features. It is then important to estimate the relative error introduced by these characteristics in the measurement of the volume of material removed.
The typical surface produced by means of μEDM finishing operations is characterized by a distinctive isotropic pattern made of craters. While waviness can be considered negligible, Ra depends on the selected process parameters but is hardly lower than 0.1 µm. The rounding of the edges is a consequence of tool wear and sparking gap. The draft angle of holes walls is caused by secondary discharges induced by the debris that are being flushed out of the working area.
A blind hole having a diameter of about 500 µm and a depth of 435 µm was machined in milling configuration driving the 300 µm tool electrode through circular interpolations, on a sacrificial workpiece made of Stavax ESR, a modified AISI 420 mould steel, with a set of process parameters typical for finishing operations and an incremental depth of 0.5 µm. The cylindrical pocket was then cross sectioned relative to the centre axis in order to characterize all the surfaces and all possible form errors. The surfaces on both walls and floor of the pockets were characterized with a confocal microscope and the corner rounding radius and walls draft angle were measured with an optical CMM.
SEM images (figure 5.8-B) and confocal measurements of the cross sectioned pocket show that floor and wall surfaces have comparable surface roughness. As a consequence, when the cylindrical tool-probe is used to measure the diameter and depth of the cavity it touches craters peaks instead of the average profile of surfaces (figure 5.7), producing a systematic under-estimation of the quantity of material removed during the erosion of the pocket. The volume that is under-estimated per unit of surface was evaluated examining portions of floor and wall surfaces with the confocal microscope and it was evaluated that up to 0.7% of the pocket volume was not considered because

of surface roughness. The corners rounding radius on the floor of the pocket was measured with the optical CMM to be about 45 µm and the related over-estimation of the pocket volume was evaluated to be within 1% for a blind hole with a diameter of 500 µm and a depth of 400 µm.
In figure 5.8-A it is possible to appreciate the angle of inclination of the walls of the pocket, that was measured with the optical CMM to be about 0.7 degrees. The presence of the draft angle introduces an error that depends not only on the extent of the walls slope but also on the depth at which the diameter of the pocket is measured.

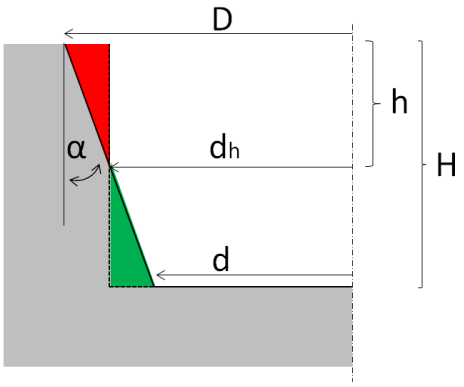

Figure 5.6: Dimensional characteristics of the machined blind holes.

As a matter of fact the draft angle leads to an over-estimation of the volume removed when the hole diameter is measured close to the top surface and at the opposite it involves an under-estimation when the measurement is carried out close to the floor of the cavity (figure 5.7). In the worst case and for a blind hole with a diameter of 500 µm and a depth of 400 µm, the error can be as high as 3% of the pocket volume. However, the exact depth h at which the diameter should be measured in order to nullify the measurement error can be calculated by imposing the equivalence between the real volume of the truncated cone and the volume of the measured imaginary cylinder. The result is represented by equation 5.1, where D is the top diameter, d is the bottom diameter and α is the taper angle as in figure 5.6.

$$h = \frac{D - \sqrt{\frac{1}{3} \cdot (D^2 + D \cdot d + d^2)}}{2 \cdot \tan \alpha} \tag{5.1}$$

Assuming that the characteristics of surface finish and corners rounding are independent of hole dimensions, the relative errors they induce on volume measurements can be combined together and studied in relation to depth and diameter of the feature (figure 5.10).

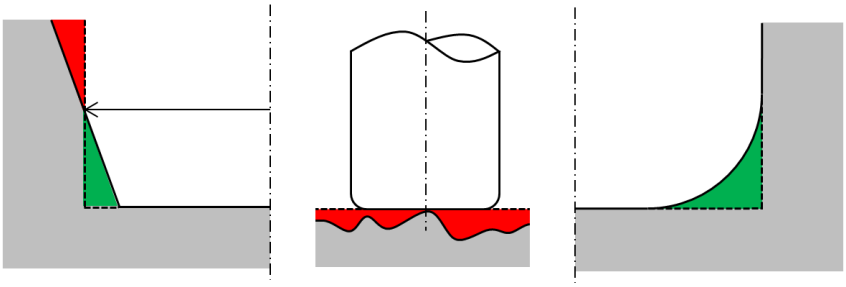

Figure 5.7: Representation of the principal causes of error in measuring the volume of a blind hole produced by EDM. Draft angle, surface roughness and corner rounding.

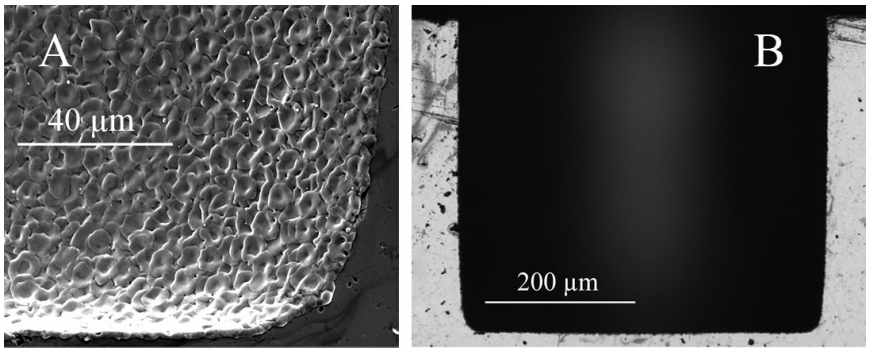

Figure 5.8: SEM image (A) and micrograph (B) of the cross section of a blind hole characterized by a diameter of about 515 µm and a depth of about 435 µm. Corners rounding have a radius of about 45 µm and draft angle is less than 1 degree.

5.5.2 Dimensional measurements

The volume of material removed during the machining of the cylindrical pocket, the selected reference feature in this work, can be estimated by measuring the diameter and depth separately. It is thus important to estimate the uncertainty in dimensional measurements performed on the μEDM in similar conditions, in order to evaluate the applicability of the short-circuit detection method.

Cylindrical probe

The use of a cylindrical tool electrode as the probe in a CMM enables on-machine dimensional measurement of microfeatures and in particular of the diameter and depth of the cylindrical pocket used as reference for the volume of material removed evaluation.
A through-hole and a step specimen as in figure 5.3 were used as references to compare results of measurements carried out on the μEDM machine with a cylindrical tool having a diameter of 0.1 mm and a CMM.
The step specimen was obtained assembling a calibrated steel gauge block having a nominal length of 0.100 mm on a larger flat surface as illustrated in figure 5.3-B; the assembly was calibrated with Werth CMM using a tactile probe. The through hole with a diameter of about 500 µm was machined by μEDM on the gauge block with finishing process parameters and an axial depth of cut of 0.5 µm.
The uncertainty of dimensional measurements performed by the μEDM machine was determined by using the experimental method given in ISO 15530-3 [46]. To this end, the diameter of the through-hole was measured on the μEDM machine acquiring 30 discrete points equally spaced along the circumference as in figure 5.3-A, while the height of the step specimen was measured as in figure 5.3-B. Measurements were repeated 20 times, unclamping and repositioning the specimen before each repetition as prescribed by ISO 15530-3. Reference calibrations of the diameter and depth were performed using the Werth multisensor CMM.
The experiments performed on the step specimen showed that the expanded uncertainty (determined with a coverage factor k = 2 for an approximated confidence level of 95%) for depth measurements (unidirectional measurements of the step height along the Z axis of the μEDM machine) is equal to 1.3 µm. These experiments showed good repeatability: the standard deviation of the 20 repetitions is 0.26 µm.

The experiments performed on the through-hole showed that the diameter measurements (multidirectional measurements of the hole on the X-Y plane of the μEDM machine) are subject to a systematic error quantified in 3.1 µm. After correcting this systematic error, the expanded uncertainty of diameter measurements was 1.9 µm. The standard deviation of the 20 measurement repetitions was 0.5 µm. These results show that the step height measurements are performed better (with lower uncertainty and repeatability) than diameter measurements; this was definitely expected also because step height measurements are unidirectional, while diameter measurements are multi-directional.

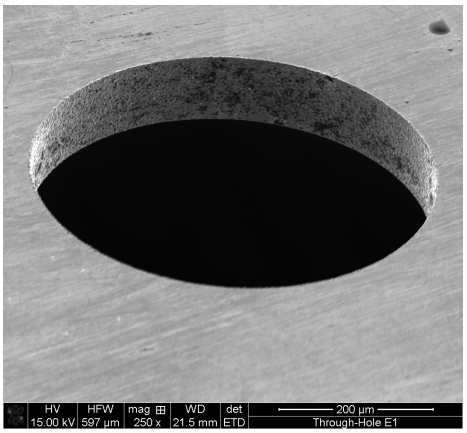

Figure 5.9: Image of the 500 µm through hole drilled by μEDM on the 0.1 µm thin steel plate and used as specimen for the evaluation of on-machine measurements uncertainty.

Propagation of uncertainty from dimensional measurements to volume measurements has been evaluated for the volume calculation of a blind hole, assuming that diameter and depth are uncorrelated variables. Results show that the relative volume measurement uncertainty is lower than 3% for holes larger than 400 µm in diameter and deeper than 100 µm.

Spherical probe

The systematic error observed in section 5.5.2 is most likely related to the surface roughness of both probe and specimens tested in previous experiments. Indeed, it is very difficult to achieve a complete and satisfactory geometrical characterization of the cylindrical probe as well as the specimens using the laser micrometre or the CMM, because of their poor surface finish, which is distinguished by the typical μEDM craters (figure 5.5 and 5.9).

A number of experiments were performed using as probe a calibrated sphere made of steel and with a diameter of 2 mm. In order to hold the sphere with the spindle of the μEDM machine, it was necessary to provide it

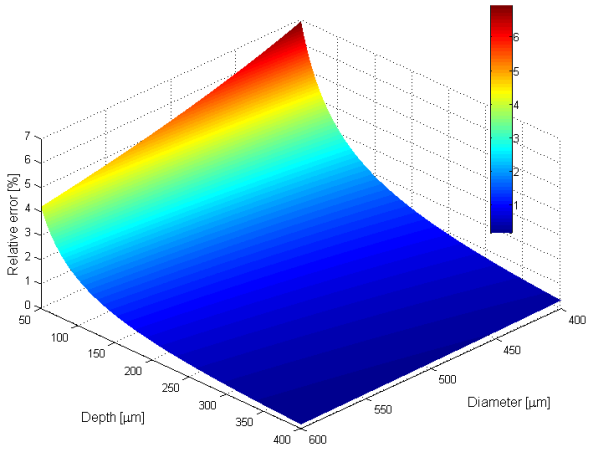

Figure 5.10: Graphical representation of the relative error affecting volume measurements of a blind hole, as a consequence of surface roughness and corners rounding, relatively to depth and diameter of the feature.

with a 0.3 mm stem. To this end, a blind hole was machined on the sphere by electrical discharge drilling and then a portion of the 0.3 mm tungsten carbide tool-electrode was inserted on the hole and soldered.

Figure 5.11: Image of the 2 mm spherical probe clamped on the Sarix SX-200 spindle, while approaching the 10 mm reference sphere.

The assembled spherical probe, held in position by the spindle of the Sarix-SX 200 can be seen in figure 5.11. The diameter measurements were performed on the upper half of the sphere corresponding to different X-Y planes.
According to ISO 10360-5:2010, the probing error of size P_{STU} is equal to 1.6 µm and the probing error of form P_{FTU} is equal to 1.8 µm. The multi-directional measurements of the sphere diameter, performed parallel to X and Y axes and at different Z levels, have an uncertainty U_B equal to 2 µm.
These results suggest that the ex-

panded uncertainty of 1.9 µm evaluated in section 5.5.2 and relative to the measurement of the through hole with a cylindrical tool-probe can be considered as a valid indication about the performance of the measurement method. However, the problem of surface roughness of both tool and specimen, as well as other possible influencing factors such as the presence of dielectric fluid and debris require further investigations.

5.6 Influence of dielectric fluid and debris

On-machine measurements are necessary to calibrate the on-line tool wear compensation method for the selected set of process parameters, electrodes materials and dielectric fluid.

The automated procedure consist in three phases: the machining of a cylindrical pocket, the measurement of tool wear and then the evaluation of the volume of material removed. After the machining, the cylindrical pocket is inevitably contaminated with dielectric fluid and debris. Although the blind hole can be washed with a flush of clean dielectric fluid and then dried with compressed air, which are provided on the workpiece through dedicated nozzles, it is important to determine the influence of the dielectric fluid and debris on measurements.

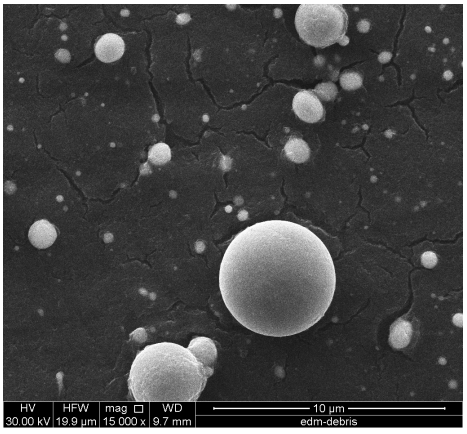

Figure 5.12: SEM image of debris produced during a μEDM process.

5.6.1 Dielectric Fluid

In order to evaluate the influence of dielectric fluid over the diameter measurements, a number of experiments were performed repeating the same measurement procedure in three different conditions: perfectly dry specimen, presence of a thin film of dielectric on its surface, specimen completely submerged into the dielectric fluid.
For the experiments a cylindrical probe with a diameter of about 0.2 mm was used to measure the diameter of the 10 mm steel sphere, as illustrated in figure 5.1. The diameter measurements were performed on different planes parallel to X and Y axes. The distance between the top of the sphere and

Z level	Dry		Wet	Submerged	
mm	average	σ		average	σ
-0.5	4.362	0.0012	4.359	4.361	0.0009
-1.5	7.135	0.0016	7.133	7.134	0.0015
-2.5	8.660	0.0004	8.658	8.658	0.0007
-3.5	9.537	0.0006	9.536	9.536	0.0005

Table 5.3: Evaluation of the influence of the dielectric fluid on the measurement of the diameter of the 10 mm sphere. Values are reported in mm.

the plane of the measurement is reported in the first column of table 5.3. The experiment was repeated 3 times for dry and submerged conditions, and one time for wet conditions.
As reported in table 5.3, the differences between average values of measurements performed in dry, wet and submerged conditions are within the variability of repetitions, which is represented by the standard deviation (σ). There is no evidence that the presence of dielectric between tool-probe and specimen surface was affecting the measurements.

5.6.2 Debris

The features measured on Sarix SX-200 are exposed to contamination of small particles, that are produced during the machining processes.

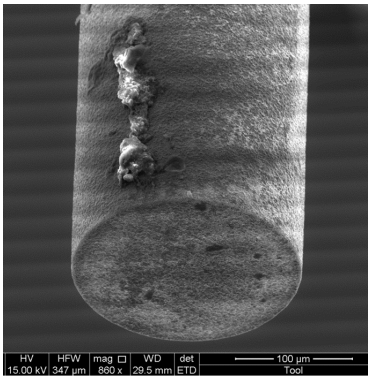

Figure 5.13: SEM image of the 0.2 mm cylindrical tool-probe after over 200 repeated measurements.

Although the surfaces are washed by the flush of dielectric fluid and compressed air, some debris can be trapped in the cavities of the workpiece and get in touch with the tool-probe electrode during the measurements.
The size of debris particles produced by μEDM have a size ranging from few nanometers to few microns (figure 5.12), hence, they can sensibly affect the measurements.
When surfaces are not accurately cleaned, the particles that are left on the surface can be collected on the tool-probe surface, modifying the shape of the tool-probe, as in figure 5.13, and invalidating the results.

Chapter 6

TWD and MRD assessment

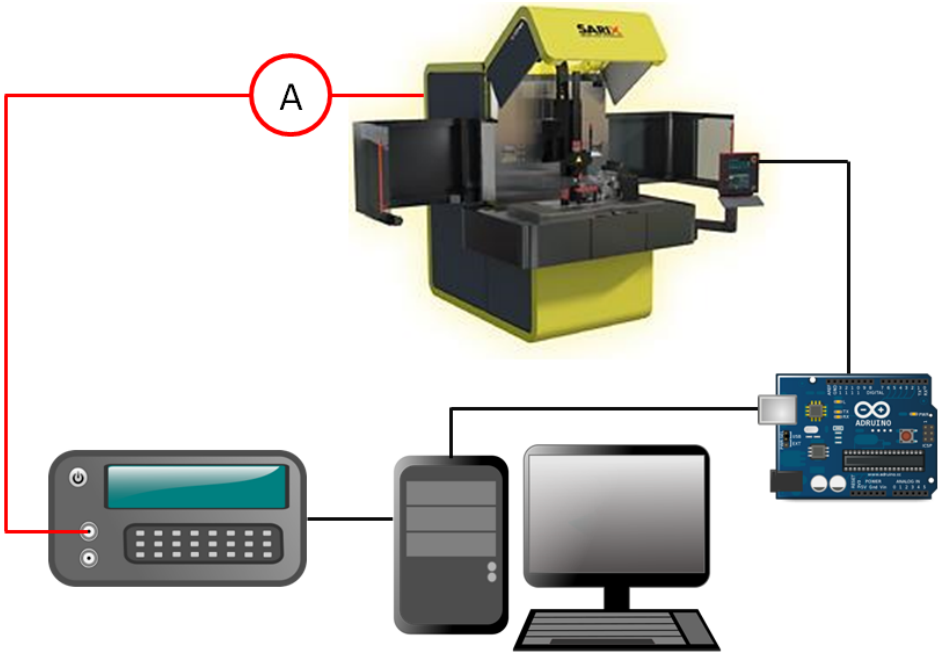

Figure 6.1: Setup used for the evaluation of MRD and TWD. Agilent 53131A frequency counter is used to count discharges and the communication between Matlab and the μEDM machine is established via a custom serial protocol.

Tool Wear per Discharge (TWD) and Material Removal per Discharge (MRD) are required for the on-line tool wear compensation method based

on discharge counting. The evaluation of TWD and MRD is performed by counting the discharges with a frequency counter (section 3.6) and measuring the tool wear and the volume of material removed from the workpiece. The method to perform on-machine measurements by exploiting the short circuit detection system of the μEDM machine has been described and tested in chapter 5. The uncertainty of multi-directional dimensional measurements performed with this method has been evaluated to be of 2 µm. The relative error affecting the measurements of the volume of material removed during the machining of a cylindrical pocket has been evaluated to be less than 3-5%, depending on the dimensions of the reference feature (figure 5.10).
MRD and TWD are evaluated before actual machining, accordingly to the specific combination of electrodes materials, dielectric fluid and process parameters. The accuracy of the tool wear compensation method based on MRD and TWD depends on the variability during the machining operation of these two parameters. As reported by Bleys [47], the on-line tool wear compensation method based on TWD has the drawback that an initial error on the estimation of the TWD produces a continuously increasing machining error.
It is therefore important to verify the consistency of the TWD and MRD during machining. A number of experiments were carried out in order to evaluate TWD and MRD for a wide range of process parameters settings [33,48]. The following paragraphs include the description of the procedure that has been developed to evaluate automatically the TWD and MRD and the results relative to one set of process parameters (energy index 105, tables 3.1 and 3.4).

6.1 Setup of the experiments

The experiments were conducted with the setup illustrated in figure 6.1. A cylindrical pocket with a diameter of 500 µm, the reference feature already used for the experiments described in chapters 3 and 5, was machined by μEDM in milling configuration as previously described, in section 3.1.1.
Discharge counting was performed on the current signal by means of a current probe developed in house and a frequency counter, Agilent 53131A which offers 10 digits per second of frequency/period resolution, a bandwidth of 225 MHz and a time interval resolution of 500 ps.
The volume of material removed during the experiments from both electrodes, was evaluated by means of on-machine measurements and following

the procedure described in chapter 5.
Tungsten carbides rods, with a nominal diameter of 300 mm, were used as tool electrodes, while the workpiece material was a martensitic stainless steel (Uddeholm Stavax ESR). An hydrocarbon oil was used as dielectric fluid (HEDMA 111).

6.1.1 Procedure

The aim of these experiments was to evaluate the value and to verify the consistency of TWD and MRD values during a machining operation, for a given combination of tool and workpiece electrodes, dielectric fluid and set of process parameters. For the implementation of the on-line tool wear compensation method based on TWD and MRD in an industrial environment, standard routines must be developed for the on-machine experimental determination of TWD and MRD. Automatic procedures have been developed by preparation of a parametric part program customizable by the user through the machine console.
In the experiments described here, the program was used for the generation of cylindrical cavities by removing material layer by layer in milling mode, with a layer thickness of 0.9 µm. The cavities were 500 µm in diameter and were generated by means of circular interpolations in 6 incremental steps with an actual depth of approximately 100 µm per step (total more than 500 µm), with discharge counting and recording of the number of discharges for each step. At the end of each step, the diameter and the depth of the cavity were measured on the machine using the electrode as a touch probe in a Coordinate Measuring Machine. The diameter measurements were performed at about half of the total depth of the step, in order to take into account the taper angle of the machined hole in the estimation of MRD as suggested by the geometrical analysis of te pocket, that was carried out in section 5.5.1. The diameter measurement procedure consisted in probing 8 points on the pocket circumference, which corresponds to 4 diameters. For improved measurement reliability, each point was probed five times. The depth of the cavity was measured by probing the centre of its bottom and a reference point on the surface close to the pocket at the centre with the electrode. The probing was repeated five times. The linear tool wear was calculated as the difference on tool length measurements performed before and after each step of the pocketing operation. The tool length was obtained as the average value of five measurements, performed by touching a reference point on the workpiece surface and recording the Z coordinate position

relative to the machine axes.
The diameter of the tool electrode can be measured beforehand, as in this case, with a length measuring instrument, or during the automatic procedure, by means of the laser scan micrometer of the wire dress unit.
The test was repeated four times.

6.1.2 Tool electrode diameter

All the phases of the procedure for the evaluation of MRD and TWD was performed with tungsten carbide tools having a nominal diameter of 300 µm (tolerance declared by manufacturer of +1 and -4 µm).
The material removal per discharge was measured on the machine with the procedure described in 5.2. The tool tip was used as a touch probe in a coordinate measuring machine and the volumetric tool wear per discharge was measured on the basis of linear tool wear measurements. For this reason, in order to have a more accurate estimation of MRD and TWD it was necessary to measure the effective diameter of the tool electrode.
The tool diameter was measured with a Tesatronic TT 20 electronic length measuring instrument and a GT22 vacuum axial probe by Tesa, mounted on a measuring stand. The measurement were repeated 50 times randomly along the first 20 mm from the tool tip, repositioning the tool electrode before each measure. As a result the mean value of the tool electrode diameter was estimated to be 296 µm, with a standard deviation of ±1 µm.

6.2 Analysis of TWD and MRD variability

The standard routine for TWD and MRD evaluation was tested with energy index 105, which corresponds to an average discharge energy of 13 µJ (table 3.4). The results of the tests are reported in table 6.1. The results relative to the first step, corresponding to the first 90 µm in depth, were not reported in the table and figures because they are affected by unstable machining which is typical for the very first layers of the toolpath.

6.2.1 TWD

The average values and standard deviations of the four repetitions are shown in figure 6.2. The data relative to approximately the first 90 µm of depth have been discarder because they are influenced by the machining instability of the beginning of the machining process. The average TWD value stabilizes

Rep. 1	depth	0.1703	0.2584	0.3461	0.4330	0.5183
	TWD	3.00	2.95	2.96	2.98	2.97
	MRD	12.87	12.74	12.60	12.48	12.31
Rep. 2	depth	0.1823	0.2732	0.3630	0.4516	0.5381
	TWD	2.75	2.75	2.83	2.85	2.93
	MRD	12.58	12.85	12.78	12.60	12.50
Rep. 3	depth	0.1784	0.2634	0.3508	0.4388	0.5262
	TWD	3.08	3.07	2.98	2.97	2.96
	MRD	12.63	12.31	12.62	12.66	12.53
Rep. 4	depth	0.1721	0.2592	0.3475	0.4347	0.5215
	TWD	3.03	3.00	2.98	2.96	2.93
	MRD	12.97	12.70	12.82	12.61	12.55
Avg.	depth	0.1758	0.2635	0.3519	0.4395	0.5260
	TWD	2.97	2.94	2.93	2.94	2.95
	MRD	12.76	12.65	12.70	12.59	12.47
St. Dev.	depth	0.0056	0.0068	0.0077	0.0084	0.0087
	TWD	0.15	0.14	0.07	0.06	0.02
	MRD	0.19	0.24	0.11	0.08	0.11

Table 6.1: Average volumes (μm^3) of material removed from the workpiece (MRD) and tool (TWD) electrode per discharge. Values are reported for the last five steps in depth (mm) as average and standard deviation of the four repetitions.

at a value of 2.95 µm^3 along the pocketing operation, and values vary in a range that is approximately 1% of the average TWD. This result is coherent with results reported in [33, 49].
The absence of a trend makes the TWD suitable for the implementation of the tool wear compensation based on discharge counting.

6.2.2 MRD

The results of the experimental tests for MRD determination are shown in figure 6.3. MRD is not constant during machining, with a decreasing trend with the progress of the machining operation. This result is in accordance with results reported in [32] for drilling, where a correction factor was introduced to account for the decreasing material removal efficiency. However in drilling EDM the flushing efficiency decreases strongly with increasing depth, affecting the observed MRD. At higher depths, where MRD reaches stabilization, the variation between repeated MRD measurements is approximately 2% for the considered energy level. While the observed scatter of the MRD measurements can be regarded as acceptable, the decreasing trend observed at the lower depths makes the implementation of tool wear compensation based on MRD difficult. The reasons for such a trend are probably related to the efficacy of the flush of dielectric fluid in removing the debris particles from the sparking gap, but are not completely understood.
Some considerations can be deduced from the analysis of the on-machine measurement procedure. The cavity step depth is measured in the centre of the cavity while a rounding of the bottom occurs at the periphery. Consequently the volume for the first step is over estimated, leading to a larger apparent MRD. Such overestimation occurs only for the first step, while for the following steps it is compensated by the excess material remaining as a consequence of the rounding effect in the previous step. The rounding radius is larger for higher average discharge energies, thus the absolute error on the MRD measured on the first layer is larger at higher energies. However the relative error on the measured volumes, and thereby on the calculated MRD, decreases with the increase of the total removed volume per step.
For the cavity diameter values and actual step depth used in the experiments presented above, the calculated relative error contribution on the step volume, and therefore on the MRD value, due to this effect is approximately 0.33%. In addition to the above error, the rounding of the tool electrode induces an overestimation of the cavity diameter for the first step.
With the diameter values used in these experiments, the maximum corresponding error is approximately 4% on the measured volume for the first

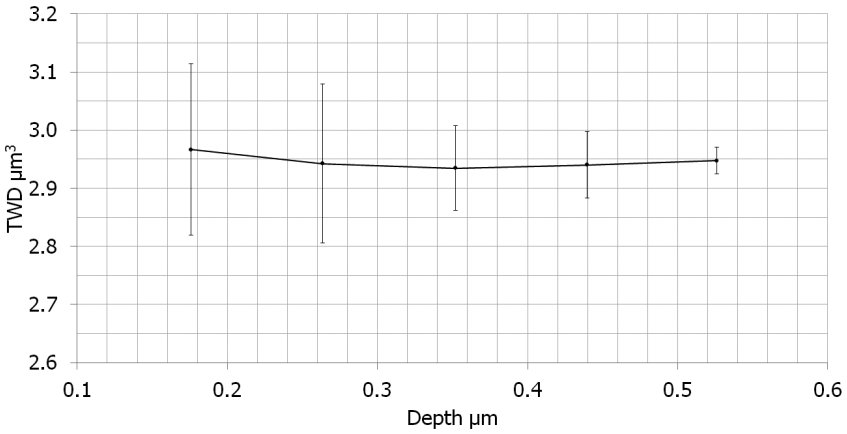

Figure 6.2: Variability of TWD along the pocketing operation. Average values of 4 repetitions, energy 105.

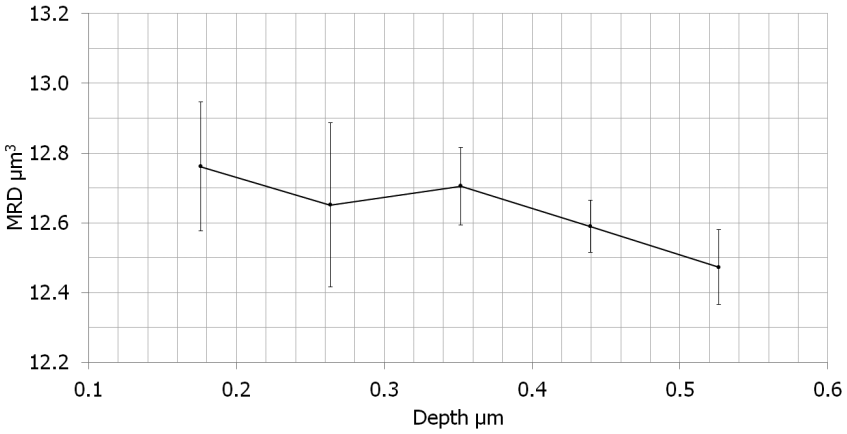

Figure 6.3: Variability of MRD along the pocketing operation. Average values of 4 repetitions, energy 105.

step. The discussed error contributions are not sufficient to justify quantitatively the decreasing trend of the MRD observed for the process settings with the highest average discharge energy as shown in figure 2, which is therefore expected to be a characteristic of the process, most probably due to the secondary discharges that occur on the cylindrical surface of the electrode while machining at greater depths [25].

6.3 In-process experimental re-estimation

It appears that by using the proposed approach, overall TWD and MRD estimation errors in the order of 3% can be expected. However this problem can be overcome by performing periodical measurements of the tool length and pocket depth during machining (while counting the discharges), thereby allowing an in-process experimental re-estimation of the TWD and MRD which is then updated for the subsequent machining. Using this approach, the diagrams in figures 6.2 and 6.3 are used only for the initial estimation of the TWD which is in turn used until the first control is performed. It is important to notice that for fine TWD and MRD assessment the on-machine measurement uncertainty becomes critical. Therefore sufficient wear length should be allowed between subsequent controls in order to reduce the relative measurement error [50].

6.4 TWD and MRD at different machine parameters settings

The procedure described in section 6.1.1 was applied to evaluate the TWD and MRD relative to the same process parameters settings that were examined in section 3.1 to characterize their discharge energy distributions.
These tests were carried out by machining the same reference feature and with the procedure followed in the previous paragraphs, but down to a depth of about 200 µm. The experiments were repeated five times. Results of the average values of the measured TWD and MRD for the five repetitions are reported in figure 6.4.
In general, higher average discharge energies yield higher TWD and MRD.

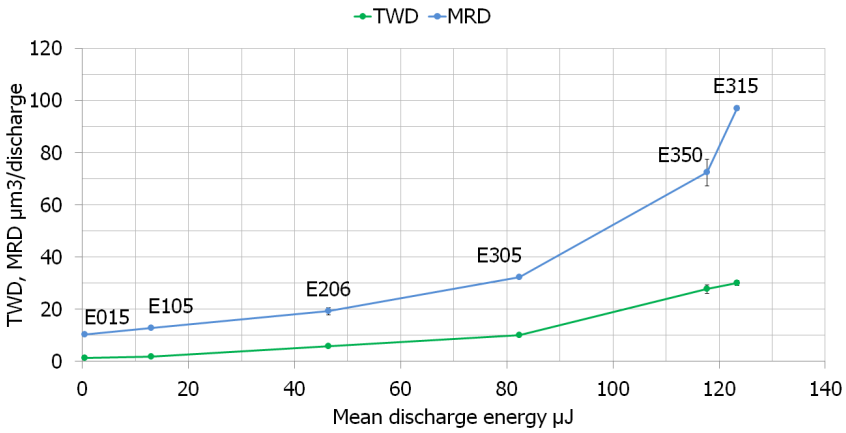

Figure 6.4: Average values of MRD and TWD for different set of process parameters.

Chapter 7

Applications

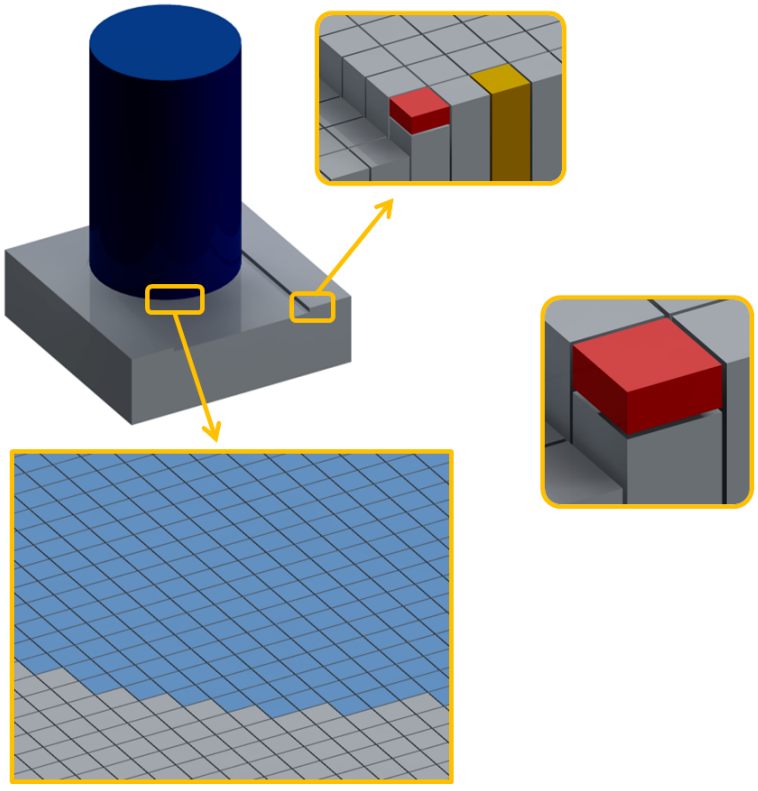

Figure 7.1: Voxel discretization of tool and workpiece electrodes used in the software tool for the simulation of the material removal process.

7.1 A test bench framework

The feasibility and reliability of the on-line tool wear compensation method based on TWD and MRD has been verified by comparing the trend of the tool wear and material removal per discharge measured during a machining process and the response of the method simulated accordingly to the counted discharges [33, 48].

The relative error of the method implemented by using TWD and MRD values preliminarily estimated with the procedure described in section 6.1.1, and without reassessment during machining, was calculated to be less than 3%.
The research activities are now oriented to testing and comparing the results achieved with different on-line tool wear compensation strategies based on TWD and MRD and the optimization of the parameters of the tool wear compensation models. To this end, a test bench framework was developed (section 6.1) to study different on-line tool wear compensation algorithms and evaluate their performance when applied to the machining of microfeatures, from simple cavities to free-form surfaces (figure 7.2).

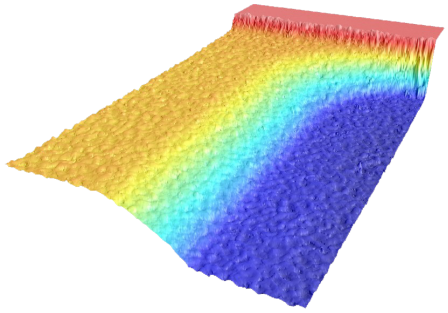

Figure 7.2: Portion having an area of 320 x 600 µm^2 of a free-form surface machined in μEDM milling configuration by implementing the on-line tool wear compensation algorithm based on TWD. The image was acquired with a Sensofar $PL\mu$ neox 3D optical profiler and 100x objective.

The capabilities of the setup were evaluated by performing a number of preliminary tests. An example is provided in the following paragraphs.

7.1.1 Setup

The on-line tool wear compensation method based on TWD was implemented by exploiting the setup described in section 6.1. A Matlab script was driving the tool movements step-by-step, adjusting the Z axis coordinate in order to compensate for the tool wear that was calculated on the basis of the number of discharges retrieved from the Agilent 53131A frequency counter.

The Matlab script accepts generic ISO-6983 (G-Code) from any CAM software and breaks the toolpath into steps with a maximum predefined length. At the end of every step the number of discharges occurred during the last movement is read from the frequency counter and converted in tool wear by the TWD based tool wear compensation model implemented into the Matlab script. The cumulated tool wear is then subtracted from the absolute Z axis coordinate and the command for the following step is sent to the Sarix Machine thorough the custom interface (chapter 4). A part program running on the Sarix machine executes the commands received from the Matlab script.

7.1.2 Experiment

The on-line tool wear compensation method has been tested in the machining of a 800 x 700 µm rectangular pocket with a 200 x 100 µm island in the middle of the cavity (figure 7.3).

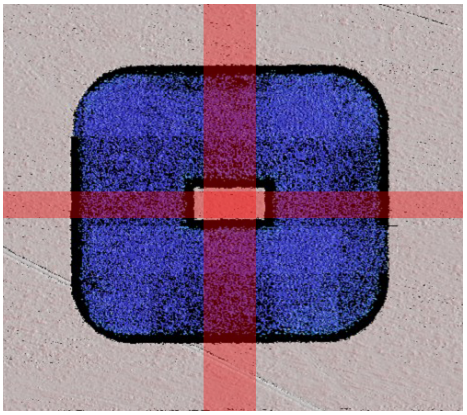

Figure 7.3: 3D reconstruction of the pocket made of 16 images stitched with 25% of overlap, acquired with a Sensofar $PL\mu$ neox 3D optical profiler. Red areas were acquired with a higher resolution 100x lens to perform more accurate depth measurements.

The nominal depth of the pocket was 40 µm. A tungsten carbide rod having a diameter of 296 µm (section 6.1.2) was used as tool electrode, together with pre-finishing process parameters (energy index 105 in table 3.1) and an hydrocarbon oil as dielectric fluid. The stock material was removed layer by layer from the block made of Uddeholm Stavax ESR steel, by following a rectangular toolpath. The toolpath was prepared on a CAM software, exported as generic ISO-6983 (G-Code) and imported into the software tool developed in Matlab to test the tool wear compensation method. The machining was performed by compensating the tool wear in steps of 300 µm along the toolpath.

TWD is assumed to be a constant characteristic of the process, hence, no TWD re-assessment was performed during machining.

The tool electrode length was measured at the beginning and at the end of the machining process, by following the procedure described in [44] and at the same reference point on the workpiece surface.
The geometries of the microfeature were characterized by means of a Sensofar $PL\mu$ neox 3D optical profiler. The depth of the pocket was measured as the difference between the Z coordinates measured on the floor of the cavity and on the top surface, in four different areas: at 0, 90, 180 and 270 degrees relatively to the centre of the island. Given the large dimensions of the microfeature, it was necessary to stitch 4 x 4 images taken with the 20x lens to acquire the whole geometry (figure 7.3). The 20x lens is characterized by a vertical resolution of 20 nm. The 100x lens, which has a the vertical resolution of 2 nm, was used to acquire two 17 x 1 stitching along the X and Y directions and passing through the centre of the pocket. The depth measurements were performed on the 3D images acquired with the higher magnification lens.

7.1.3 Results

The micromachining of the pocket lasted about one and a half hours.
The overall linear tool wear was estimated by subtracting the tool length measured before and after machining. The difference between the linear tool wear measured by touching the workpiece surface and the value calculated during the process by discharge counting is 2 µm.
The depth values measured with the confocal microscope are reported in table 7.1. The error in the table is the deviation of the measured depth from the specification, and the results shows that it is homogeneously distributed on the floor of the cavity.
Considering that the nominal depth of the pocket was 40 µm and the average error is 1.4 µm, the relative error can be estimated to be 3.5%.
This result is in line with the experiments performed in [33, 48].

7.2 Material removal simulation

The prediction of tool wear and stock material removal is of paramount importance for the accurate estimation of process statistics and tool path generation in CAM softwares as well as process control [36]. This can be achieved by representing the process with a model.
One possible approach to define a model to describe the EDM process is

ΔZ µm	Avg	Std	Error
North	38.7	0.01	1.3
East	38.4	0.01	1.6
South	38.5	0.05	1.5
West	38.8	0.02	1.2
avg	38.6		1.4
std	0.17		

Table 7.1: Depth of the microfeature measured with a confocal microscope in four different areas, and relative error (nominal depth 40 µm).

theoretical-analytical [51]: starting from the solid-state physics, thermodynamics and the electrodynamics of the process a model is defined to correlate machining results to technology parameters. But the assumptions that are taken during the simplification of the complex EDM process often leads to significant difference between model estimations and experimental results.
The thermo-electrical principles of the process are exploited for the definition of the model [52], through heat diffusion equations [53]. The plasma channel of the discharge is considered as the heat source, and the heat transmission through the electrodes material is studied at steady conditions. Once the temperature map on the workpiece and the melting temperature of the material are known, it is possible to predict crater shape and dimensions. In [54] crater dimensions are predicted by considering the local stress generated by the discharge relatively to the yield strength of the electrode material. The numerical model based on heat transfer equations presented in [55] includes latent heat for melting and evaporation. The simulation contemplates the debris effect on the discharge process, in particular on sparking gap and discharge voltage.

Alternatively, the model can be defined by replacing the assumptions with experimental data, in this case the model is called semi-empirical. The results are in general more accurate but semi-empirical models are defined for specific purposes and are valid only for a narrow range of its characteristic parameters, or working conditions. In [56, 57] the Taguchi statistical test was adopted to evaluate the influence of different process parameters on machining performance. The results of the statistical tests were then employed to define a number of dimensionless quantities, in order to predict machining performances given a set process parameters.
Geometric models are often used to describe the process at a single spark

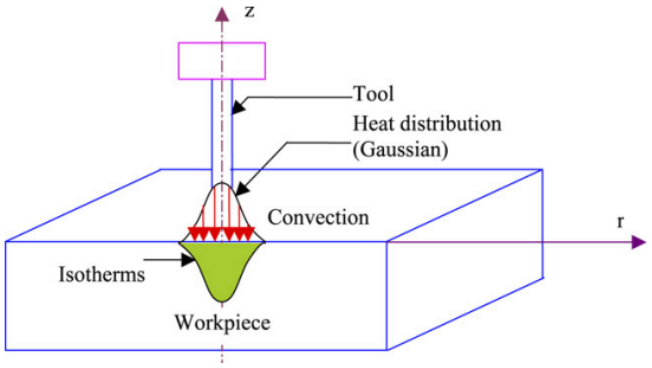

Figure 7.4: Example of model based on the heat transfer equations. Schematic sketch of Gaussian heat distribution in powder mixed EDM [55].

level. Solids can be represented through analytical formulation [58], molecular dynamics [59, 60], Z-Map [61] and R-Map [62].

The last two methods are a specialization of ray casting, where the volume of material is discretized with a resolution of the atoms or arbitrary voxels, grids and matrix cells. These models are suitable for 2D and 3D representation of tool and workpiece, and are often implemented in software tools used for the simulation of die-sinking, wire, drilling and milling EDM processes [62–66]. For instance, the geometrical model was applied to the reverse simulation of the EDM process [67].

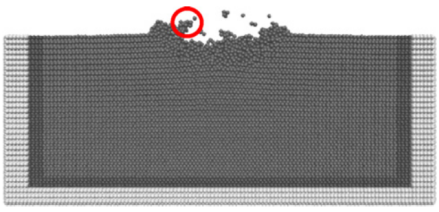

Figure 7.5: Example of geometrical representation of a discharge with the molecular dynamics approach. Cross section of electrode at 8.4 ps after dielectric breakdown [59].

In micro EDM the discharge gap dimensions are comparable to surface roughness and irregularities, especially in finishing and super-finishing operations [58], hence, the resolution of the geometrical model should be enough to describe the surface topography. Indeed, even defects that are characteristic of the electrodes materials, such as pores, can influence the results of simulations [59].

7.2.1 Material removal simulation tool

A tool for material removal simulation has been developed in Matlab. The tool allows accurate representation of the machined geometry which can be used for verification of the progress of the machining operation as well as for improved tool trajectory definition and tool wear compensation for the following process steps. The input to the simulation tool consists of a list with the tool positions and the corresponding number of counted discharges. In order to increase the resolution of the toolpath, the path interval is divided in any preferred number of segments within the simulation module and the amount of discharges corresponding to each segment is calculated by dividing the discharges counted for the whole path interval by the number of segments.
Solids and the material removal process are geometrically represented by an algorithm that was inspired by Z-Map models [61]. Tool and workpiece electrodes are discretized in a number of $2\,^1/_2$D voxels with square footprint equal to the average area of the discharge craters measured for the specific process settings.
The tool is able to manage any desired voxel size and a geometrical model to represent the single discharge crater can be implemented. However, the computational time is proportional to the resolution of the simulation.
The processing time was minimized by choosing a square shape with a lateral size close to the average crater size as voxel. Since the amount of reduction in height of the single voxel depends on its lateral dimension, as the volume removed by a single spark is constant and equal to the MRD, this is the minimum acceptable resolution for the simulation. Indeed, when voxels are too small the voxel height reduction caused by a single discharge is exaggerated and the accuracy of the simulation is compromised.
The tool electrode is considered in the simulation as having a diameter equal to the actual diameter plus two times the lateral discharge gap (which is determined experimentally). For each segment, the couple of voxels on tool and workpiece that have minimum distance are identified and the Z coordinate of the workpiece voxel is reduced by an amount equal to the MRD divided by the voxel area. Thus the volume removed from the voxel corresponds to MRD. If more than one tool-workpiece voxels couples with the same distance are found (as happens at the beginning of the operation), a random choice is operated automatically. The output of the simulation tool consists of a file of the machined part in STL and SDF formats. The STL file can be imported in a generic CAM software for the generation of the tool trajectory for the following machining operation. The SDF file can be

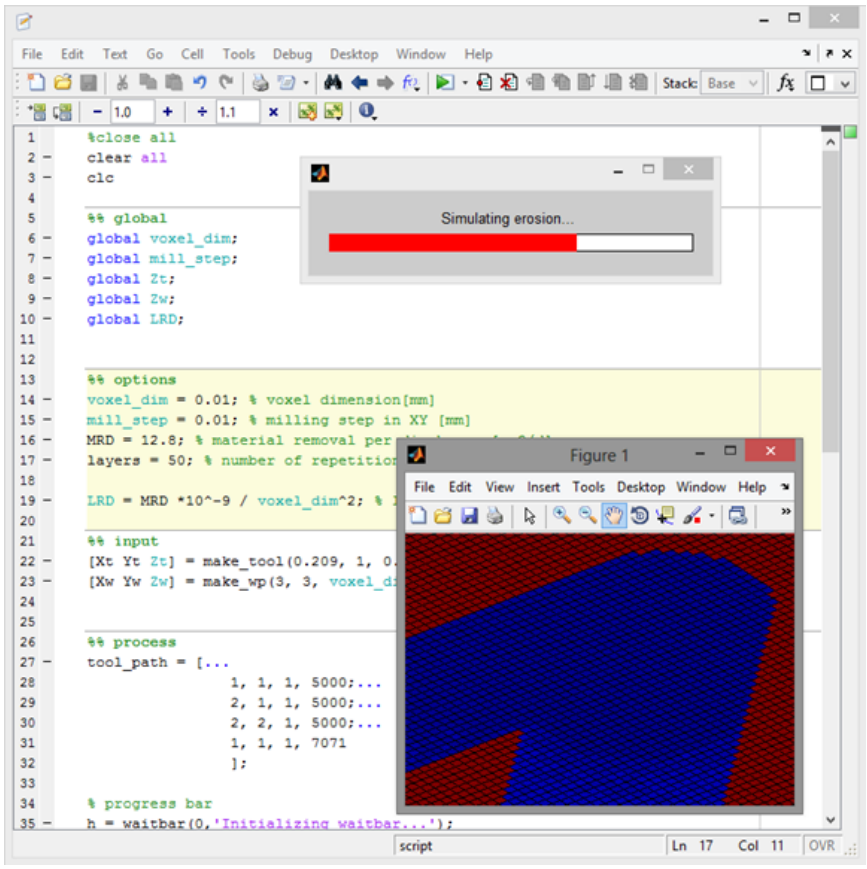

Figure 7.6: Material removal simulation tool.

imported in programs such as SPIP for measurement of part geometry.

7.2.2 Validation of material removal simulation tool

Experimental validation of the material removal simulation tool was obtained by comparing the geometrical characteristics of the microfeatures obtained from the machining operation and from the simulation tool. Here are reported two different tests, the first one involved the machining of a straight groove 500 µm in length, with full radial engagement of the tool electrode (slotting, figure 7.7) while the second one produced a square pocket with a square island in the middle of the cavity (figure 7.8). In both tests the tool electrode was dressed using the machine WEDG unit to a diameter of 200 µm and process parameters settings corresponding to energy index 105

(average discharge energy 12 µJ) were used. The discharge gap was measured to be 5.5 µm by means of Confocal and SEM measurements on dedicated tests, while the crater diameter was measured to be approximately 10 µm. No tool wear compensation was applied and discharges were counted during machining. For the simulation, the actual tool path segments, counted discharges, tool diameter and lateral sparking gap were given as input. MRD was assumed constant and equal to 12.4 μm^3.

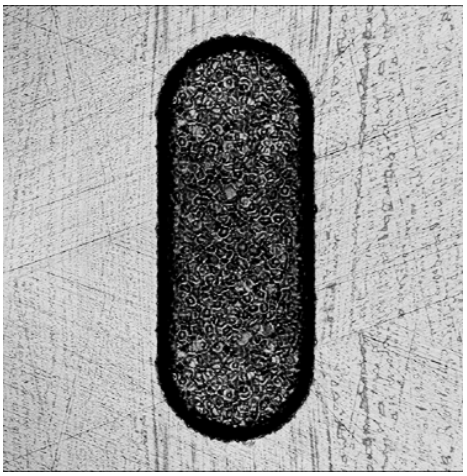

Figure 7.7: Straight groove with a length of 500 µm and a width of about 210 µm.

The groove was machined in 10 steps, each consisting of 20 layers with nominal layer depth of 0.9 µm, for a total nominal depth of 180 µm (actual depth 77 µm). At the end of each step of 20 layers, the number of discharges was recorded and the groove floor was measured at half the path length by means of touches using the tool electrode. Machining was simulated layer by layer, with a motion resolution of 10 µm in x-y directions. Table 7.2 shows the comparison between the groove depth as measured on the machine and the corresponding values from the simulation for each of the steps of 20 layers each. An overall good agreement between measured and simulated material removal is observed. With the exception of the first layer, the maximum depth error of the material removal simulation is 1.2 µm for a total depth of 77 µm. The error in the first layer is likely to be due to alignment errors of the workpiece on the machine fixture. The square pocket was machined in 50 layers, with a basic trajectory consisting of 4 segments and nominal layer depth of 0.9 µm. Discharges were recorded at each layer at the end of each side. Simulation was performed layer by layer, with a motion resolution of 10 µm in X-Y directions. The comparison between the machined and simulated pocket profile along one of its sides is shown in figure 7.8, showing a very good agreement between measurements and simulation. These results confirm the reliability of material removal simulation based on discharge counting and MRD estimation.

	Actual depth µm									
Step N	1	2	3	4	5	6	7	8	9	10
Measure	0.7	14.3	21.8	29.5	37.6	46.5	53.7	61	69.2	77.2
Sim.	5.4	13.2	20.6	28.4	36.6	45	53	61.5	69.8	78.4
Error	4.7	1.1	1.2	1.1	1	1.5	0.7	0.5	0.6	1.2

Table 7.2: Results of validation of material removal simulation.

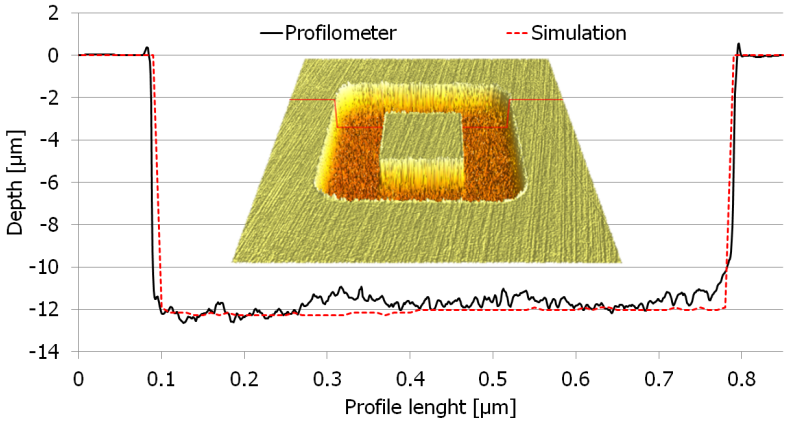

Figure 7.8: Square pocket with a square island used as experimental validation of the simulation tool. The channel is approximately 210 µm in width. Depth profile comparison along one side of the pocket.

Chapter 8

Energy efficiency analysis

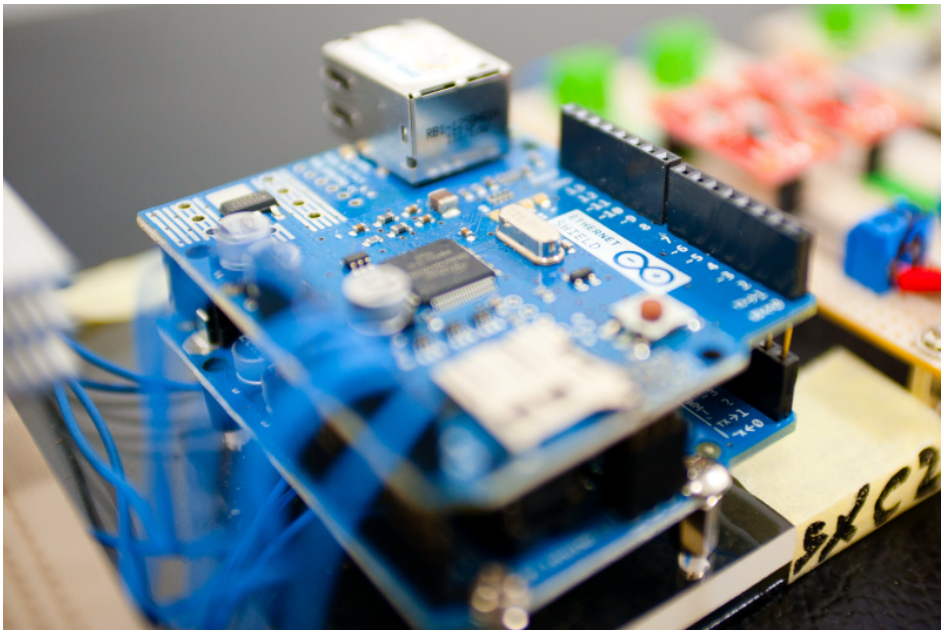

Figure 8.1: Image of the acquisition system, which is composed by an Arduino Uno microcontroller board and Ethernet Shield, plus voltage and current sensors.

8.1 Sustainability

Sustainability has become an important issue in all spheres of life. This will be the case for many years to come, or at least until we find an as yet unknown solution. Sustainability focuses on safeguarding natural resources against exploitation, in the name of productivity and competitiveness, by manufacturing and service organizations. It is a major concern in many countries and is leading to strict regulations regarding the impact of products and services during their manufacturing, use and disposal.
Government regulations, profit and not-for-profit organizations, as well as internal strategic objectives, employee safety, cost savings, productivity and quality are pushing companies around the world to seriously think about their sustainable business practices both in manufacturing and services. As a consequence, the interest in environmentally friendly manufacturing is increasing.
Anastas and Warner define green chemistry as the design, development, and implementation of chemical products and processes to reduce or eliminate the use and generation of substances hazardous to human health and the environment [68]. It is possible to define green manufacturing, green marketing and green supply chain in a similar way [69].
Sustainability is about building a society in which a proper balance is created between economic, social and ecological aims. Sustainability can be pursued at different levels: business, product design, supply, production, distribution, remanufacturing/recycling. Production sustainability includes managing the processes with sustainable input such as energy, people, equipment and machines with the objective of reducing waste, rework, inventory and delays as well as reducing carbon footprint.
With the rising to new records of prices per kWh and the introduction of taxes related to Green House Gas (GWP) emissions, energy is being considered by industrial enterprises as a valuable resource which requires to be strategically planned and managed with more and more sophisticated optimization strategies. Accordingly to recent studies [70], electricity monitoring in manufacturing companies should be performed in 3 levels or orders: factory, department, and unit process. Examining the lower level, energy bills can be sensibly eased by reducing machine tools energy wastes. To accomplish this task different approaches are available, from product design optimization and life cycle management to production plant scheduling and tool machine ecodesign. What all these approaches have in common is the requirement of complete transparency of energy usage among the entire manufacturing facilities. To this end, it is necessary to implement a detailed

grid of meters to characterize energy consumption over time, plus an informatics system capable of logging data from such meters, process it and visualize human readable results in support to management and decision making.
In addition, power metering systems can report a wide range of parameters to characterize voltage quality, which is very important especially in applications that are sensitive to voltage sags, surges and disturbances, such as high precision manufacturing. As a matter of fact, electricity is probably unique in being a product which is manufactured, delivered and used at the same instant of time [71] and it is important for the company to monitor if contract claims are respected by providers as with any other variable input.
In this chapter, a mini framework for developing a sustainable manufacturing or business in general, through on-line energy consumption monitoring is presented. The system for the on-line energy consumption monitoring of an industrial process will be described in detail and then applied to a micro EDM milling machine.

8.1.1 Energy efficiency in micro EDM

In order to achieve the objectives described in the introduction of this chapter, it was necessary to implement a modular system for on-line energy consumption monitoring that could be easily adapted to the different configurations of existing production facilities. In this work only one process was considered, but all the most relevant subsystems of the μEDM machine were analysed, with an experimental setup that could be easily replicated and adapted to monitor the energy consumption of different machines. The system was employed to acquire data and gain a better understanding of the total amount of energy involved in the process, the quota dissipated by each main component of the machine. Then the results obtained from the data analysis were used to suggest strategies to increase the energy efficiency of the process.
On-line energy monitoring [72–75] and modelling of energy consumption of industrial processes at macro scale [76–81], have already been studied and a number of works have already been published on this topic. At micro scale, instead, and in particular in micro EDM there are only few investigations [82].
Energy efficiency in μEDM can be evaluated by comparing the total energy of the discharges, which are instrumental in material removal, and the overall energy consumption of the process, including all the necessary auxiliary equipment. The total energy of the discharges occurring during a μEDM

process can be easily evaluated experimentally by counting the number of discharges occurring during the machining process and then by multiplying it by the mean discharge energy that is characteristic for the selected set of process parameters (section 3.3, table 3.4).
Although only a small percentage of the discharge energy is effectively spent to remove material from the workpiece, because energy is converted into heat and then almost completely dissipated by conduction into the electrodes and dielectric fluid [1], total discharge energy will be considered in this work.
In order to perform a μEDM process, a number of auxiliary components are required and, given the small amount of material that is removed in micromachining processes, it is expected that the energy required by the auxiliaries is dominant. Nevertheless, an estimation of the energy consumption of the machine subsystems is valuable because it can suggest procedures and strategies for the optimization of process parameters and improvements of the machine hardware, oriented to the reduction of the overall energy consumption of the micromachining process.

8.2 Measuring the electrical energy consumption

In general, the electrical energy consumption is calculated by (8.1):

$$E = \int P(t)\mathrm{d}x \tag{8.1}$$

where $P(t)$ is electric power as a function of time t. Instant power P is a product between instant voltage U and instant current I. When using an AC (sinusoidal) current supply to power a linear system, by definition composed by Ohm loads, the power used on a load can be simply calculated by eq. (8.2):

$$P = V_{\mathrm{RMS}} \cdot I_{\mathrm{RMS}} \tag{8.2}$$

where the root mean square (RMS) value of an arbitrary variable x is calculated by eq. (8.3):

$$x_{\mathrm{RMS}} = \sqrt{\frac{1}{n}\sum_{i=1}^{n}(x^2 + \bar{x}^2)} \tag{8.3}$$

But most of the production machines consist of several subsystems with linear, capacitive and inductive loads. In this case, equation (8.2) gives the apparent and not the real power. To calculate energy consumption at a

given time, the sum of instant power over the observed time is calculated using the following equation (8.4):

$$P(t) = U(t) \cdot I(t) \tag{8.4}$$

8.3 Experimental setup

The machine that has been selected for the energy efficiency investigations in this work is a Sarix SX-200 (1.1), state of the art in micro electrical discharge machining and capable of performing micro EDM milling, drilling, die-sinking and grinding operations.
The machine consists of three main sub systems with different electrical elements: the main C structure which includes the spindle, motors, actuators and other equipment to perform machining, the control unit (SX-CU) with generators and logic boards to drive the process and the dielectric unit (SX-DA) for filtering, cooling and pumping the dielectric liquid. The flushing of dielectric liquid, which in this case is a low viscosity hydrocarbon oil, is provided by a pump directly on the machining area through a hose.
Only the minimum indispensable electrical components are left in the main C structure, in order to increase the thermal stability and hence the machining accuracy of the process. As a consequence, the SX-CU control unit is composed of many electrical components: several electric cards, a computer, a laser micrometer display unit, input/output interfaces and man-machine console. The most important electric cards are: the 5V, 12V, 24V, 36V general purpose power supplies (GPS), a security control unit (SCU), motors control unit (MCU) that drive the motors of the axes, erosion power supply (PWR) that generates the power required for erosion, micro pulse shape generator (MPS) that modulates electrical discharge pulses and monitors in real time machining parameters, process performances and collisions.
The SX-DA dielectric unit instead is connected to the SX-CU only for communications purposes and sources the power from the grid through a dedicated plug. SX-DA is equipped with two electrical pumps necessary for flushing (P1) and for cooling and filtering (P2) the dielectric fluid, the auxiliaries such as power supply, electro valves, temperature and pressure sensors, logic boards, SX-CU communication interface board, relays, safety switches, circuit breakers.
In Table 8.1 are listed the main components of the machine that were monitored during the experiments. The μEDM machine was also using compressed air for the functioning of the high pressure dielectric pump, pneu-

Location	Code	Description	Channel
SX-CU	CU-MAIN	Main plug of dielectric unit SX-CU	A1-CH1
SX-CU	PC	On-board computer	A3-CH1
SX-CU	MCU	Motors Control Unit	A3-CH2
SX-CU	MPS	Micro Pulse Shape generator	A3-CH3
SX-CU	C	C axis 24V power supply	A4-CH1
SX-CU	XY	X and Y axes 36V power supply	A4-CH2
SX-CU	Z	Z axis 36V power supply	A4-CH3
SX-CU	PWR	Erosion Power supply	A4-CH4
SX-DA	DA-MAIN	Main plug of dielectric unit SX-DA	A1-CH2
SX-DA	P1	Pump: low pressure flushing circuit	A2-CH1
SX-DA	P2	Pump: cooling and filtering circuit	A2-CH2
SX-DA	DA-AUX	Machine ancillaries	A2-CH3

Table 8.1: List of the main subsystem of the μEDM machine considered for the energy consumption evaluation.

matic actuators and cleaning of the tool electrode before the measurements at the laser micrometer. The SX-DA was using the water provided by a chiller at 20.0 °C to control the temperature of the dielectric fluid inside the SX-DA main tank. The energies related to the air compressor and chiller were not considered in this work.
The energy consumption of the μEDM machine and its subsystems was measured by means of an Arduino based framework that will be described in section 8.3.1. The energy consumed for the removal of the material from the workpiece electrode was evaluated by counting the number of discharges occurring during the machining process with an Agilent 53131A frequency counter, and then multiplying the resulting number of discharges by the value of average energy per discharge relative to the process parameters settings used in the experiment (table 3.4).

8.3.1 Arduino energy monitor

The energy consumption of the μEDM machine and its main subsystems (table 8.1), was measured, recorded, processed, and displayed on-line by an Arduino based framework.
The system is capable to reading analogue signals from current and voltage sensors, converting them to digital values, performing mathematical oper-

ations, storing the results in a database, and finally providing the most relevant information in human readable format on the screen of a computer, while the machining process is running. Other secondary but important requirements were considered, in order to encourage the implementation of this system in small and medium industries: costs, dimensions, invasiveness of the system over machine operation were reduced to minimum, while ease of use and modularity were enhanced to make it easily adaptable to different machines. Results were made remotely accessible for the on-line monitoring of the process and for the following analysis of the recorded data.
To satisfy these requirements, a system has been composed as in figure 8.2 by: the necessary number of current and voltage sensors, a microcontroller board to process signals from sensors, Ethernet connection for data transfer, and a web server to store and display results.
The microcontroller board chosen for this work is an Arduino Uno, which sports an Atmel ATmega328 microcontroller clocked at 16 MHz, 2 KB SRAM and 6 analogue inputs with 1024 levels analogue to digital converter at a nominal sampling rate of 10 MS/s. Ethernet shield has been added to each Arduino Uno board (8.1) to be able to send data to the remote server through existing Ethernet network.
Current sensors have been selected from commercially available products and are based on Hall-effect integrated circuits. In this work, two types of ACS 712 sensors were necessary: one with a maximum peak current of 5 A and another one with a peak current of 20 A. Voltage sensors instead have been assembled in-house and are based on a voltage divider circuit. These sensors are able to scale down the voltage signal from 220 V AC and 12 or 24 or 36 V DC to the 0-5 V range that is accepted by the microcontroller Analog-to-Digital Converter (ADC). All current and voltage sensors, as well as Arduino Uno boards were powered by a dedicated 9 V power supply unit through a 5 V voltage regulator, in order to stabilize the DC voltage required by all the elements of the system.
Results from the data elaborated with Arduino are sent over Ethernet to a remote server using UDP protocol. On the server, incoming data was read out, stored and visualized on a graphical user interface by a script written in Processing language.

Arduino Uno and Ethernet Shield

Arduino Uno AVR RISC-based 8 bit microcontroller has a clock speed of 16 MHz, which theoretically should give enough computational power to sample current and voltage signals, perform calculations and send elaborated

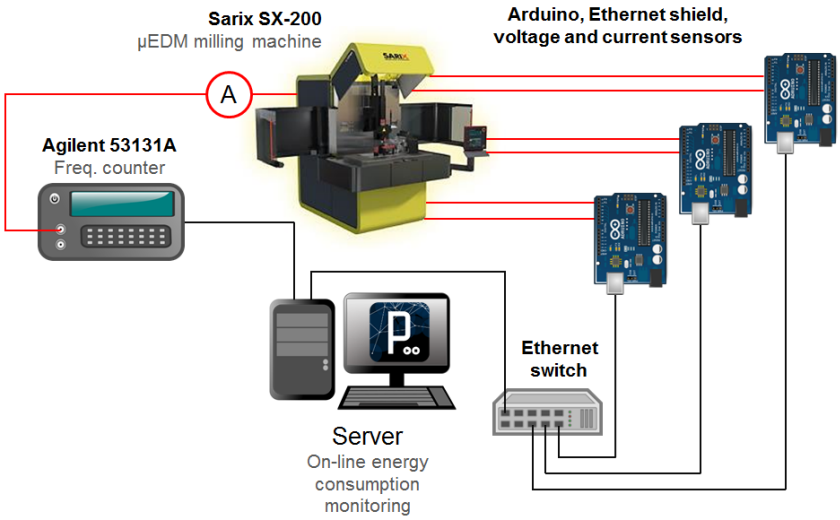

Figure 8.2: Arduino based framework for the remote and on-line energy consumption monitoring of the μEDM process.

data to the server. However the programming language is not optimized for floating point calculations, hence operations with variables can occupy the microcontroller for several clock cycles, reducing the number of samples that are acquired per second.
Arduino Uno microcontroller board is built around the ATmega328 chip, which has 2 KB SRAM. As a consequence, the maximum number of elements that can be stored in memory is very limited. As an example, no more than 512 unsigned long variables, that are 4 bytes in size, can be initialized having a total of 2048 byte SRAM available. This is just a theoretical estimation, the actual limit is lower. In any case it is evident that it is not possible to use SRAM to store values for a long period of time, it can be used as a small buffer but the data must be saved into a remote server. Hence, the data elaborated by the microcontroller was sent to a computer that will store and display it to the user in a human readable format. Arduino Uno is not capable to perform multiple operations in parallel; as a consequence it is important to minimize data transfer time because the time spent to send data to the remote server corresponds to a pause in the operation of sampling the signals from sensors. Arduino Uno boards are usually connected to computers with a virtual serial port through USB. The maximum speed of the serial port is limited to 115.2 kbps and it is not suitable for connecting many Arduino boards to the same computer. To achieve a

better performance in data transfer an Ethernet Shield was added to the Arduino Uno boards, in order to be able to use Ethernet protocols such as HTTP, TCP/IP or UDP. In this case not only the transmission speed is drastically increased (nominal transfer rate of 10 Mbps) but the connection between microcontrollers and server is extremely simplified, with the added possibility to supplant complicated wired connections with a wireless router. UDP was selected among the available protocols over Ethernet, trading a negligible quota of data transmission reliability for a substantial increase in speed.

The analogue to digital converter (ADC) of the ATmega328 microcontroller by default is capable to convert analogue signals at a rate of about 10 Ksps, which is sufficient in sampling a voltage/current signal characterized by a frequency of 50 Hz. However in practice the sampling rate of the system is sensibly slower than the conversion rate of the ADC, because in this case it is affected by the time necessary to transfer data over Ethernet, the number of channels that are read and the computational load between analogue channel readout, especially when values are stored as floating numbers. Indeed, the 6 analogue inputs/outputs of the microcontroller board are multiplexed and hence read successively, with two important negative outcomes: first, when reading the signals from multiple sensors the sampling rate decreases to a fraction; secondly, channels are not read simultaneously but there is a short time interval between each channel readout.

It is evident that an increase in ADC speed, or conversion rate, would be doubly beneficial in diminishing the influence on results of the issues described above. Interestingly, the ATmega328 datasheet specifies that the ADC by default is under clocked at 125 KHz, while it can withstand clock frequencies up to 200 KHz without any side effect, or 1000 KHz with a marginal loss in resolution [83]. After setting the prescaler of the ADC clock to 32, which corresponds to a clock speed of 500 kHz, it was possible to acquire during the experiments from 850 to 1150 samples per second, depending on the number of channels and the complexity of calculations.

In order to monitor energy and power, voltage and current sensors are required. Voltage sensors are voltage divider circuits, while current sensors are commercially available breakouts that are based on an Allegro Microsystem ACS712 integrated circuits. Amplitude and offset trimmers of the output signal have been adjusted to fit the range accepted by Arduino analogue input pins, with the assistance of an oscilloscope.

The nominal resolution of Arduino Uno internal ADC is 10 bit, which corresponds to 1024 levels on a measured range, and the accepted voltages at the input ports are in the range of $0 \div 5$ V. This means that the resolution

of voltage sensors is about 0.6 V, given that the amplitude of the voltage signal is $\pm 220\sqrt{2}$, while the resolution of current measurements is 0.014 A for $0 \div 5$ A current sensors and 0.055 A for $0 \div 20$ A current sensors.

Arduino software

As any software in general, the Arduino script accepts some values as inputs, processes them, and provides the results at the output. The inputs in this case are signals between 0 and 5 V originating from current and voltage sensors that are connected to the analogue input/output pins. The Arduino software has to accomplish the following tasks repetitively: to read analogue values as fast as possible, to perform the necessary calculations to obtain the desired values, and finally to send them to the server.
The microcontroller board is equipped with 6 analogue inputs. One of them is allocated to a voltage sensor and the other five are available for current sensors. Voltage and current values required to calculate real power have to be acquired in the very same instant, but as discussed in section 8.3.1, in Arduino the analogue inputs are multiplexed and as a consequence they are not read simultaneously but successively. However, if the analogue channels are read fast enough relative to the frequency of the input signal, then this difference can be neglected. This is very important to properly calculate instant power (8.4). The software executed by the microcontroller cycles between three main loops:

- a loop to acquire all the values from the ADC
- a loop to perform calculation on the acquired values
- a loop to send the data to the server

This structure enables the acquisition of all the voltage and current signals in a sequence. A simpler structure is achieved by executing only one loop through the channels and performing the data acquisition, post-processing and transmission for one channel at a time. However, in this case the time discrepancy between the acquired signals would be larger.
In the first loop analogue channels are read subsequently and converted to digital values as fast as possible and values are just stored into variables. In the second step calculations are performed: variables are scaled to the physical values according to the prior defined calibration gain and offset factors. Calibration factors, for each sensor were determined as described in section 8.3.1. As mentioned before, the SRAM is not capable of storing a large number of variables and data transmission is not fast enough to

send a direct stream of sensor values, hence real power, RMS of voltage and RMS of current are continuously calculated with running algorithms (8.5) at maximal sampling rate, and results are sent to server with a time interval of 1 second.

$$RMS_{i+1}^2 = RMS_i^2 + \frac{Val_i^2 - RMS_i^2}{i} \tag{8.5}$$

$$P_{i+1} = P_i + \frac{U_i \cdot I_i - P_i}{i} \tag{8.6}$$

In the formulas (8.5) and (8.6) above, V_i and I_i are instant values of voltage and current respectively, $V \cdot I$ is instant power, P is real or average power, RMS can represent voltage or current RMS depending on the parameter associated to Val. Equations (8.5) and (8.6) were obtained as follows:

$$\begin{aligned}
\bar{x}_n &= \frac{1}{n}\sum_{i=1}^{n} x_i \\
&= \frac{n-1}{n}\frac{1}{n-1}\left(\sum_{i=1}^{n-1} x_i + x_n\right) \\
&= \frac{n-1}{n}\frac{1}{n-1}\sum_{i=1}^{n-1} x_i + \frac{n-1}{n}\frac{1}{n-1}x_n \\
&= \frac{n-1}{n}\left(\frac{1}{n-1}\sum_{i=1}^{n-1} x_i\right) + \frac{1}{n}x_n \\
&= \bar{x}_{n-1} + \frac{1}{n}\left(x_n - \bar{x}_{n-1}\right)
\end{aligned} \tag{8.7}$$

where x can be rms of voltage or electric current or average power [72]. Other values that are calculated and stored in memory are: size of the sample (number of inputs contributing to the calculation of the mean value), microcontroller time reference at the beginning of the sampling and number of periods of the sampled sine wave signals. Identification number, time reference, number of samples, voltage RMS, voltage frequency, and for each current channel frequency, current RMS, real power, are converted with a predefined pattern into a binary packet that is then sent to the server, every second. While these values are sent to the server, the information from sensors are lost, but using UDP data transfer protocol it was possible to limit the blackout time to less than 5 milliseconds.

Server

Since raw data is processed in Arduino and results are transmitted to the server every second, data throughput is moderate, and consequently server hardware requirements are also moderate. A laptop with a 2 GHz Intel Core2Duo processor and 4 GB of RAM was more than sufficient to run the server application and record the data incoming from the acquisition system.
Data is sent by the four Arduino boards to the server through an Ethernet connection using UDP protocol at a predefined UDP port. The software on the server that manages the incoming data was written in Processing programming language, because of the similarities with Arduino programming language and the open-source license. The software is continuously listening to the predefined UDP port and once a packet of binary data is received the variables are decoded and stored in a database. Results were monitored in real time through the graphical user interface and then processed using Matlab for further analysis.

Calibration of the sensors

Calibration of voltage and current sensors was performed using a multimeter as reference and a dedicated software for both server and Arduino. The procedure allows to calculate the offset of the analogue signal, and then to estimate the gain by matching the two RMS values read from the multimeter and the sensor.
Alternating current (AC) in general is varying through all the sensor range and depending on the setting of the trimmers on sensor breakout can show a response curve that is not perfectly linear at the extreme values. For this reason current sensors have been calibrated in direct current (DC) but at different values within the sensor range. A calibration circuit was made with a variable 0 to 12 V power supply capable to provide up to 6 A and a suitable high power resistor in order to dissipate from 0 to about 5 A, which is the range of currents sensed during experiments. The calibration procedure was applied at different current values for each sensor, with ranges of nominal current values that depends on sensor application, and repeated 5 times. In figure 8.3 example of data from calibration procedure relative to sensor A2-CH2 (SX-DA cooling and filtering circuit pump) tested in a range from -4 to +4 A, which shows an almost linear response curve. In this case, the coefficients of the calibration function were obtained fitting the data with a one degree polynomial function. As an example, the equation 8.8 represents

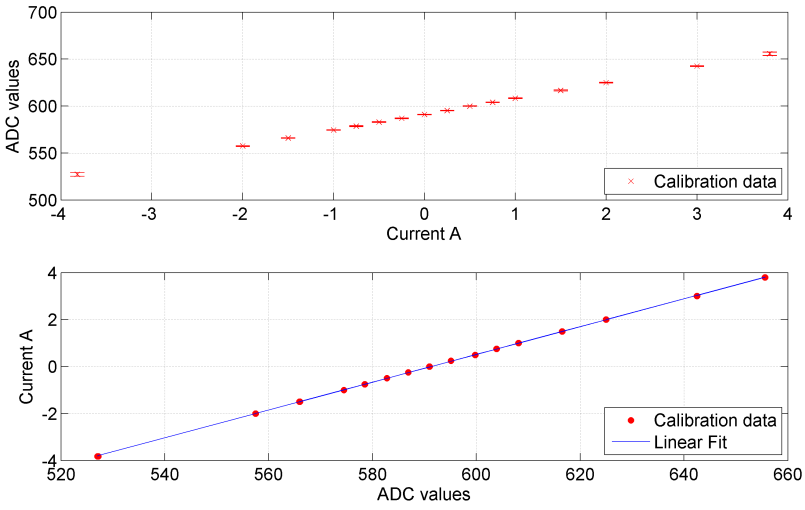

Figure 8.3: Average values with relative standard deviations of the data acquired during the 5 repetitions of the calibration procedure of a current sensor. From these values the calibration curve for current sensor is obtained by performing a polynomial fit in Matlab software.

the linear regression of the calibration curve in figure 8.3.

$$\text{current} = -34.99 + 0.05918 \cdot \text{ADC} \tag{8.8}$$

8.4 Experiments

The energy consumption of the machine was measured while performing a pocketing operation of a circular cavity with a diameter and depth of about 530 µm and 30 µm respectively, on a block of mold steel in milling configuration and with a tungsten carbide tool electrode.
The energy efficiency of the process was tested on a wide range of process parameters (table 3.1), ranging from fine-finishing (energy index 015) to pre-roughing (energy index 350). The performance of each set of process parameters was tested with a dedicated experiment, that was repeated 3 times and average values were then considered. The experiment related to energy index 350 was repeated 10 times to evaluate the reliability of the acquisition system.

Energy	N. of	Radius µm		Depth µm		Time s	
index	obs.	mean	σ	mean	σ	mean	σ
E015	3	174	0.6	52.9	0.6	258.1	1
E105	3	213	0.4	30.4	0.7	260.2	1
E206	3	363	4.4	46.4	0.3	264.9	0
E250	3	284	0.5	29.8	0.7	263.1	0
E300	3	354	0.3	38.0	0.2	266.3	1
E305	3	991	0.8	35.7	0.5	265.0	5
E315	3	410	0.3	40.8	0.4	264.6	1
E350	10	263.3	0.5	30.0	0.4	413.0	0

Table 8.2: Average values of the geometrical characteristics of the features machined during the experiments and duration of the material removal operation (erosion time).

Energy consumption was calculated from the data recorded on the server by the acquisition system described in previous sections. The main variables that are stored in the database about every one second for each channel are the time reference of the record, voltage RMS, current RMS and real power. In order to be able to expand this work in future, by comparing results relative to different working conditions and process parameters, the results have been related to unit of material removed. The volume of material removed has been measured after the experiment with an optical profilometer.

8.5 Results

A 3D image of the microfeatures machined during the experiments (figure 8.4) were acquired with a Sensofar PLμ Neox confocal microscope, and then the diameters and depths were measured with Image Metrology SPIP software. The volume of material removed during the EDM process was calculated from diameter and depth values and results are reported in table 8.2.

The arduino based data acquisition system was started before the machining process and was stopped after the tool electrode was cut at the end of each experiment. The data relative to the machining time frame, and consequently the time that was required to remove the material of the cylindrical pocket, were extracted by means of a script in Matlab by using the current signals as indicators of the status of the machine. As a matter of fact

the pulse generator, the spindle and the pump for the flushing of dielectric on the workpiece are turned on just at the beginning of machining and then turned off exactly at the end of the operation.

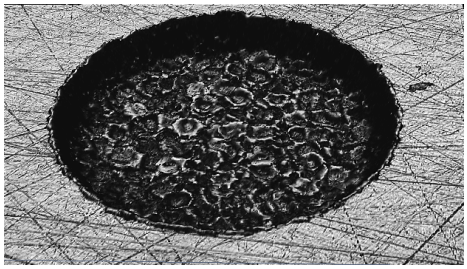

Figure 8.4: Confocal image of a blind hole machined by µEDM with a set of process parameters typically used for roughing (E350), having a diameter of about 528 µm and a depth of about 30 µm.

They are turned on again towards the end of the experiments to cut the tool electrode, as it is possible to notice in figure 8.7. The machining operation was lasting from 257 to 413 seconds, depending on the process parameters settings, as reported in table 8.2.
The values stored in the database were processed in Matlab in order to compare the energy efficiency of different machining operations. Real power has been averaged through the machining time, energy consumption has been calculated as described in section 8.2 and finally the energy consumption relative to each subsystem per unit of volume of material removed was obtained from the geometrical characteristics of the machined holes and energy consumption. Results are reported in table 8.3.

The results reported in tables 8.2 and 8.3 show a good repeatability of the measures and hence suggest that the acquisition system is reliable.
The measured average real power of 292 W, relative to the tank pump, is compatible with the manufacturer specifications, which rate the power consumption to 300 W.
The data represented in figure 8.7 was available during the process, enabling on-line analysis and providing valuable information about the on-going machining operation. For instance, a machine malfunction can be promptly identified and eventually prevented by searching for anomalies in the signals, such as large deviations from standard values.
The column chart in figure 8.6 shows that the power required by the SX-CU for the machining operations with different process parameters settings can be considered constant. There is a slight variation in the power absorbed by the SX-DA between different energy indexes, but this is not related to differences in process parameters because they have no effect on the SX-DA performance.

kJ/mm^3	E015	E105	E206	E250	E300	E305	E315	E350
CU-MAIN	4.0	8.3	9.0	11.0	10.5	31.7	11.6	15.8
PC	0.8	1.6	1.8	2.2	2.1	6.2	2.3	3.1
MCU	0.6	1.3	1.4	1.8	1.7	5.1	1.9	2.6
MPS	0.3	0.5	0.5	0.6	0.6	1.9	0.7	0.9
C	0.3	0.6	0.7	0.9	0.8	2.4	0.9	1.2
X Y	0.5	1.0	1.1	1.3	1.2	3.7	1.3	1.9
Z	0.3	0.6	0.7	0.9	0.8	2.5	0.9	1.2
PWR	0.1	0.1	0.1	0.2	0.2	0.5	0.2	0.2
DA-MAIN	6.8	14.3	15.3	18.8	18.1	54.3	19.7	27.2
P1	1.6	3.4	3.6	4.4	4.3	12.8	4.7	6.6
P2	4.6	9.7	10.4	12.8	12.3	37.1	13.7	20.1
DA-AUX	0.8	1.6	1.7	2.1	2.0	6.1	2.2	3.2

Table 8.3: Average energy consumption per cubic millimetre of material removed during the μEDM process.

This result can be explained by the difference between total discharge energy and total machine energy in table 3.4. Total discharge energy is evaluated by multiplying the average discharge energy, relative to the process parameters settings considered, by the number of discharges counted during the experiments. Total machine energy, instead, is measured with the voltage and current sensors at the main plugs of SX-CU and SX-DA. The variation in total discharge energy due to different process parameter settings is several orders of magnitude smaller than total machine energy, and hence it is negligible.

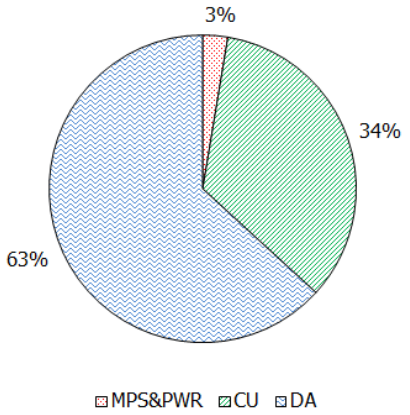

Figure 8.5: Energy consumption distribution during a pre-roughing machining process (energy index 350).

For this reason, the differences of the results in table 8.3 between process parameters settings is due almost exclusively to the difference in machining time (table 8.2).

Energy index	N. of discharges	Total discharge energy J	Total machine energy kJ
E015	11463600	2.8	120.0
E105	522475	6.1	146.4
E206	247364	16.0	248.9
E250	70894	7.7	193.6
E300	54427	9.2	241.6
E305	44676	4.4	676.8
E315	43287	6.5	281.0
E350	78712	15.3	281.7

Table 8.4: Energy required for the material removal calculated as average discharge energy multiplied by the number of discharges and total energy consumption of the μEDM process, relatively to different process parameters settings.

The pie chart in figure 8.5 shows that also the quota of energy consumed by the pulse generators during the process is negligible when compared to total machine energy. In particular the SX-DA unit is absorbing more than 60% of the total energy consumption of the machine.
The Sankey diagram in figure 8.8 was drawn on the basis of the mean values relative to experiments E350 and gives a clear overview of the energy losses through all the main subsystems of the μEDM machine.

8.6 Possible improvements and best practices

The two pumps used for flushing, filtering and cooling the dielectric fluid, in the μEDM machine tested during the experiments, are consuming together more than all the other components of the machine (figure 8.5). These should be the first elements of the machine to be taken into consideration for an energy efficiency optimization.
Indeed, the SX-DA unit is probably oversized because the flow rate of dielectric fluid is always more than sufficient to completely flood the working area and it has to be reduced by means of a ball valve. The pump dedicated to the cooling and filtering of the dielectric fluid is always on once the machine is armed. A more efficient management of the SX-DA could be possible by implementing a smart logic control to turn on the two pumps only when flushing, cooling and filtering are strictly necessary.

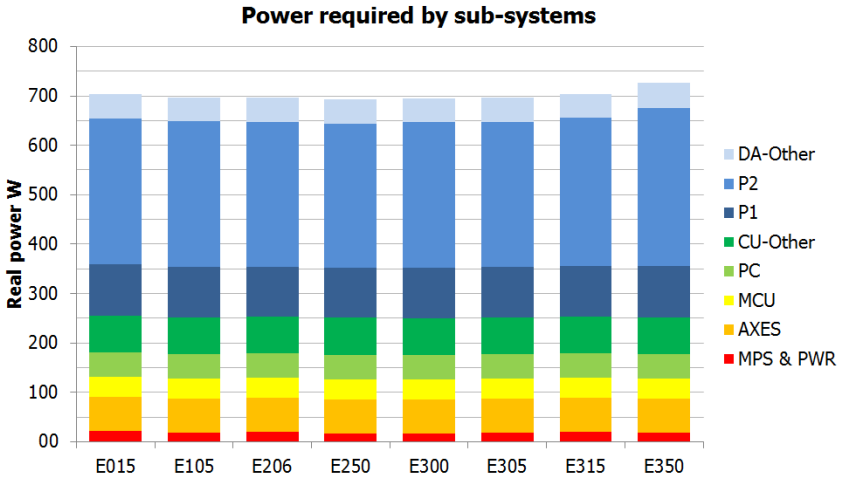

Figure 8.6: Average values of power required during the machining process with different process parameter settings.

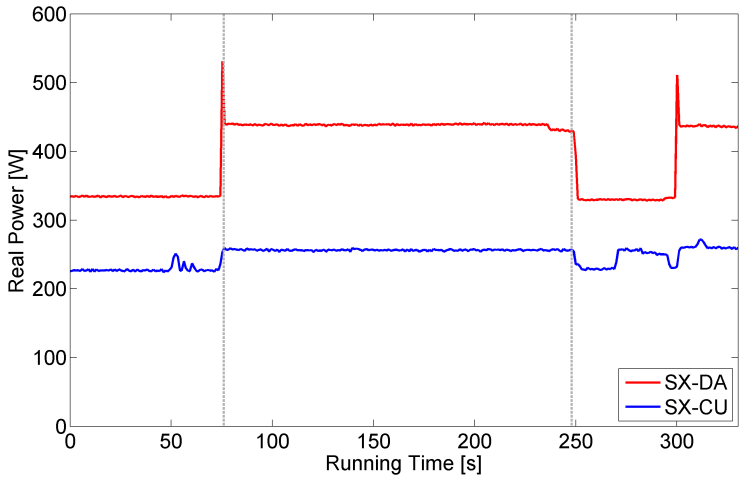

Figure 8.7: Real power data as recorded by the acquisition system of the SX-DA unit. The activity of the pump that flushes the dielectric on the workpiece was used as reference to identify the machining operations along the acquisition timeframe.

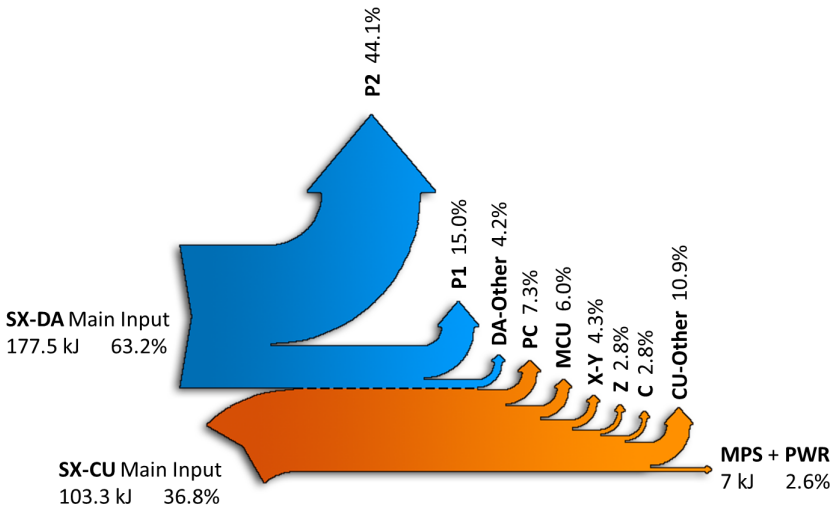

Figure 8.8: Sankey diagram illustrating the distribution of energy in a pre-roughing μEDM process (energy index 350).

At the same time, the strategies implemented in the CAM software could be optimized in order to minimize the overall machining time. For instance, the on-machine fabrication of microtools at the wire dress unit, usually represents a relevant quota of the total machining time. As a consequence, sensible energy savings can be obtained by reducing both the time required by the fabrication procedure and the number of tools that are used in a process. With the current version of the firmware of the machine, a fresh tool is fabricated at the beginning of every machining operation, and the tool that was used in the previous one is dumped even if not completely worn out. Tool length should be correctly sized in order to avoid the waste of the portion of tool that is in excess and the time spent for its fabrication. Machining process parameters, such as feed rate (gain) and layer depth, should be optimized in order to minimize the machining time, whenever possible. Indeed, figure 8.6, suggests that productivity and energy consumption of the process are inversely proportional.

Chapter 9

Conclusions

Micro Milling EDM is an attractive solution for the manufacturing of microcomponents but in order to exploit its peculiar characteristic for high accuracy micromachining, it is necessary to increase the performance of the process.
The small cylindrical tool electrodes used in micro milling μEDM are subject to severe wear during machining. As a result, the tool length and shape is changing during the process, producing form errors on the machined microfeatures. Thus, a tool wear compensation method is required in order to achieve high accuracy machining in Milling μEDM.
In this work, an on-line tool wear compensation method based on discharge counting and tool wear per discharge was proposed. The average discharge energy of sampled discharges, relative to a wide range of process parameter settings, was analysed and its variability during long and deep machining pocketing operations evaluated. Specific software tools were programmed in Matlab and optimal trigger values for discharge counting were defined.
Through extensive experimentation and data acquisition it was demonstrated that the variability of mean discharge energy, tool wear and material removal per discharge can be neglected, under the condition of stable machining and constant process parameter settings.
A strategy to perform on-machine volume measurement was developed and the repeatability and uncertainty of measures were studied. An evaluation of the errors affecting μEDM on-machine measurements was carried out. While probing speed can influence the repeatability and the accuracy of a measurement, tool-probe diameter and presence of dielectric fluid showed negligible effects on probing surfaces with a relatively good surface finish.
The uncertainty of dimensional measurements performed by the μEDM

milling machine was evaluated both for diameter and depth measurements. Results show a good repeatability and expanded uncertainties below 2 µm after correction of systematic errors on diameter measurements.
It is then possible to conclude that the measurement errors can be limited within 3% of the volume, by defining accurately the reference pocket dimensions and with an appropriated measurement procedure. Hence μEDM measurements based on the short-circuit system is suitable for calibration of tool wear compensation strategies.
A custom interface and protocol developed to command the μEDM machine from Matlab programming language was developed and successfully tested. This achievement enabled the definition of an automatic procedure for on-machine measurement of the material removal and tool wear per discharge. The procedure was tested with a wide range of process parameters. The variability of MRD and TWD values were evaluated. While TWD reached stability after few machining layers, MRD showed a decreasing trend with the progress of the machining operation, reaching stabilization after a certain depth depending on the energy level. The accuracy of MRD estimation was found higher for process parameters combinations yielding lower average discharge energies. In such conditions tool wear compensation based on MRD is expected to be most efficient.
As a result, it is possible to conclude that the tool electrode wear can be effectively compensated on the basis of discharge counting without the implementation of a pulse discrimination system. The method was applied in a preliminary experiment for the machining of a test feature by μEDM milling with satisfactory results.
Exploiting the information on MRD and counted discharges during a machining operation, a material removal simulation tool for accurate workpiece representation of the machined geometry has been developed and validated. The simulation tool can be used for verification of the progress of the machining operation as well as for improved tool trajectory definition and tool wear compensation for the following process steps.
Finally, the energy efficiency of the μEDM machine was analysed by using a low-cost, modular framework for remote energy monitoring specifically developed for this task, by employing open-hardware and open-source software. A number of expedients to gain in energy efficiency of the μEDM machine and process were suggested.

Bibliography

[1] M Kunieda, B Lauwers, K.P. Rajurkar, and B.M. Schumacher. Advancing EDM through Fundamental Insight into the Process. *CIRP Annals - Manufacturing Technology*, 54(2):64–87, January 2005.

[2] Eckart Uhlmann, Sascha Piltz, and Ulrich Doll. Machining of micro/miniature dies and moulds by electrical discharge machiningRecent development. *Journal of Materials Processing Technology*, 167(2-3):488–493, August 2005.

[3] K.P. Rajurkar, G. Levy, a. Malshe, M.M. Sundaram, J. McGeough, X. Hu, R. Resnick, and a. DeSilva. Micro and Nano Machining by Electro-Physical and Chemical Processes. *CIRP Annals - Manufacturing Technology*, 55(2):643–666, January 2006.

[4] Bernd M Schumacher. After 60 years of EDM the discharge process remains still disputed. *Journal of Materials Processing Technology*, 149(1-3):376–381, June 2004.

[5] B Sen, N Kiyawat, P K Singh, S Mitra, J H Ye, and P Purkait. Developments in electric power supply configurations for electrical-discharge-machining (EDM), 2003.

[6] K P Rajurkar and S M Pandit. Formation and Ejection of EDM Debris. *Journal of Engineering for Industry*, 108(1):22, 1986.

[7] Masanori KUNIEDA and Kenji YANATORI. Study on debris movement in EDM gap. *International journal of electrical machining*, 2:43–49, 1997.

[8] H.K. Kansal, Sehijpal Singh, and Pradeep Kumar. Technology and research developments in powder mixed electric discharge machining (PMEDM). *Journal of Materials Processing Technology*, 184(1-3):32–41, April 2007.

[9] Y.F. Luo. An evaluation of spark mobility in electrical discharge machining. *IEEE Transactions on Plasma Science*, 26(3):1010–1016, June 1998.

[10] Shuvra Das, Mathias Klotz, and F Klocke. EDM simulation: finite element-based calculation of deformation, microstructure and residual stresses. *Journal of Materials Processing Technology*, 142(2):434–451, November 2003.

[11] Dominiek Reynaerts, Paul-henri Heeren, and Hendrik Van Brussel. Microstructuring of silicon by electro-discharge machining (EDM) part I " theory. 60(c):212–218.

[12] K.H Ho and S.T Newman. State of the art electrical discharge machining (EDM). *International Journal of Machine Tools and Manufacture*, 43(13):1287–1300, October 2003.

[13] U. Maradia, M. Boccadoro, J. Stirnimann, I. Beltrami, F. Kuster, and K. Wegener. Die-sink EDM in Meso-Micro Machining. *Procedia CIRP*, 1:166–171, January 2012.

[14] Z Y Yu, H Shen, and Management Systems Engineering. High Aspect Ratio and Complex Shaped Blind Micro Holes. (1):1–4.

[15] K.H Ho, S.T Newman, S Rahimifard, and R.D Allen. State of the art in wire electrical discharge machining (WEDM). *International Journal of Machine Tools and Manufacture*, 44(12-13):1247–1259, October 2004.

[16] T Kaneko and M Tsuchiya. Three-dimensional numerically controlled contouring by electric discharge machining with compensation for the deformation of cylindrical tool electrodes. *Precision Engineering*, 10(3):157–163, 1988.

[17] Z Y Yu and M Fujino. Micro-EDM for Three-Dimensional Cavities - Development of Uniform Wear Method -. 47:169–172, 1998.

[18] T. Masuzawa. State of the Art of Micromachining. *CIRP Annals - Manufacturing Technology*, 49(2):473–488, January 2000.

[19] T Masuzawa and HK Tönshoff. Three-dimensional micromachining by machine tools. *CIRP Annals-Manufacturing Technology*, 1997.

[20] D.T Pham, S.S Dimov, S Bigot, a Ivanov, and K Popov. Micro-EDMrecent developments and research issues. *Journal of Materials Processing Technology*, 149(1-3):50–57, June 2004.

[21] a. Kojima, W. Natsu, and M. Kunieda. Spectroscopic measurement of arc plasma diameter in EDM. *CIRP Annals - Manufacturing Technology*, 57(1):203–207, January 2008.

[22] Kai Egashira, Akihiro Matsugasako, Hachiro Tsuchiya, and Makoto Miyazaki. Electrical discharge machining with ultralow discharge energy. *Precision Engineering*, 30(4):414–420, October 2006.

[23] Fuzhu Han, Shinya Wachi, and Masanori Kunieda. Improvement of machining characteristics of micro-EDM using transistor type isopulse generator and servo feed control. *Precision Engineering*, 28(4):378–385, October 2004.

[24] M. Kunieda, a. Hayasaka, X.D. Yang, S. Sano, and I. Araie. Study on Nano EDM Using Capacity Coupled Pulse Generator. *CIRP Annals - Manufacturing Technology*, 56(1):213–216, January 2007.

[25] J. Murray, D. Zdebski, and a.T. Clare. Workpiece debris deposition on tool electrodes and secondary discharge phenomena in micro-EDM. *Journal of Materials Processing Technology*, 212(7):1537–1547, July 2012.

[26] R Snoeys, D Dauw, and M Jennes. Survey of EDM Adaptive Control and Detection Systems. *CIRP Annals - Manufacturing Technology*, 31(2):483–489, 1982.

[27] D Dauw and R Snoeys. On the Derivation and Application of a Real-Time Tool Wear Sensor in EDM. *CIRP Annals - Manufacturing Technology*, 35(1):111–116, 1986.

[28] D T Pham, A Ivanov, S Bigot, K Popov, and S Dimov. A study of micro-electro discharge machining electrode wear. *Proceedings of the Institution of Mechanical Engineers, Part C: Journal of Mechanical Engineering Science*, 221(5):605–612, 2007.

[29] Yao-Yang Tsai and Takahisa Masuzawa. An index to evaluate the wear resistance of the electrode in micro-EDM. *Journal of Materials Processing Technology*, 149(1-3):304–309, June 2004.

[30] Eckart Uhlmann and Markus Roehner. Investigations on reduction of tool electrode wear in micro-EDM using novel electrode materials. *CIRP Journal of Manufacturing Science and Technology*, 1(2):92–96, January 2008.

[31] P. Bleys, J.-P. Kruth, and B. Lauwers. Sensing and compensation of tool wear in milling EDM. *Journal of Materials Processing Technology*, 149(1-3):139–146, June 2004.

[32] E. Aligiri, S.H. Yeo, and P.C. Tan. A new tool wear compensation method based on real-time estimation of material removal volume in micro-EDM. *Journal of Materials Processing Technology*, 210(15):2292–2303, November 2010.

[33] G. Bissacco, H.N. Hansen, G. Tristo, and J. Valentincic. Feasibility of wear compensation in micro EDM milling based on discharge counting and discharge population characterization. *CIRP Annals - Manufacturing Technology*, 60(1):231–234, January 2011.

[34] Jian-Zhong Li, Lu Xiao, Hui Wang, Hui-Lan Yu, and Zu-Yuan Yu. Tool wear compensation in 3D micro EDM based on the scanned area. *Precision Engineering*, 37(3):753–757, July 2013.

[35] Jayakumar Narasimhan, Zuyuan Yu, and Kamlakar P. Rajurkar. Tool Wear Compensation and Path Generation in Micro and Macro EDM. *Journal of Manufacturing Processes*, 7(1):75–82, January 2005.

[36] K P Rajurkar and Z Y Yu. 3d micro-edm using cad/cam. *CIRP Annals-Manufacturing Technology*, 49(1):127–130, 2000.

[37] P. Bleys, J.-P. Kruth, B. Lauwers, a. Zryd, R. Delpretti, and C. Tricarico. Real-time Tool Wear Compensation in Milling EDM. *CIRP Annals - Manufacturing Technology*, 51(1):157–160, January 2002.

[38] JAE WON JUNG, YOUNG HUN JEONG, Byung-Kwon MIN, and SANG JO LEE. Model-Based Pulse Frequency Control for Micro-EDM Milling Using Real-Time Discharge Pulse Monitoring. *Journal of manufacturing science and engineering*, 130(3).

[39] J Valentinčič, I Sabotin, G Tristo, G Bissaco, and S Bigot. Tooling and microinjection moulding of bottom grooved micromixers. In *Proceedings of the 10th International Conference on Multi-Material Micro Manufacture*, pages 2–5, San Sebastián, Spain, 2013.

[40] Izidor Sabotin, Gianluca Tristo, Mihael Junkar, and Joško Valentinčič. Two-step design protocol for patterned groove micromixers. *Chemical Engineering Research and Design*, 91(5):778–788, May 2013.

[41] T Masuzawa, M Fujino, K Kobayashi, T Suzuki, and N Kinoshita. Wire Electro-Discharge Grinding for Micro-Machining. *CIRP Annals - Manufacturing Technology*, 34(1):431–434, 1985.

[42] V. Schulze, P. Weber, and C. Ruhs. Increase of process reliability in the micro-machining processes EDM-milling and laser ablation using on-machine sensors. *Journal of Materials Processing Technology*, 212(3):625–632, March 2012.

[43] Dong-Yea Sheu. Study on an evaluation method of micro CMM spherical stylus tips by -EDM on-machine measurement. *Journal of Micromechanics and Microengineering*, 20(7):075003, July 2010.

[44] Giuliano Bissacco, Gianluca Tristo, and Josko Valentinčič. Assessment of Electrode Wear Measurement in Micro EDM Milling. In *Proceedings of the 7th International Conference on Multi-Material Micro Manufacture*, pages 155–158, Singapore, 2010. Research Publishing Services.

[45] S. Carmignato and E. Savio. Traceable volume measurements using coordinate measuring systems. *CIRP Annals - Manufacturing Technology*, 60(1):519–522, January 2011.

[46] ISO 15530-3:2011, Geometrical product specifications (GPS) – Coordinate measuring machines (CMM): Technique for determining the uncertainty of measurement – Part 3: Use of calibrated workpieces or measurement standards.

[47] P. Bleys. *Electrical Discharge Milling. Technology and tool wear compensation.* PhD thesis, Katholieke Universiteit Leuven, 2004.

[48] G Bissacco, G Tristo, H.N. Hansen, and J. Valentincic. Reliability of electrode wear compensation based on material removal per discharge in micro EDM milling. *CIRP Annals - Manufacturing Technology*, 62(1):179–182, January 2013.

[49] G. Bissacco, J. Valentincic, H. N. Hansen, and B. D. Wiwe. Towards the effective tool wear control in micro-EDM milling. *The International Journal of Advanced Manufacturing Technology*, 47(1-4):3–9, May 2009.

[50] J Valentinčič, G Bissacco, and G Tristo. On machine measurements of electrode wear in micro EDM milling.

[51] E. Weingärtner, F. Kuster, and K. Wegener. Modeling and simulation of electrical discharge machining. *Procedia CIRP*, 2:74–78, January 2012.

[52] Nizar Ben Salah, Farhat Ghanem, and Kaïs Ben Atig. Numerical study of thermal aspects of electric discharge machining process. *International Journal of Machine Tools and Manufacture*, 46(7-8):908–911, June 2006.

[53] Z Katz and CJ Tibbles. Analysis of micro-scale EDM process. *The International Journal of Advanced Manufacturing Technology*, 25(9-10):923–928, September 2004.

[54] Ajit Singh and Amitabha Ghosh. A thermo-electric model of material removal during electric discharge machining. *International Journal of Machine Tools and Manufacture*, 39(4):669–682, April 1999.

[55] H.K. Kansal, Sehijpal Singh, and Pradeep Kumar. Numerical simulation of powder mixed electric discharge machining (PMEDM) using finite element method. *Mathematical and Computer Modelling*, 47(11-12):1217–1237, June 2008.

[56] Pei-Jen Wang and Kuo-Ming Tsai. Semi-empirical model on work removal and tool wear in electrical discharge machining. *Journal of Materials Processing Technology*, 114(1):1–17, July 2001.

[57] Kuo-Ming Tsai and Pei-Jen Wang. Semi-empirical model of surface finish on electrical discharge machining. *International Journal of Machine Tools and Manufacture*, 41(10):1455–1477, August 2001.

[58] C Tricarico, R Delpretti, and DF Dauw. Geometrical simulation of the EDM die-sinking process. *CIRP Annals-Manufacturing Technology*, 1988.

[59] Xiaodong Yang, Jianwen Guo, Xiaofei Chen, and Masanori Kunieda. Molecular dynamics simulation of the material removal mechanism in micro-EDM. *Precision Engineering*, 35(1):51–57, January 2011.

[60] Yongshun Zhao, Xingquan Zhang, and Kazuo Yamazaki. Molecular Dynamics simulation for EDM Die-Sinking. 1(c):1–5, 1980.

[61] Yongshun Zhao, Xingquan Zhang, Xianbing Liu, and Kazuo Yamazaki. Geometric modeling of the linear motor driven electrical discharge ma-

chining (EDM) die-sinking process. *International Journal of Machine Tools and Manufacture*, 44(1):1–9, January 2004.

[62] M Yang and Eungki Lee. NC verification for wire-EDM using an R-map. *Computer-Aided Design*, 26(9):733–740, 1996.

[63] Kenji Morimoto and Masanori Kunieda. Sinking EDM simulation by determining discharge locations based on discharge delay time. *CIRP Annals - Manufacturing Technology*, 58(1):221–224, January 2009.

[64] Young Hun Jeong and Byung-Kwon Min. Geometry prediction of EDM-drilled holes and tool electrode shapes of micro-EDM process using simulation. *International Journal of Machine Tools and Manufacture*, 47(12-13):1817–1826, October 2007.

[65] Segon Heo, Young Hun Jeong, Byung-Kwon Min, and Sang Jo Lee. Virtual EDM simulator: Three-dimensional geometric simulation of micro-EDM milling processes. *International Journal of Machine Tools and Manufacture*, 49(12-13):1029–1034, October 2009.

[66] Fuzhu Han, Masanori Kunieda, Tomoko Sendai, and Yoshihito Imai. High Precision Simulation of WEDM Using Parametric Programming. *CIRP Annals - Manufacturing Technology*, 51(1):165–168, January 2002.

[67] Masanori Kunieda, Wataru Kowaguchi, and Takashi Takita. Reverse Simulation of Die-Sinking EDM. *CIRP Annals - Manufacturing Technology*, 48(1):115–118, January 1999.

[68] Paul Anastas and Nicolas Eghbali. Green chemistry: principles and practice. *Chemical Society Reviews*, 39(1):301–312, 2010.

[69] Angappa Gunasekaran and Alain Spalanzani. Sustainability of manufacturing and services: Investigations for research and applications. *International Journal of Production Economics*, 140(1):35–47, November 2012.

[70] Eoin ODriscoll and Garret E. ODonnell. Industrial power and energy metering A state of the art review. *Journal of Cleaner Production*, October 2012.

[71] D.J. Start. A review of the new CENELEC standard EN 50160. In *IEE Colloquium on Issues in Power Quality*, volume 1995, pages 4–4, Coventry, 1995. IEE.

[72] Andrej Lebar, Luka Selak, Rok Vrabič, Peter Butala, and Others. Online Monitoring, Analysis, and Remote Recording of Welding Parameters to the Welding Diary. *Strojni{š}ki vestnik-Journal of Mechanical Engineering*, 58(7-8):444–452, 2012.

[73] Shaohua Hu, Fei Liu, Yan He, and Tong Hu. An on-line approach for energy efficiency monitoring of machine tools. *Journal of Cleaner Production*, 27:133–140, May 2012.

[74] Thomas Behrendt, André Zein, and Sangkee Min. Development of an energy consumption monitoring procedure for machine tools. *CIRP Annals - Manufacturing Technology*, 61(1):43–46, January 2012.

[75] a. Vijayaraghavan and D. Dornfeld. Automated energy monitoring of machine tools. *CIRP Annals - Manufacturing Technology*, 59(1):21–24, January 2010.

[76] Joost R. Duflou, John W. Sutherland, David Dornfeld, Christoph Herrmann, Jack Jeswiet, Sami Kara, Michael Hauschild, and Karel Kellens. Towards energy and resource efficient manufacturing: A processes and systems approach. *CIRP Annals - Manufacturing Technology*, 61(2):587–609, January 2012.

[77] Nancy Diaz, Elena Redelsheimer, and David Dornfeld. Energy Consumption Characterization and Reduction Strategies for Milling Machine Tool Use. In Jürgen Hesselbach and Christoph Herrmann, editors, *Glocalized Solutions for Sustainability in Manufacturing*, pages 263–267. Springer Berlin Heidelberg, Berlin, Heidelberg, 2011.

[78] S. Kara and W. Li. Unit process energy consumption models for material removal processes. *CIRP Annals - Manufacturing Technology*, 60(1):37–40, January 2011.

[79] C. Herrmann, S. Thiede, S. Kara, and J. Hesselbach. Energy oriented simulation of manufacturing systems Concept and application. *CIRP Annals - Manufacturing Technology*, 60(1):45–48, January 2011.

[80] Y. Seow and S. Rahimifard. A framework for modelling energy consumption within manufacturing systems. *CIRP Journal of Manufacturing Science and Technology*, 4(3):258–264, January 2011.

[81] F Draganescu, M Gheorghe, and C V Doicin. Models of machine tool efficiency and specific consumed energy. *Journal of Materials Processing Technology*, 141(September 2002):9–15, 2003.

[82] J.L. Liow. Mechanical micromachining: a sustainable micro-device manufacturing approach? *Journal of Cleaner Production*, 17(7):662–667, May 2009.

[83] Jonathan Oxer and Hugh Blemings. *Practical Arduino: Cool Projects for Open Source Hardware*. Apress, 2009.

Appendix A

Current and voltage waveforms and discharge energy histograms relative to energy indexes 015, 206, 250, 305, 315 and 350.

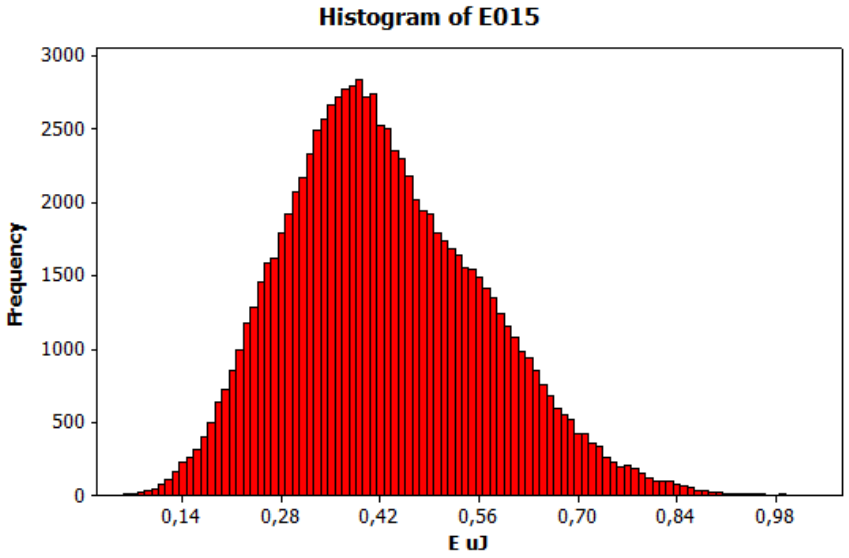

Figure 1: Energy distribution of discharge population relative to energy index 015.

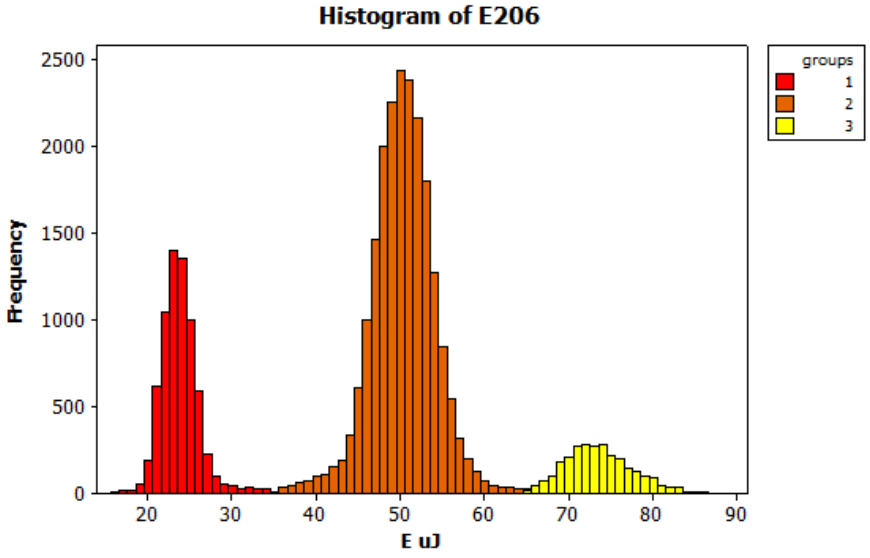

Figure 2: Energy distribution of discharge population relative to energy index 206.

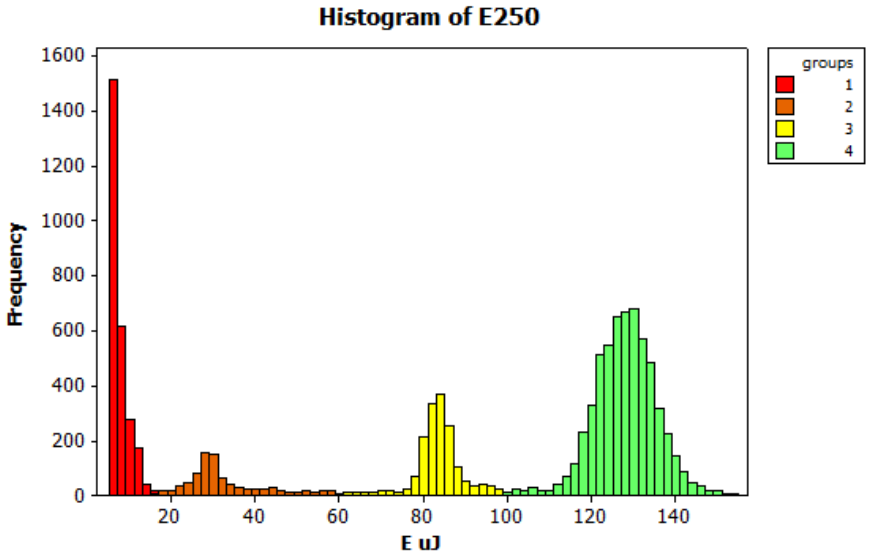

Figure 3: Energy distribution of discharge population relative to energy index 250.

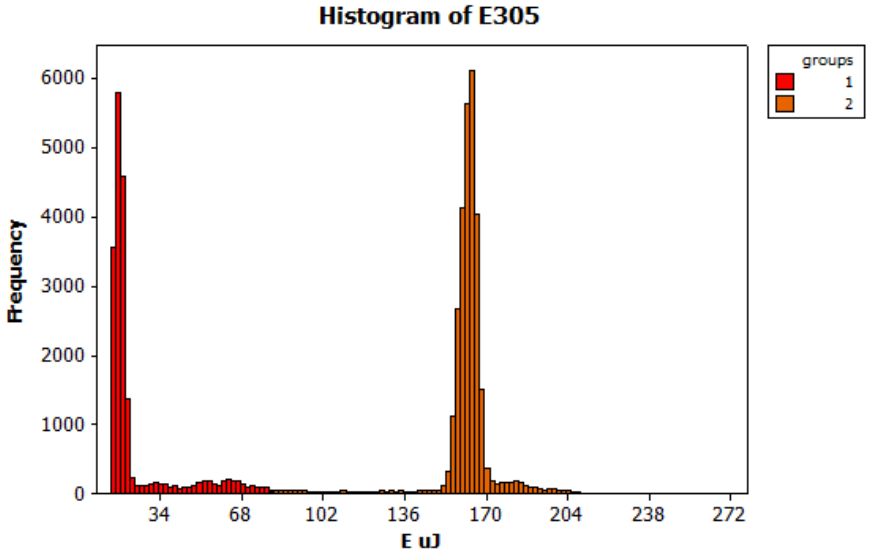

Figure 4: Energy distribution of discharge population relative to energy index 305.

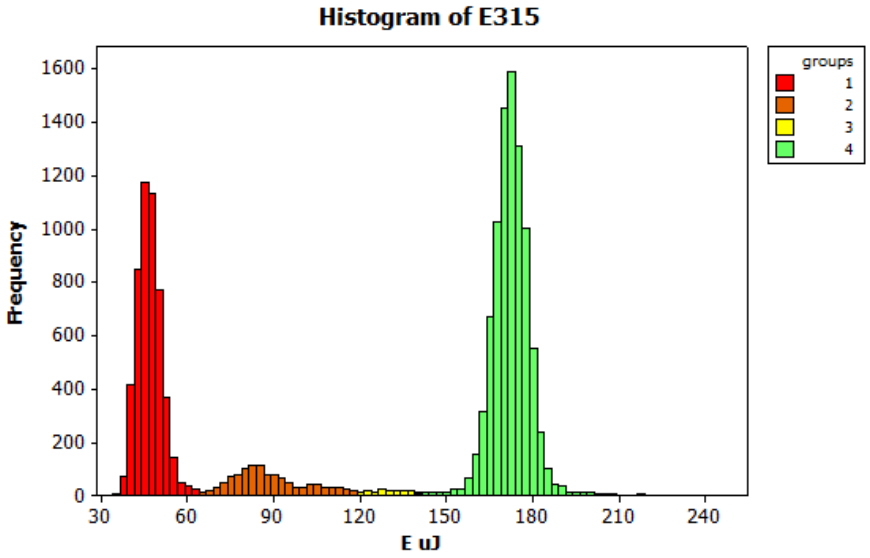

Figure 5: Energy distribution of discharge population relative to energy index 315.

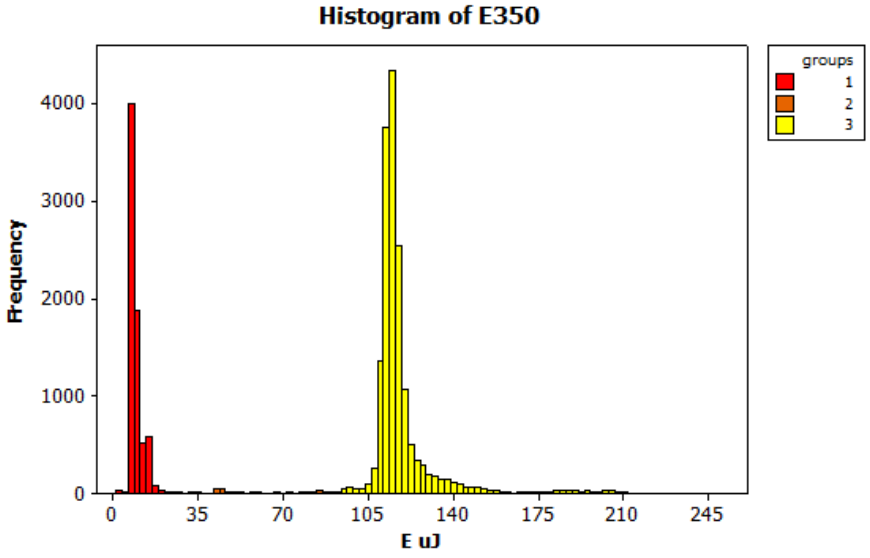

Figure 6: Energy distribution of discharge population relative to energy index 350.

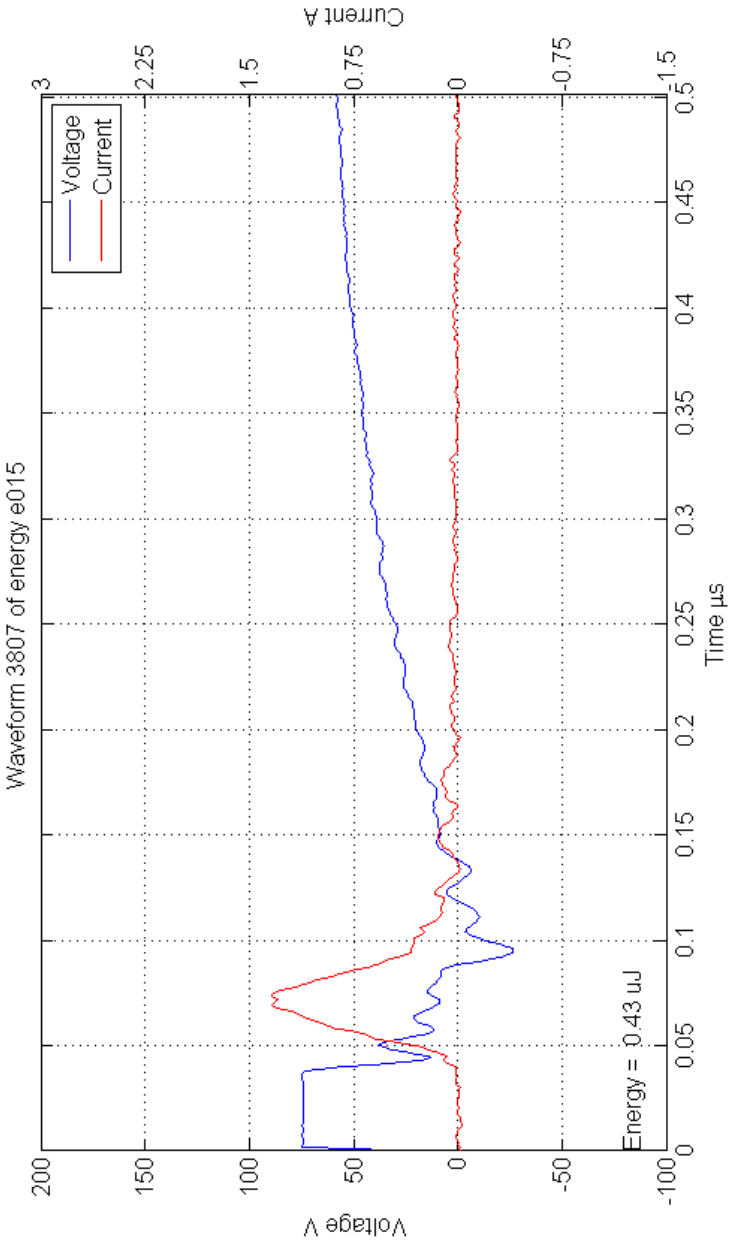

Figure 7: Typical voltage and current waveforms relative to energy index 015.

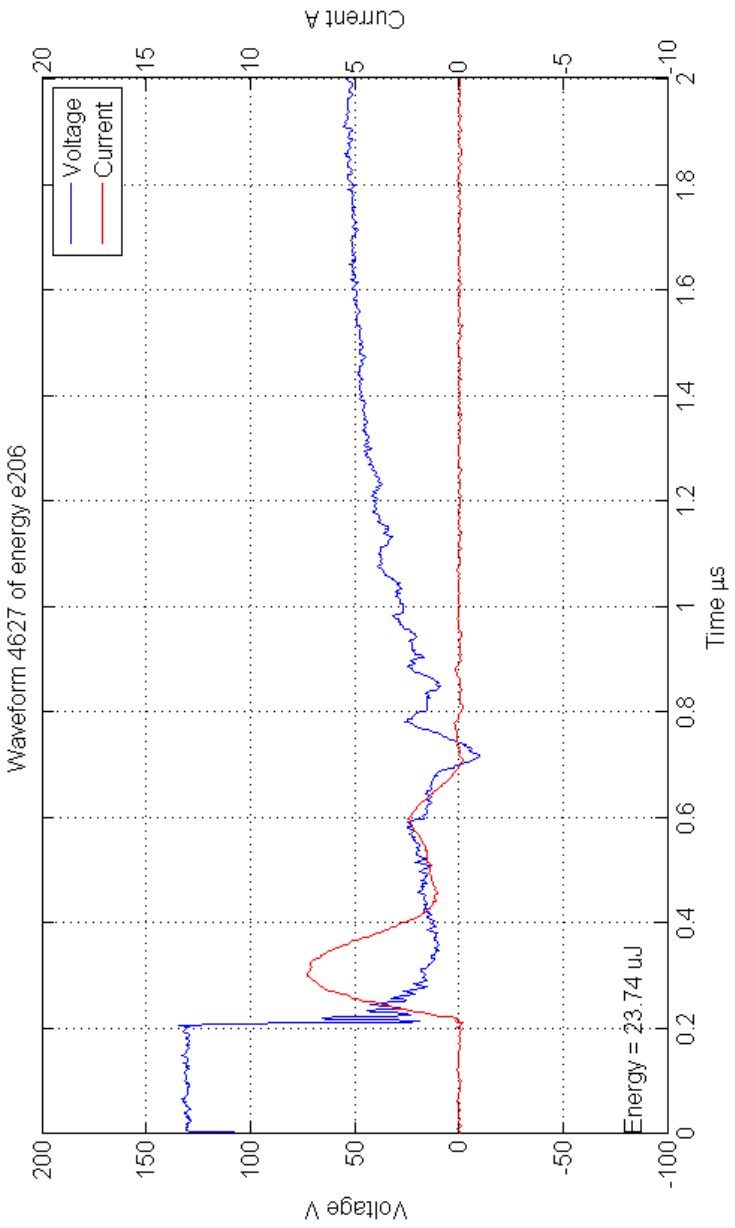

Figure 8: Typical voltage and current waveforms relative to energy index 206, group 1.

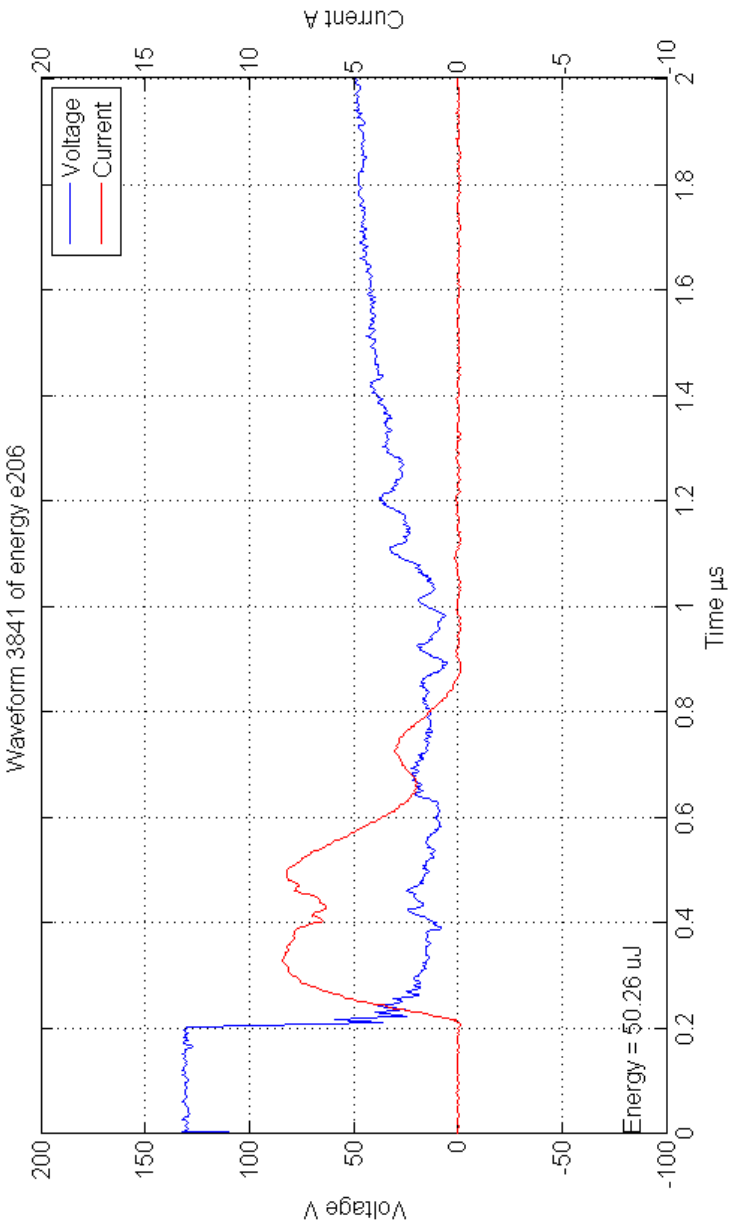

Figure 9: Typical voltage and current waveforms relative to energy index 206, group 2.

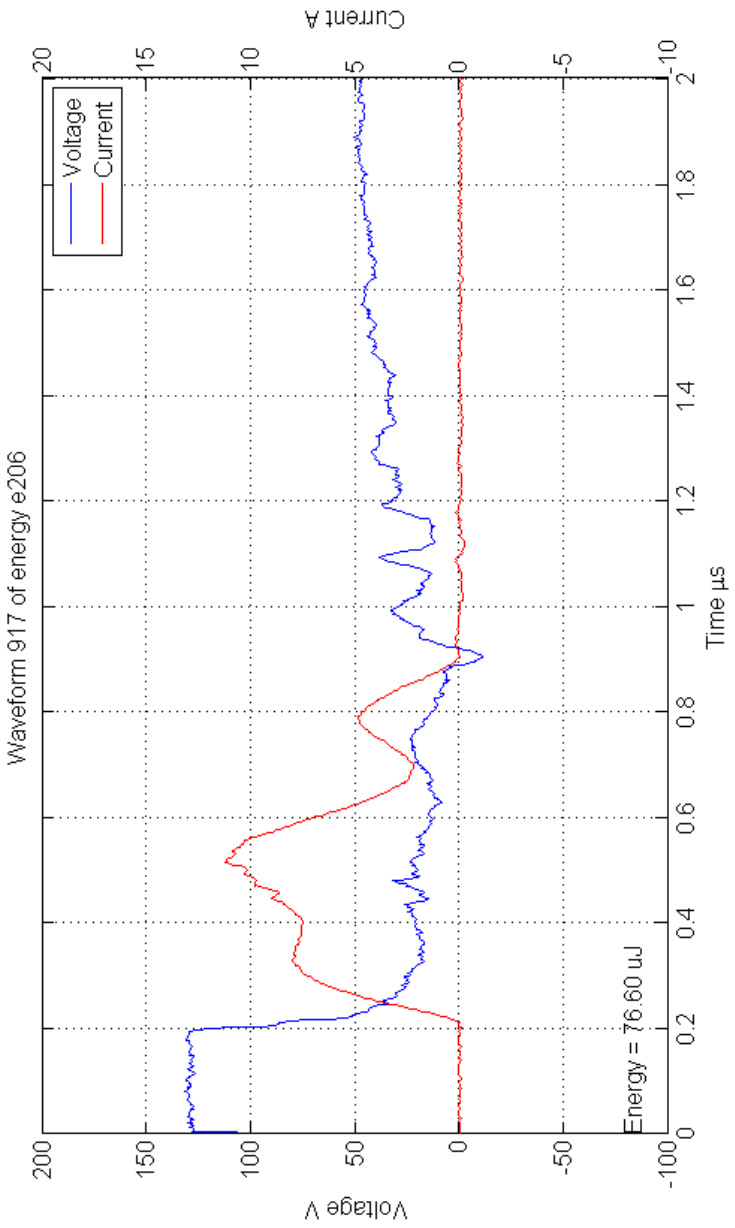

Figure 10: Typical voltage and current waveforms relative to energy index 206, group 3.

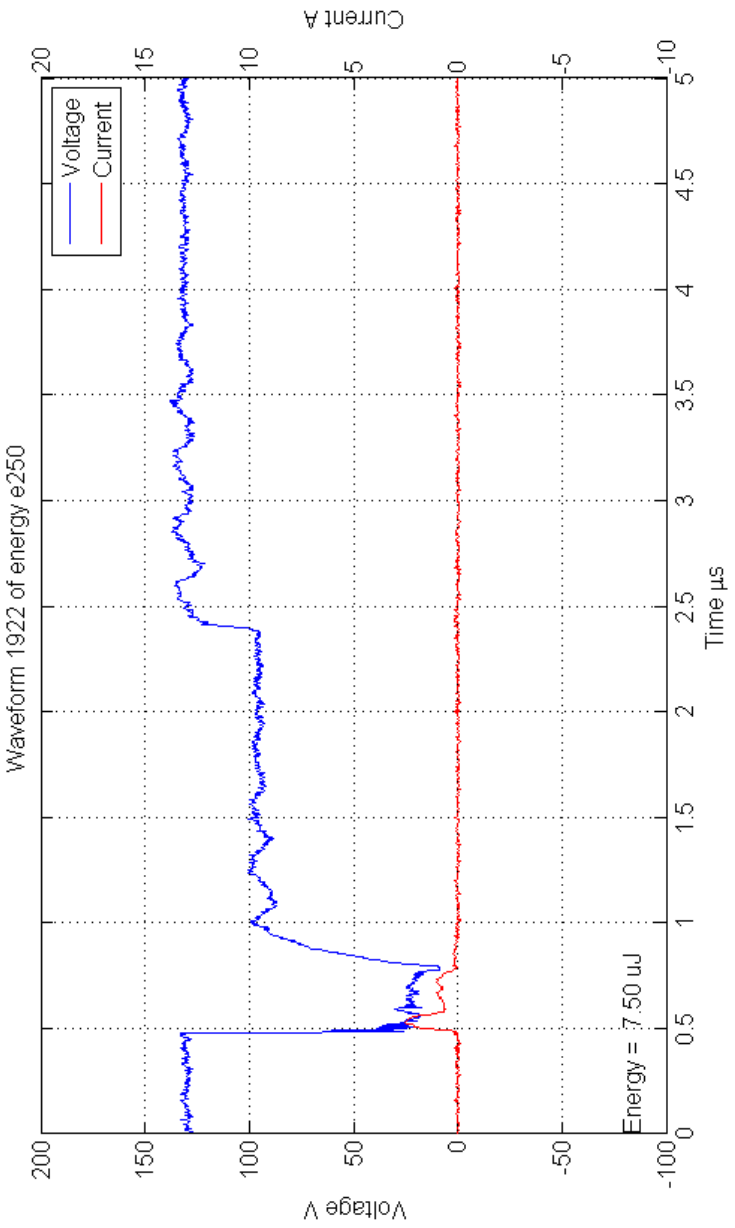

Figure 11: Typical voltage and current waveforms relative to energy index 250, group 1.

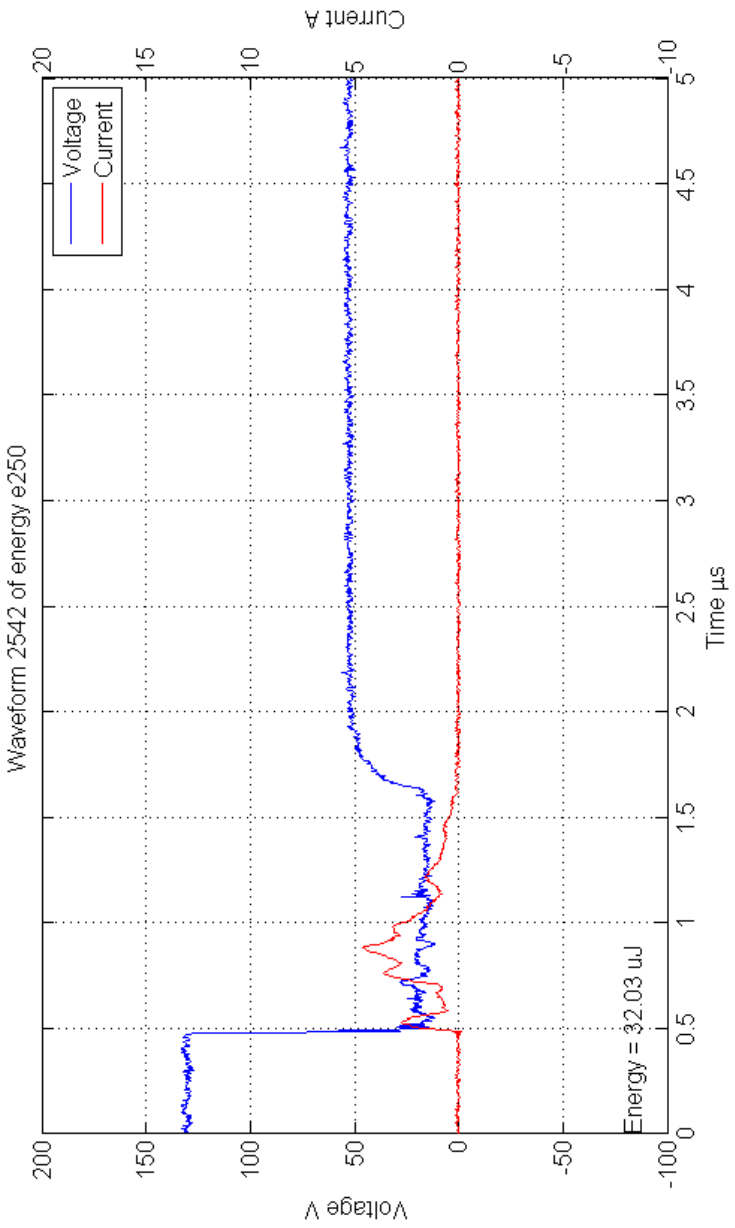

Figure 12: Typical voltage and current waveforms relative to energy index 250, group 2.

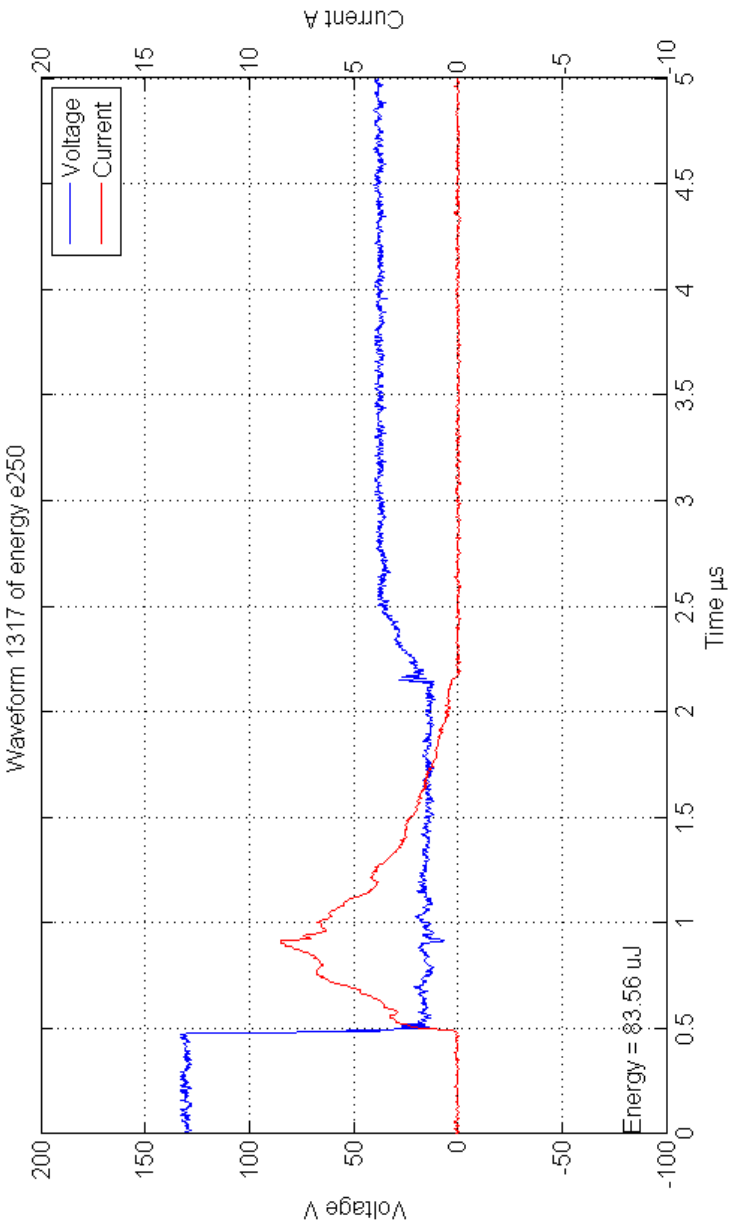

Figure 13: Typical voltage and current waveforms relative to energy index 250, group 3.

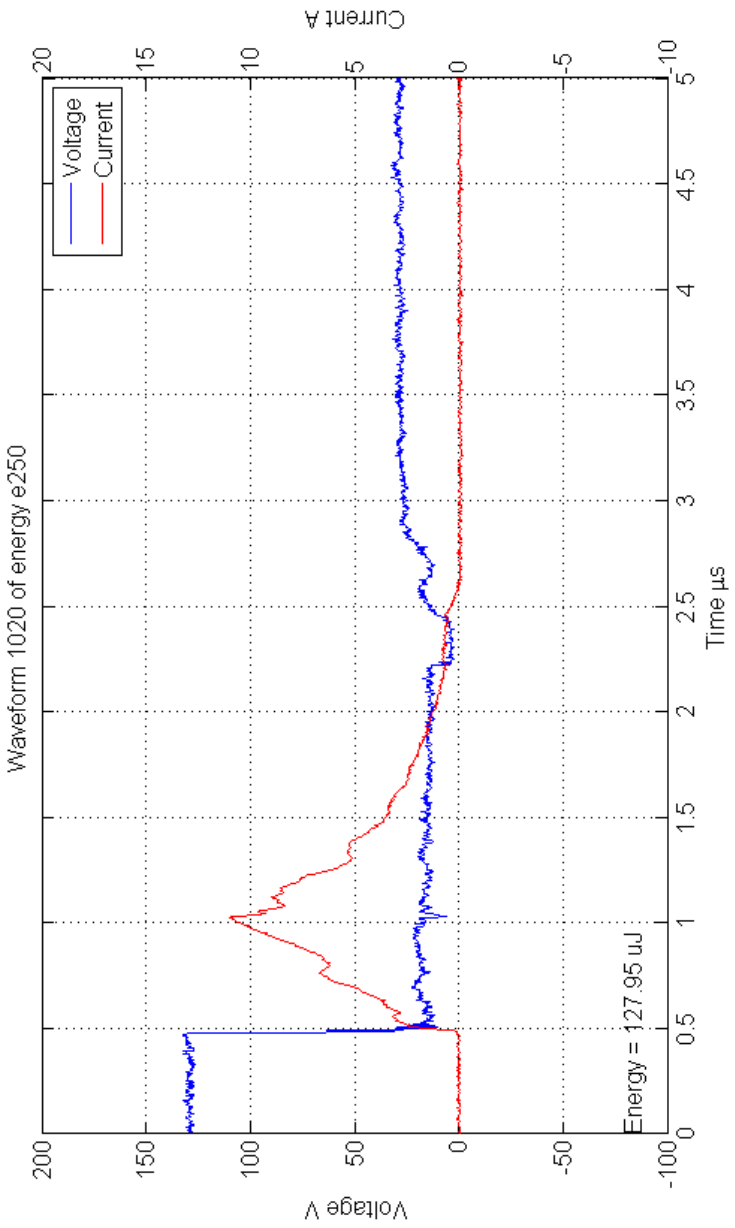

Figure 14: Typical voltage and current waveforms relative to energy index 250, group 4.

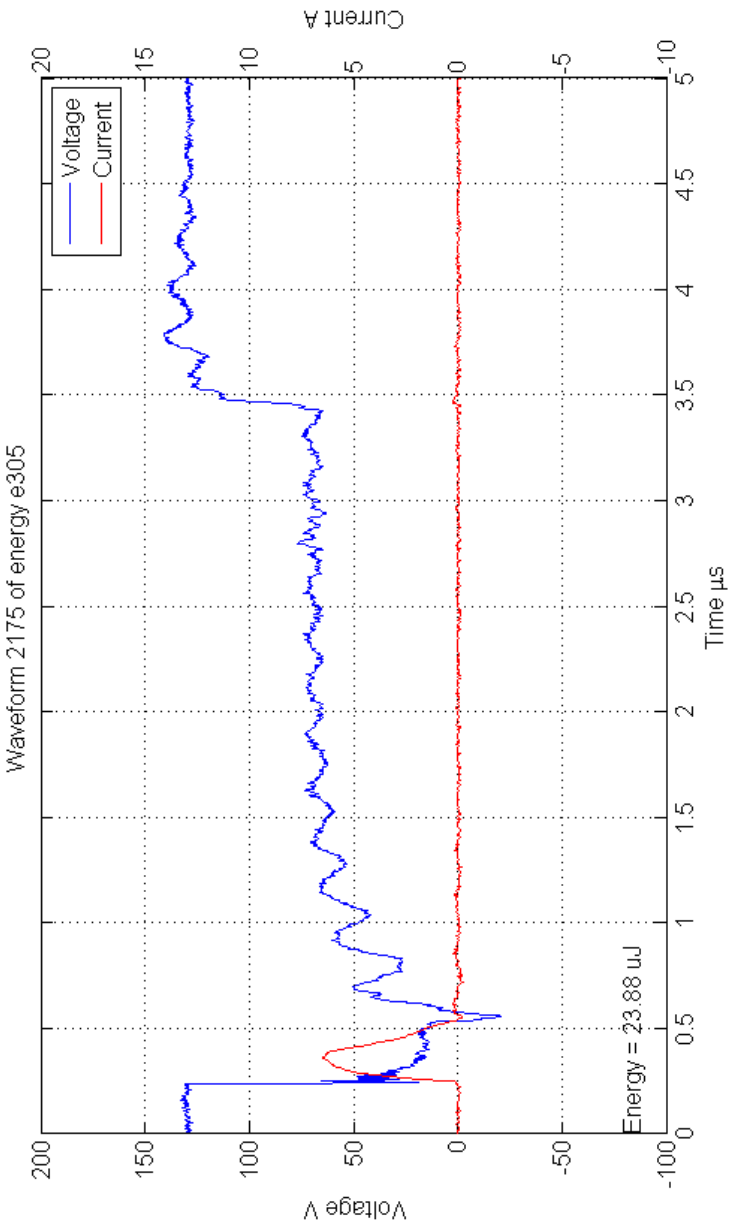

Figure 15: Typical voltage and current waveforms relative to energy index 305, group 1.

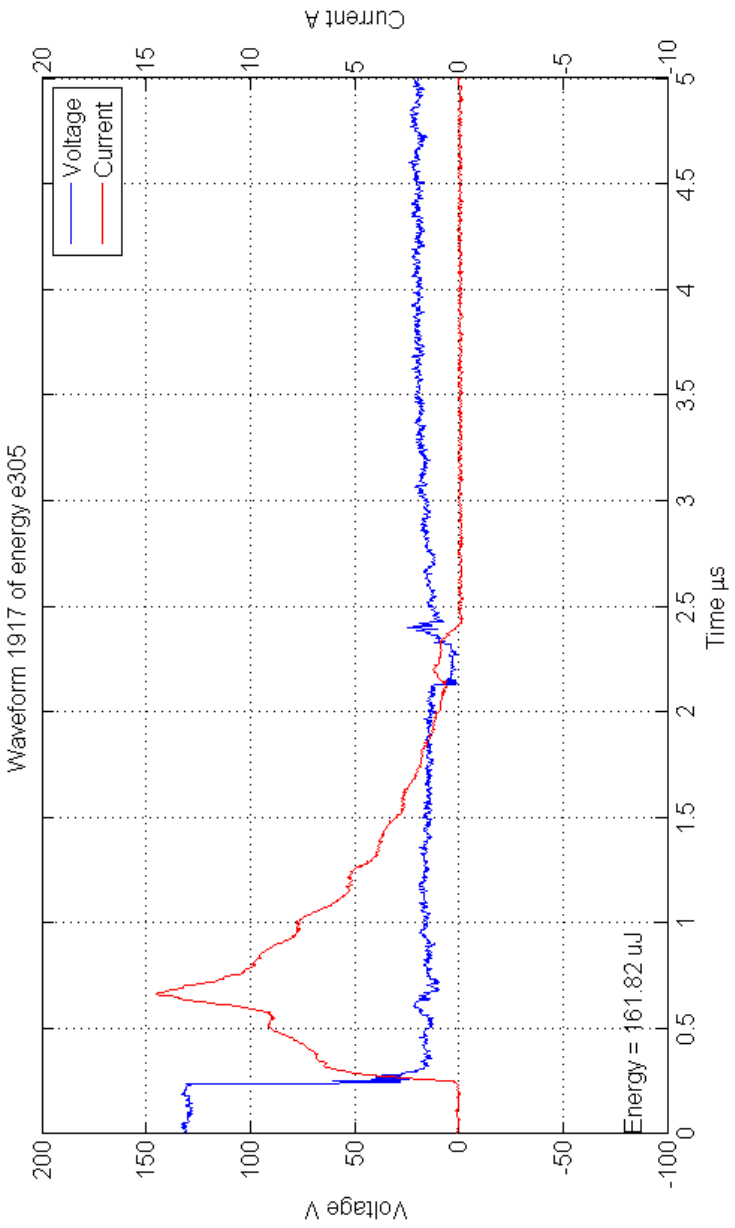

Figure 16: Typical voltage and current waveforms relative to energy index 305, group 2.

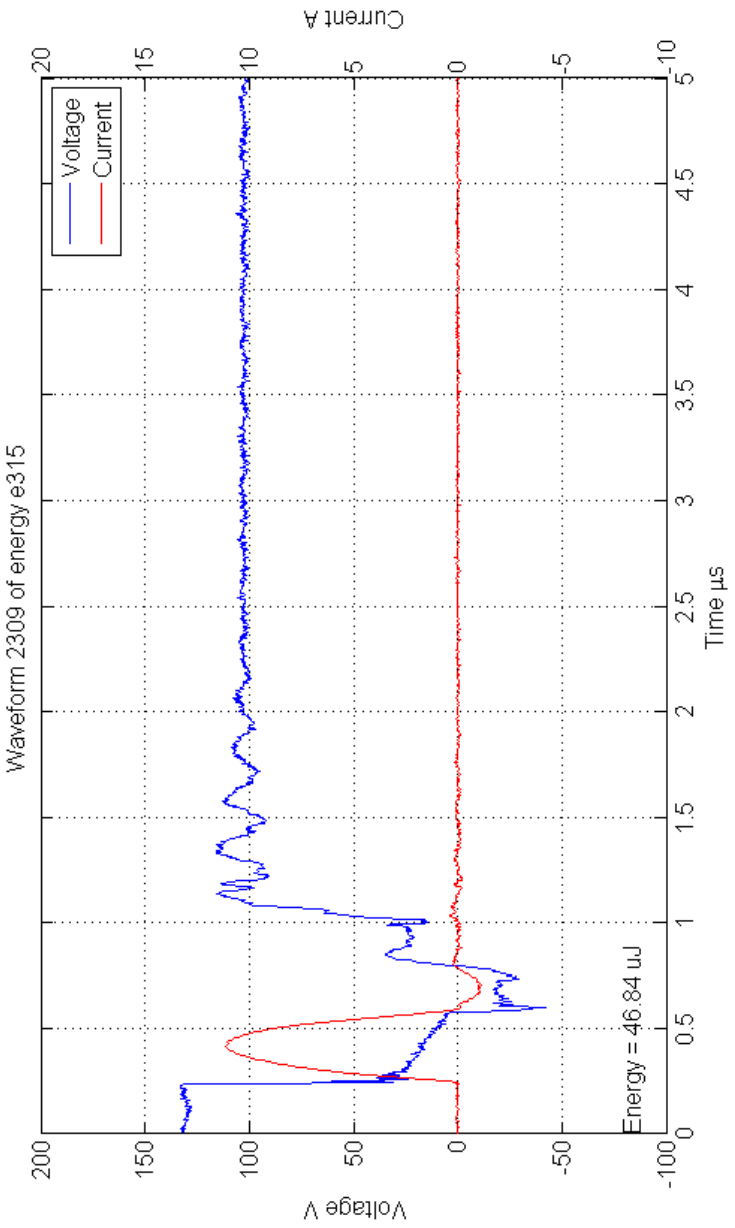

Figure 17: Typical voltage and current waveforms relative to energy index 315, group 1.

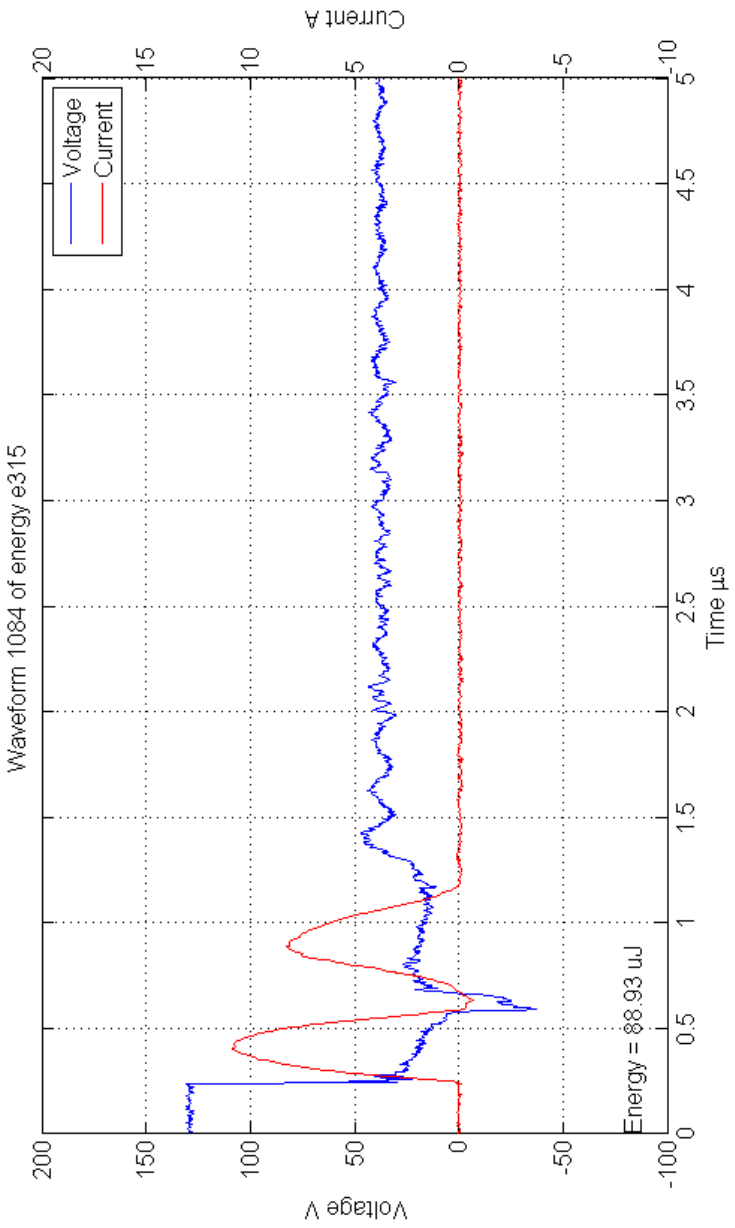

Figure 18: Typical voltage and current waveforms relative to energy index 315, group 2.

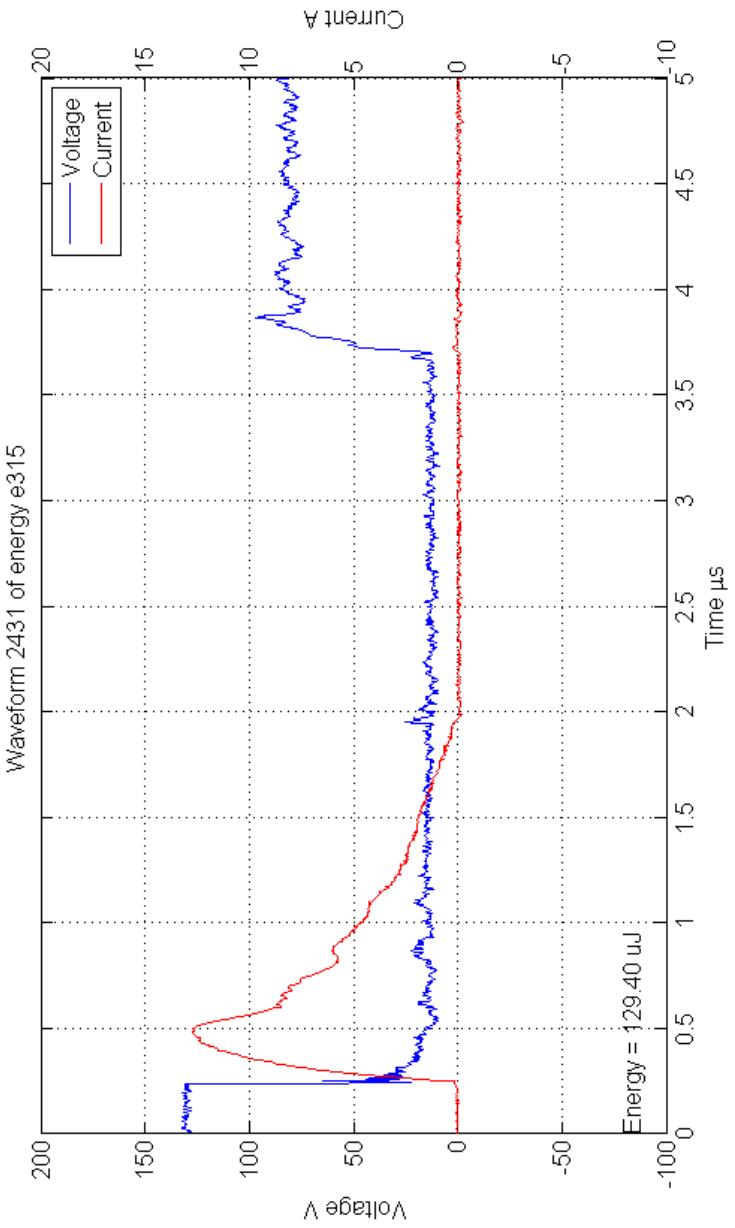

Figure 19: Typical voltage and current waveforms relative to energy index 315, group 3.

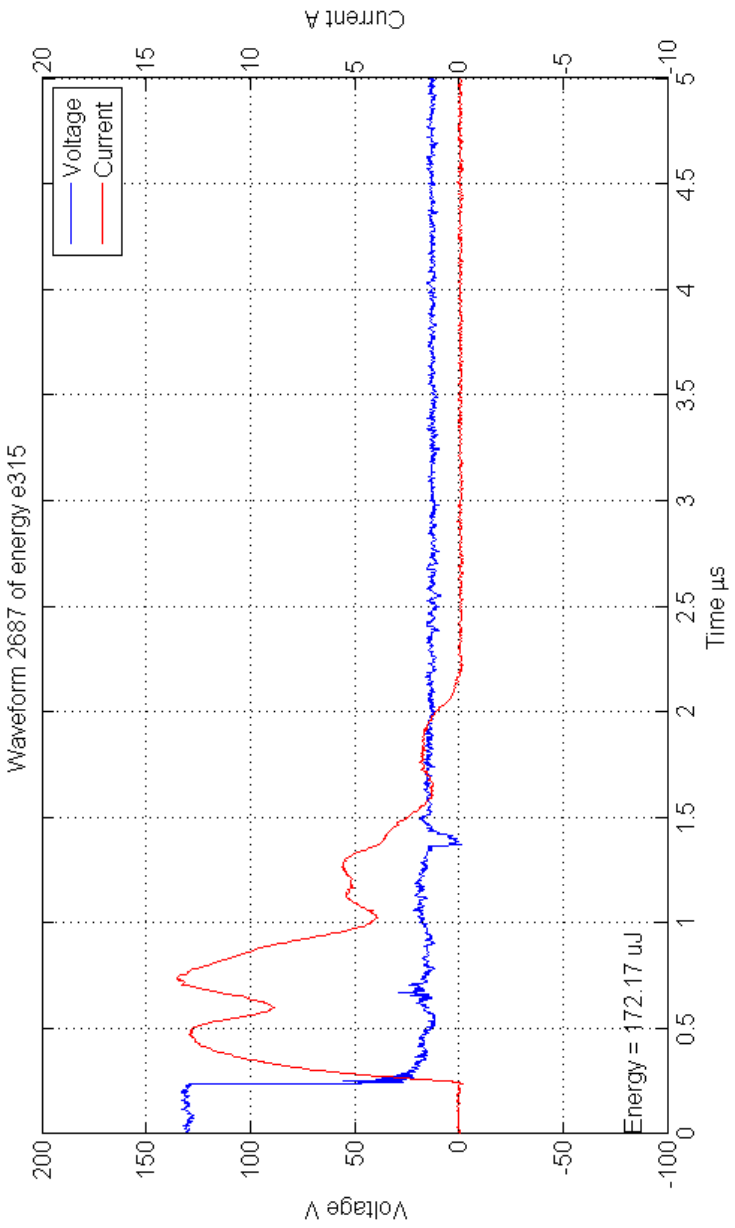

Figure 20: Typical voltage and current waveforms relative to energy index 315, group 4.

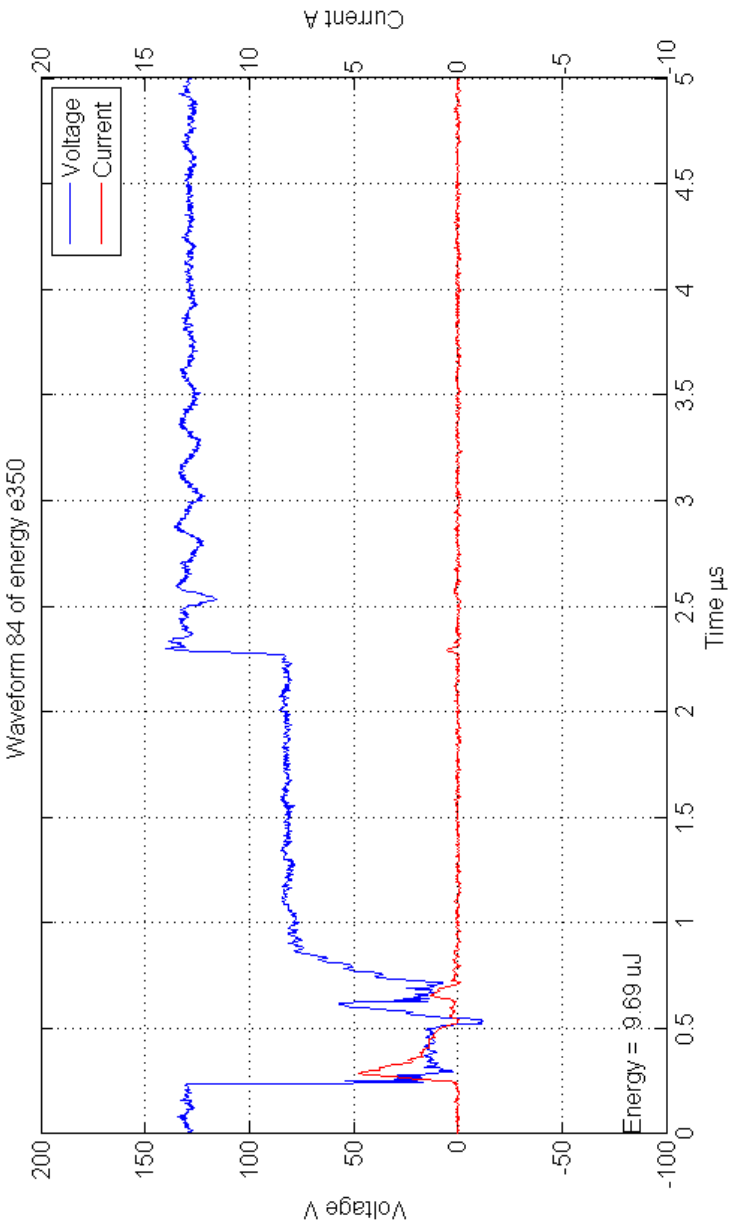

Figure 21: Typical voltage and current waveforms relative to energy index 350, group 1.

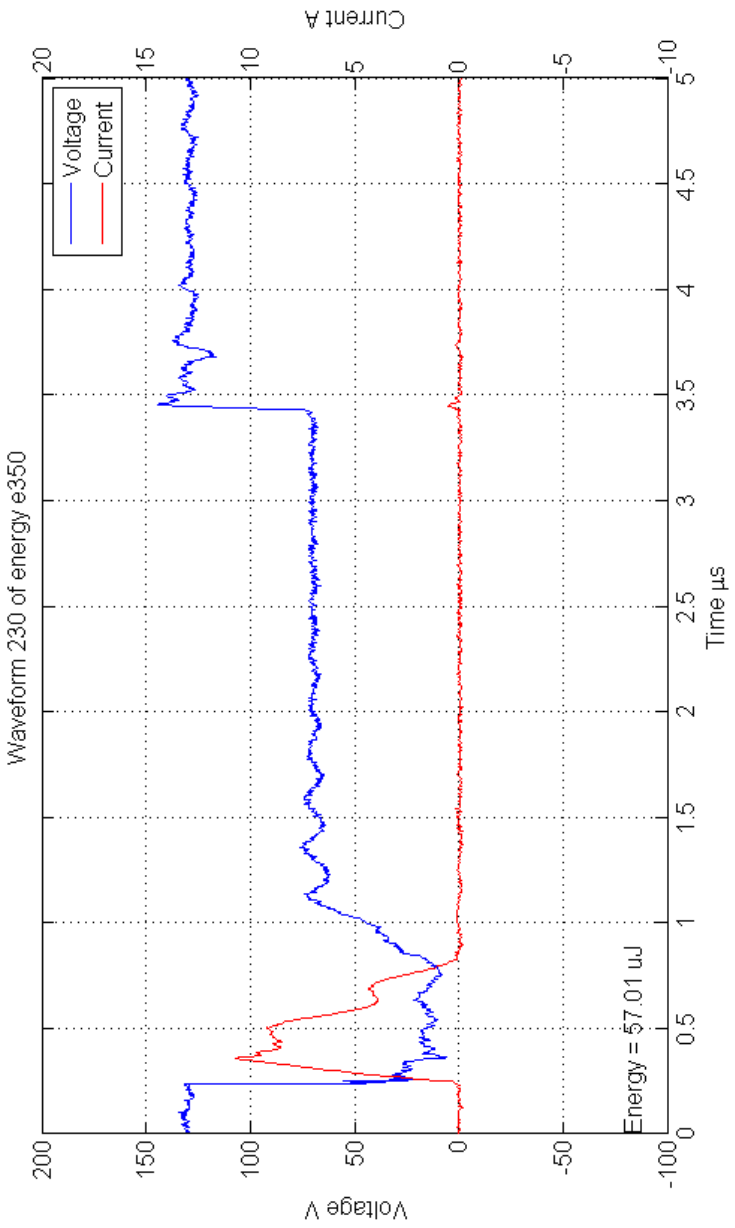

Figure 22: Typical voltage and current waveforms relative to energy index 350, group 2.

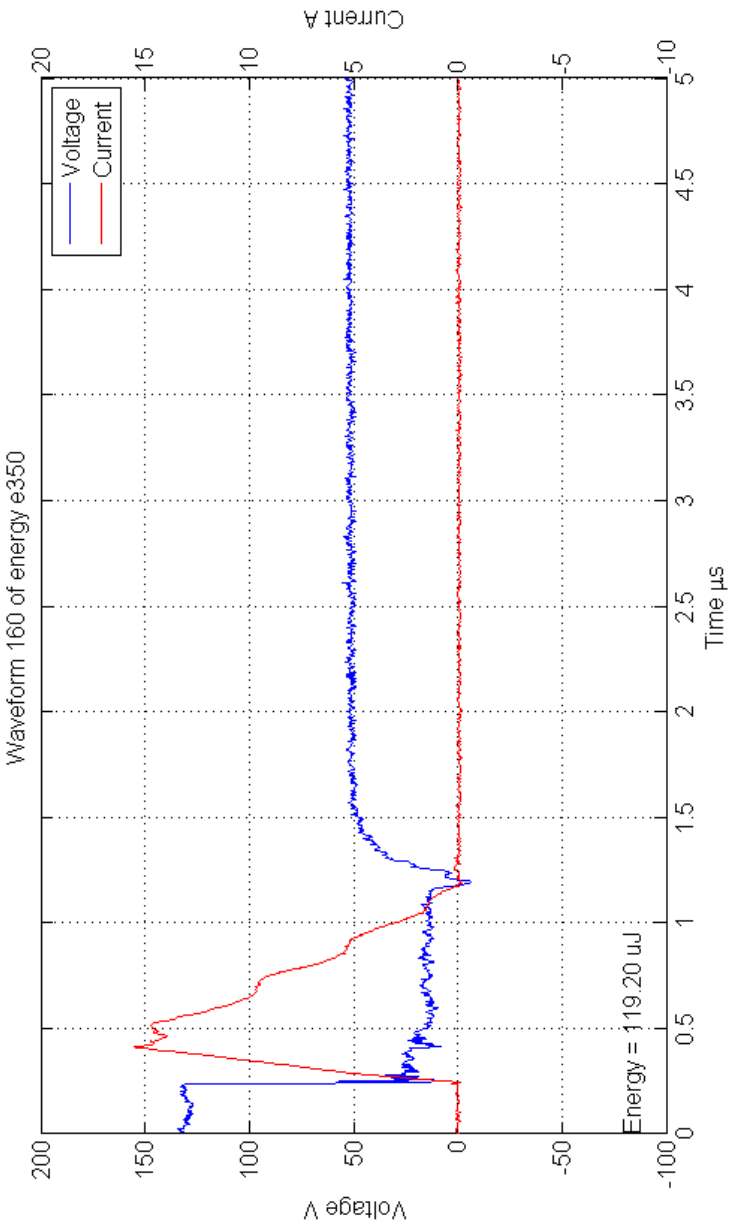

Figure 23: Typical voltage and current waveforms relative to energy index 350, group 3.